Cement and Concrete Research

Hydration and interactions between pure and doped C3S and C3A in the presence of different calcium sulfates

--Manuscript Draft--

Manuscript Number:	CEMCON-D-22-00338R1
Article Type:	Research paper
Keywords:	C3S; C3A; calcium sulfate; Polymorphism; Hydration
Corresponding Author:	José S. Andrade Neto, M.Sc. Universidade Federal do Rio Grande do Sul BRAZIL
First Author:	José S. Andrade Neto, M.Sc.
Order of Authors:	José S. Andrade Neto, M.Sc.
	Paulo R. de Matos
	Angeles G. De la Torre
	Carlos E. M. Campos
	Sandro M. Torres
	Paulo J. M. Monteiro
	Ana Paula Kirchheim
Abstract:	This research studied the hydration of C3S-C3A-calcium sulfate systems made of combinations of two C3S (pure triclinic and Al-doped monoclinic), two C3A (pure cubic C3A and Na-doped orthorhombic), and two calcium sulfates (gypsum and hemihydrate). For each system, the hydration of four different SO3 contents (0.25-2.0 wt%) was assessed by calorimetry. The optimum SO3 content was fixed from calorimetry results, and the mixtures were evaluated by in-situ XRD and TGA. The type of C3S was the factor that most affected the sulfate balance of the systems. The mixes with Al-C3S produced a higher amount of ettringite in the first hours, resulting in much earlier sulfate depletions when compared to the mixes with pure C3S. The mixes with ort-C3A also showed faster sulfate depletion due to its higher reactivity compared with cb-C3A. Finally, the replacement of gypsum by hemihydrate resulted in faster sulfate depletion caused by the faster hemihydrate dissolution.
Suggested Reviewers:	Daniel Jansen Friedrich Alexander University Erlangen Nuremberg: Friedrich-Alexander-Universitat Erlangen-Nurnberg daniel.jansen@fau.de Dr. Jansen has several important publications regarding cement hydration, especially using in-situ XRD, one of the most important techniques of the present study. Furthermore, in his recent studies, Dr. Jansen has addressed the topic of sulfate demand on Portland cements, which is one of the present study topics.
	Luca Valentini Padua University: Universita degli Studi di Padova luca.valentini@unipd.it Dr. Valentini has several publications on cement chemistry and hydration, including some of them using in-situ XRD.
	Maria Juenger, PhD The University of Texas at Austin mjuenger@mail.utexas.edu Professor Juenger has several important publications on cement hydration.
	Daniel Wagner Friedrich Alexander University Erlangen Nuremberg: Friedrich-Alexander-Universitat Erlangen-Nurnberg daniel.w.wagner@fau.de Dr. Wagner has some interesting publications on the impact of aluminum on C3S

	hydration. Therefore his expertise might be helpful here as one of our major findings is that aluminum doping impacts the sulfate demand of C3S_C3A_Calcium sulfate systems. Dr. Wagner's publications: Influence of aluminium on the hydration of triclinic C3S with addition of KOH solution - 10.1016/j.cemconres.2020.106198 Impact of KOH on the interfacial precipitation rates of C-S-H during the early hydration of C3S - 10.1016/j.cemconres.2021.106488
Opposed Reviewers:	
Response to Reviewers:	

Hydration and interactions between pure and doped C_3S and C_3A in the presence of different calcium sulfates

José S. Andrade Neto[1,a*], Paulo R. de Matos[2,b], Angeles G. De la Torre[3,c], Carlos E. M. Campos[4,d], Sandro M. Torres[5,e], Paulo J. M. Monteiro[6,f], Ana Paula Kirchheim[1,g]

[1] Programa de Pós-Graduação em Engenharia Civil: Construção e Infraestrutura / Universidade Federal do Rio Grande do Sul (UFRGS) – Av. Osvaldo Aranha 99, Centro Histórico, 90035-190, Porto Alegre/RS, Brazil

[2] Universidade Federal de Santa Maria (UFSM).

[3] Departamento de Química Inorgánica, Cristalografía y Mineralogía, Universidad de Malaga, Campus Teatinos s/n., 29071 Málaga, Spain

[4] Laboratório de Difração de raios-X, Departamento de Física, Universidade Federal de Santa Catarina (UFSC)

[5] Departamento de Engenharia Mecânica, Universidade Federal da Paraíba (UFRB)

[6] Department of Civil and Environmental Engineering, University of California, Berkeley, CA 94720, USA

[a]jose.andrade@ufrgs.br, [b]paulo.matos@ufsm.br, [c]mgd@uma.es, [d]carlos.campos@ufsc.br, [e]sandromardentorres@yahoo.co.uk, [f]monteiro@ce.berkeley.edu, [g]anapaula.k@ufrgs.br

*Corresponding author.

ABSTRACT

This research studied the hydration of C_3S-C_3A-calcium sulfate systems made of combinations of two C_3S (pure triclinic and Al-doped monoclinic), two C_3A (pure cubic C_3A and Na-doped orthorhombic), and two calcium sulfates (gypsum and hemihydrate). For each system, the hydration of four different SO_3 contents (0.25-2.0 wt%) was assessed by calorimetry. The optimum SO_3 content was fixed from calorimetry results, and the mixtures were evaluated by *in-situ* XRD and TGA. The type of C_3S was the factor that most affected the sulfate balance of the systems. The mixes with Al-C_3S produced a higher amount of ettringite in the first hours, resulting in much earlier sulfate depletions when compared to the mixes with pure C_3S. The mixes with ort-C_3A also showed faster sulfate depletion due to its higher reactivity compared with cb-C_3A. Finally, the replacement of gypsum by hemihydrate resulted in faster sulfate depletion caused by the faster hemihydrate dissolution.

Keywords: C_3S; C_3A; Calcium sulfate; Polymorphism; Hydration.

1 INTRODUCTION

Calcium sulfate, such as gypsum and/or anhydrite, is added to the Portland clinker to control the C_3A[§] hydration and prevent flash set [1]. In addition, the amount of calcium sulfate added needs to be enough to delay the renewed hydration of C_3A until after the main C_3S hydration peak. Otherwise, the C_3S hydration is hindered, negatively affecting the early strength of Portland cement (PC) concrete [1]. However, if an excess of sulfate is used, the mechanical strength decreases [1–4], and durability problems with delayed ettringite formation (DEF) in pastes cured at high temperatures may occur [5,6]. Thus, there is an optimum sulfate content in which the mixture presents the lowest shrinkage and highest compressive strength without causing quick setting and DEF problems. In a properly sulfated cement, the calcium sulfate depletion and the renewed hydration of C_3A occur after the main C_3S hydration. Therefore, factors interfering in sulfate's supply or consumption will affect the optimum sulfate content [1,7]. Sulfate ions are mainly supplied by calcium and alkaline sulfates dissolution and consumed by the ettringite formation and C-S-H adsorption [1].

Zunino and Scrivener [7] showed that increasing C_3S and C_3A fineness – and consequently their reactivities – increases the C-S-H and ettringite formation and increases the optimum amount of calcium sulfate. In addition to their fineness, the polymorphism and ion doping of C_3S and C_3A also change their reactivities [1,8–14]. However, to the best of the authors' knowledge, no systematic study regarding the aluminum doping of C_3S and C_3A polymorphism on the optimum sulfate content was reported. The correct understanding of the influence of polymorphism or ion doping on the optimization of sulfates is essential to ensure that the cements meet performance requirements.

The incorporation of aluminum in C_3S decreases its reactivity [8–11]. With aluminum-doped C_3S (Al-C_3S) dissolution, the aluminum ions are released in the solution, which is known to retard C_3S hydration [10,15–17]. The reason for that is not clear, but it may be related to the formation of C-A-S-H, which according to some authors [10,16] is not a good substrate for the C-S-H growth as the C-S-H nuclei itself, or it may be related to the condensation of aluminum-silicate species at C_3S surface [15,17]. Either way, the delay in the C_3S hydration decreases the amount of C-S-H formed in the first days and tends to

[§] C = CaO; S = SiO_2; A = Al_2O_3; H = H_2O.

reduce the amount of sulfate consumption due to adsorption by C-S-H. However, the aluminum coming from Al-C_3S dissolution may contribute to ettringite formation. Although, as pointed out by Jansen et al. [18], it is not yet clear if the aluminum coming from the alite/Al-C_3S plays a role in the sulfate demand or not. Therefore, the incorporation of aluminum in C_3S may change the optimum sulfate content of cement, but which phenomenon is predominant (i.e., lower sulfate adsorption by C-S-H or higher sulfate consumption by ettringite formation) is still not known.

Regarding the aluminates, the polymorphism of C_3A depends on the sulfate/alkali balance during clinker production and therefore the alkali content incorporated in the C_3A structure. In industrial Portland clinkers, the C_3A may be present as cubic (cb-C_3A) and/or orthorhombic (ort-C_3A) polymorphs [19,20], depending on the raw materials and fuel used. Despite forming the same hydration products (ettringite and AFm phases), ort-C_3A reacts much faster than cb-C_3A in the presence of calcium sulfate [12–14]. This will probably influence the sulfate balance in the PC hydration, but no study regarding this has been published to date, and there is a gap on this topic.

Finally, during cement milling, gypsum ($CaSO_4 \cdot 2H_2O$) may dehydrate into hemihydrate ($CaSO_4 \cdot 1/2H_2O$) and/or soluble anhydrite ($CaSO_4$), which dissolves faster than gypsum or natural anhydrite [21,22]. As shown by previous studies, gypsum delays the initial hydration of C_3S, prolonging the induction period, but enhances afterward, resulting in higher main heat flow peaks. However, no studies regarding the effect of hemihydrate on C_3S have been conducted yet. In relation to C_3A, as showed by Andrade Neto et al. [14], gypsum replacement with hemihydrate did not significantly influence cb-C_3A but accelerated ort-C_3A reaction. The authors used only one sulfate/C_3A ratio, and the effect of different gypsum/hemihydrate content on the cb- and ort-C_3A hydration needs further studies to understand better its impact on the sulfate balance of Portland cements.

Zunino and Scrivener [7] studied the T1-C_3S/cb-C_3A systems and reported that the use of hemihydrate instead of gypsum resulted in higher ettringite precipitation until the renewed hydration of C_3A. This occurs due to the faster dissolution rate of hemihydrate than gypsum, resulting in more sulfate ions in the pore solutions [7]. The higher ettringite precipitation leads to an earlier sulfate depletion, increasing the sulfate demand of the mixtures. However, how this change in sulfate source will influence the sulfate balance

of systems with Al-C_3S or with ort-C_3A, which have quite different reactivities than C_3S and cb-C_3A, is an important question to answer.

This study aims to evaluate the influence of the aluminum doping C_3S, the C_3A polymorph, and the calcium sulfate type on the hydration and sulfate demand of the system and their interactions. Additionally, the effect of calcium sulfate composition (gypsum/hemihydrate) on the C_3S and Al-C_3S hydration and the effect of different gypsum/hemihydrate contents on the cb-C_3A and ort-C_3A hydrations were studied. First, the hydration of the C_3S and C_3A polymorphs (alone and in the presence of gypsum or hemihydrate) was evaluated separately through isothermal calorimetry. Then, ternary mixes of both types of C_3S and C_3A in a constant C_3S/C_3A ratio of 92/8 were produced with four different contents of gypsum or hemihydrate and were evaluated by calorimetry. Finally, an optimum SO_3 content was fixed from these results, and the hydration of the ternary mixes was evaluated by *in-situ* XRD and TGA.

2 MATERIALS AND METHODS

2.1 Materials

Powder samples of C_3S, aluminum-doped C_3S (Al-C_3S), cubic C_3A (cb-C_3A), and orthorhombic C_3A (ort-C_3A) were acquired from Mineral Research Processing Cie (MRPC, France). The C_3S and Al-C_3S were synthesized at MRPC by heating a stoichiometric mixture of reagent grade $CaCO_3$ and SiO_2 at around 1450°C. Cb-C_3A and ort-C_3A were synthesized by heating twice at 1350°C, a stoichiometric mixture of calcium carbonate ($CaCO_3$) and alumina (Al_2O_3). For the ort-C_3A, sodium carbonate ($NaCO_3$) was also used. High purity (>96 wt%) natural gypsum ($CaSO_4{\cdot}2H_2O$) and hemihydrate ($CaSO_4{\cdot}1/2H_2O$) were used as calcium sulfate sources. Hemihydrate was prepared by heating the gypsum at 100 °C for 48 hours. Details about elemental composition and mineralogy have been reported elsewhere [11,14] and are presented in the Supplementary Materials (Tables S1 and S2). The C_3S mainly consists of triclinic (T_1) C_3S (95.7 wt%), while the Al-C_3S has 98.7 wt% of monoclinic (M_1) C_3S. The C_3S does not have aluminum in its composition, while Al-C_3S has 0.8 wt%. Cub-C_3A has 96.9 wt% of cubic C_3A, while ort-C_3A has 94.4 wt% of orthorhombic C_3A and 5.6 wt% of cubic C_3A. Finally, the gypsum contains 96.1 wt% of $CaSO_4{\cdot}(H_2O)_2$, and the hemihydrate contains 97.2 wt% of bassanite (crystalline $CaSO_4{\cdot}(H_2O)_{0.5}$).

The particle size distribution was determined by laser diffraction, using a PSA 1090 equipment from Anton Paar (Graz, Austria), using isopropanol as the dispersant, and considering Mie theory [23]. The BET surface area was determined using an ASAP 2420 equipment from Micromeritics (Georgia, USA). The physical characterization results of the raw materials are presented in Table 1.

Table 1 – Physical characterization of the raw materials.

Property	**C_3S**	**Al-C_3S**	**cub-C_3A**	**orth-C_3A**	**Gypsum**	**Hemihydrate**
BET surface area (m^2/g)	1.14	1.08	1.42	1.13	1.33	1.38
D_v 90 (μm)	16.9	32.4	30.8	28.7	51.8	40.8
D_v 50 (μm)	6.7	11.6	7.5	7.6	16.9	14.8
D_v 10 (μm)	1.5	1.7	1.6	1.8	3.6	3.5

2.2 Methods

2.2.1 *Mixture proportions and sample preparation*

Firstly, the hydration of C_3S and Al-C_3S alone and in the presence of gypsum or hemihydrate were evaluated by isothermal calorimetry (IC) (see Section 2.2.2). Table 2 presents the mix proportions of the C_3S pastes evaluated. For this purpose, a water-to-solid ratio of 0.50 by mass was used. In the mixes with gypsum or hemihydrate, the C_3S was replaced with the amount of calcium sulfate to result in an SO_3 content of 1.5 wt% (≈ 3.22-3.26 wt% of gypsum or ≈ 2.81-2.85 wt% of hemihydrate). This SO_3 content was chosen because it resulted in properly sulfated C_3S/C_3A mixes (see Section 3.1.2) and was used to analyze the ternary systems. For this purpose, the SO_3 present in C_3S and Al-C_3S were also considered, so the amounts weighed were slightly different.

Table 2 – Mix proportions of the C_3S pastes.

Id	C_3S type	Calcium sulfate type	C_3S (wt%)	Calcium sulfate (wt%)	SO_3 (wt%)	w/s ratio	Tests performed
C_3S_wo/C$	C_3S	-	100	0	0	0.5	IC
C_3S_3.22% GYP	C_3S	Gypsum	96.78	3.22	1.5		
C_3S_2.81% HEM	C_3S	Hemihydrate	97.19	2.81	1.5		
Al-C_3S_wo/C$	Al-C_3S	-	100	0	0		
Al-C_3S_3.26% GYP	Al-C_3S	Gypsum	96.74	3.26	1.5		
Al-C_3S_2.85% HEM	Al-C_3S	Hemihydrate	97.15	2.85	1.5		

The hydration of cb-C_3A and ort-C_3A, alone and in the presence of gypsum or hemihydrate, were also assessed by calorimetry. Table 3 presents the mix design of the C_3A pastes evaluated. A water-to-solid ratio of 1.0 by mass was used for these mixes because it is enough to hydrate the C_3A fully and provide good workability. Different amounts of calcium sulfate were used, resulting in mixtures with SO_3-to-C_3A ratios of 0, 0.03, 0.06 and 0.12 by weight (≈ 0, 5.9, 11.6, and 21.4 wt% of gypsum or ≈ 0, 5.2, 10.3, 19.2 wt% of hemihydrate). These values were chosen as it corresponds to the SO_3-to-C_3A ratios of the ternary mixes (see Table 4) with 0.25, 0.50 and 1.00 wt% of SO_3, respectively.

Table 3 – Mix proportions of the C_3A pastes.

Id	C_3A type	Calcium sulfate type	C_3A (wt%)	Calcium sulfate (wt%)	SO_3/ C_3A	w/s ratio	Tests performed
cb-C_3A_wo/C$	cb-C_3A	-	100	0	0	1.0	IC
cb-C_3A_5.9% GYP	cb-C_3A	Gypsum	94.1	5.9	0.03		
cb-C_3A_11.6% GYP	cb-C_3A	Gypsum	88.4	11.6	0.06		
cb-C_3A_21.4% GYP	cb-C_3A	Gypsum	78.6	21.4	0.12		
cb-C_3A_5.2% HEM	cb-C_3A	Hemihydrate	94.8	5.2	0.03		
cb-C_3A_10.3% HEM	cb-C_3A	Hemihydrate	89.7	10.3	0.06		
cb-C_3A_19.2% HEM	cb-C_3A	Hemihydrate	80.8	19.2	0.12		
ort-C_3A_wo/C$	ort-C_3A	-	100	0	0		
ort-C_3A_5.9% GYP	ort-C_3A	Gypsum	94.1	5.9	0.03		
ort-C_3A_11.6% GYP	ort-C_3A	Gypsum	88.4	11.6	0.06		
ort-C_3A_21.4% GYP	ort-C_3A	Gypsum	78.6	21.4	0.12		
ort-C_3A_5.2% HEM	ort-C_3A	Hemihydrate	94.8	5.2	0.03		
ort-C_3A_10.3% HEM	ort-C_3A	Hemihydrate	89.7	10.3	0.06		
ort-C_3A_19.2% HEM	ort-C_3A	Hemihydrate	80.8	19.2	0.12		

Mixtures of C_3S (pure C_3S or Al-C_3S) with C_3A (cb-C_3A or ort-C_3A) and different amounts of gypsum or hemihydrate were evaluated, as presented in Table 4. The C_3S/C_3A ratio was fixed at 92/8 by weight, which is the same ratio used by Zunino and Scrivener [7] and Quennoz and Scrivener [24] and is similar to the ratio usually found in Portland cement clinkers. The water/solid ratio of all mixtures was kept at 0.50 by weight. Firstly, the hydration of C_3S/C_3A pastes was evaluated by isothermal calorimetry in systems with four different contents of calcium sulfate (gypsum or hemihydrate): 0.25, 0.50, 1.00 and 1.50 wt% for the systems with C_3S and 0.50, 1.00, 1.50 and 2.00 wt% of SO_3 for the systems with Al-C_3S. These SO_3 content considered the SO_3 from C_3S, C_3A and calcium sulfate. From these results, 1.5 wt% SO_3 content was fixed for all the mixtures for the other analysis, i.e., *in situ* XRD and TGA (see sections 2.2.3, 2.2.4, and 2.2.5, respectively). This content was chosen since none of the C_3S/C_3A systems was undersulfated on this level of sulfates (for more details, see section 3.1.3).

1 Table 4 – Mix proportions of the C_3S-C_3A pastes.

Id	C_3S type	C_3A type	Calcium sulfate type	C_3S (wt%)	C_3A (wt%)	Calcium sulfate (wt%)	SO_3 (wt%)	w/s ratio	Tests performed
C_3S_(cb, ort)-C_3A_0.50% GYP	C_3S	(cb, ort)-C_3A	Gypsum	91.54	7.96	0.50	**0.25**	0.50	IC
C_3S_(cb, ort)-C_3A_1.04% GYP	C_3S	(cb, ort)-C_3A	Gypsum	91.04	7.92	1.04	**0.50**	0.50	IC
C_3S_(cb, ort)-C_3A_2.13% GYP	C_3S	(cb, ort)-C_3A	Gypsum	90.04	7.83	2.13	**1.00**	0.50	IC
C_3S_(cb, ort)-C_3A_3.22% GYP	C_3S	(cb, ort)-C_3A	Gypsum	89.04	7.74	3.22	**1.50**	0.50	IC, *in-situ* XRD, TGA
C_3S_(cb, ort)-C_3A_0.44% HEM	C_3S	(cb, ort)-C_3A	Hemihydrate	91.60	7.97	0.44	**0.25**	0.50	IC
C_3S_(cb, ort)-C_3A_0.91% HEM	C_3S	(cb, ort)-C_3A	Hemihydrate	91.16	7.93	0.91	**0.50**	0.50	IC
C_3S_(cb, ort)-C_3A_1.86% HEM	C_3S	(cb, ort)-C_3A	Hemihydrate	90.29	7.85	1.86	**1.00**	0.50	IC
C_3S_(cb, ort)-C_3A_2.81% HEM	C_3S	(cb, ort)-C_3A	Hemihydrate	89.41	7.78	2.81	**1.50**	0.50	IC, *in-situ* XRD, TGA
Al-C_3S_(cb, ort)-C_3A_1.08% GYP	Al-C_3S	(cb, ort)-C_3A	Gypsum	91.01	7.91	1.08	**0.50**	0.50	IC
Al-C_3S_(cb, ort)-C_3A_2.17% GYP	Al-C_3S	(cb, ort)-C_3A	Gypsum	90.01	7.83	2.17	**1.00**	0.50	IC
Al-C_3S_(cb, ort)-C_3A_3.25% GYP	Al-C_3S	(cb, ort)-C_3A	Gypsum	89.01	7.74	3.25	**1.50**	0.50	IC, *in-situ* XRD, TGA
Al-C_3S_(cb, ort)-C_3A_4.34% GYP	Al-C_3S	(cb, ort)-C_3A	Gypsum	88.01	7.65	4.34	**2.00**	0.50	IC
Al-C_3S_(cb, ort)-C_3A_0.94% HEM	Al-C_3S	(cb, ort)-C_3A	Hemihydrate	91.13	7.92	0.94	**0.50**	0.50	IC
Al-C_3S_(cb, ort)-C_3A_1.89% HEM	Al-C_3S	(cb, ort)-C_3A	Hemihydrate	90.26	7.85	1.89	**1.00**	0.50	IC
Al-C_3S_(cb, ort)-C_3A_2.84% HEM	Al-C_3S	(cb, ort)-C_3A	Hemihydrate	89.38	7.77	2.84	**1.50**	0.50	IC, *in-situ* XRD, TGA
Al-C_3S_(cb, ort)-C_3A_3.79% HEM	Al-C_3S	(cb, ort)-C_3A	Hemihydrate	88.51	7.70	3.79	**2.00**	0.50	IC

2

For paste preparation, 2 g of anhydrous materials (C_3S, C_3A, and calcium sulfate) were previously manually mixed in an agate mortar for 10 minutes, subsequently mixed with distilled water at 350 rpm for 2 minutes using a rotational mixer. For the calorimetry analysis, the mixing procedure was conducted in the glass ampoule used in the test. The plastic rod was left inside the glass ampoule to minimize material loss during mixing. The mixing procedure and insertion of glass ampoule in the calorimetry took less than 3 minutes after the initial contact with the water. For the TGA and *in-situ* XRD tests, the mixes were prepared in plastic vessels. For the TGA analysis, the paste remained inside the hermetically closed vessels until the hydration stoppage.

The hydration of the pastes was stopped at 8 hours, 1, 3, and 7 days for the TGA. The pastes were first ground to a fine powder using an agate mortar. Then, ~0.5 g of each paste was mixed with 25 ml of isopropanol for 30 minutes while stirring. In the sequence, the sample was filtered at a low vacuum through a nylon filter with a 15 µm opening for 10 minutes and dried in an oven at 40°C for another 10 minutes.

2.2.2 *Isothermal calorimetry (IC)*

For the IC analyses, an eight-channel Thermal Activity Monitor of Tam Air, TA Instruments (New Castle, DE, USA) was used. The pastes were mixed *ex-situ* but inside the glass ampoule, as described in item 2.2.1. A glass ampoule with distilled water was used as the reference. The amount of distilled water was defined according to Wadsö [25] to obtain a similar heat capacity of C_3S/C_3A pastes. The heat flow and the cumulative heat were recorded for 48 hours at 22 °C for all the pastes.

2.2.3 *Thermogravimetry analysis (TGA)*

The TGA of the pastes at 8 hours, 1, 3, and 7 days were performed in a TGA 2 analyzer from Mettler Toledo (Columbus, Ohio, USA). The samples were placed in open alumina crucibles under airflow, and the temperature varied between room temperature (RT) and 1000°C with a heating rate of 20 °C/min.

From TGA results, the bound water and the portlandite contents were determined. After stopping the hydration, the bound water of the pastes after stopping hydration content was assigned to the weighed loss from RT to 550°C. Eq. 1 calculates the actual bounded water and Eq. 2 determines the amount of free water [26].

$$\mathrm{BW} = \frac{\mathrm{BW_{ATD}} \cdot \mathrm{CM}}{100 - \mathrm{BW_{ATD}}} \quad (1)$$

$$\mathrm{FW} = \mathrm{TW} - \mathrm{BW} \quad (2)$$

Where BW corresponds to actual chemically bound water content; BW_{ATD} is the mass loss measured between RT and 550ºC from TGA curves; CM is the cement (C_3S + C_3A + calcium sulfate) content; TW is the total water content added (all the numbers in weight percentages).

Also, the portlandite content was determined by Eq. 3 [27].

$$Ca(\mathrm{OH})_{2,\mathrm{measured}} = \mathrm{WL}_{\mathrm{Ca(OH)_2}} \cdot \frac{\mathrm{m}_{\mathrm{Ca(OH)_2}}}{\mathrm{m}_{\mathrm{H_2O}}} \quad (3)$$

Where $\mathrm{WL}_{\mathrm{Ca(OH)_2}}$ is the weight loss due to the evaporation of water, obtained by the integration of DTG peak located in the temperature range from ~400 to ~500 ºC using the tangential method [27]; $\mathrm{m}_{\mathrm{Ca(OH)_2}}$ is the molecular mass of portlandite (74 g/mol); and $\mathrm{m}_{\mathrm{H_2O}}$ is the molecular mass of water (18 g/mol).

The total mass of solids increases with C_3S/C_3A hydration progress, as free water is bound into hydration products. Therefore, the portlandite content obtained by TGA was normalized per 100 g of paste according to Eq. 4.

$$Ca(\mathrm{OH})_{2,\mathrm{rescaled}} = Ca(\mathrm{OH})_{2,\mathrm{measured}} \cdot \frac{(100 - \mathrm{FW})}{100} \quad (4)$$

Where $Ca(\mathrm{OH})_{2,\mathrm{rescaled}}$ is the portlandite content in g/100 g of paste; $Ca(\mathrm{OH})_{2,\mathrm{measured}}$ is the portlandite content obtained by TGA; and FW is the free water content determined by TGA according to Eq. 2.

2.2.4 *In-situ X-ray diffraction (In-situ XRD)*

In-situ XRD was conducted using an X'Pert Pro (PANalytical) diffractometer operating at 45 kV and 40 mA, equipped with an X'Celerator detector with an active length of 2.122°. The following experimental setup was used: Bragg–Brentano θ-2θ geometry with a 240 mm radius goniometer; CuKα radiation with a wavelength of 1.5418 Å; a 0.04 rad Soller slit, a 10 mm beam mask, a 1° fixed anti-scatter slit, and a 1/2° fixed divergence

slit on the incident beam; a 5.0 mm fixed anti-scatter slit, a 0.04 rad Soller slit, and a 0.020 mm Ni filter on the diffracted beam; and knife-edge at the first division.

For this analysis, scans were recorded at the range from 7 to 55° 2θ with a counting time of 24.76 seconds per step, totaling about 10 minutes per scan. The fresh sample was placed on the sample holder and immediately covered with a Kapton film to prevent water loss and carbonation. The measurements started 30 minutes after the first contact between the water and the dry materials and were recorded for 48 hours. Three samples were tested alternatively, placed at an X-ray beam automatically by a robotic arm, providing an XRD pattern for each sample every 30 minutes. Immediately before each 48-hour measurement set, a corundum (α-Al_2O_3) sample covered with Kapton was measured in the same testing conditions to be used as an external standard.

Rietveld quantitative phase analysis (QPA) was conducted using TOPAS v.5 software [28], and the crystallographic information files used are detailed in Table 5. All the XRD patterns of each mix were refined together, and the same refinement steps were applied for each group of patterns (i.e., for each mix). The refinement of *in-situ* XRD data is somehow delicate since it deals with simultaneous amorphous contributions (e.g., C-S-H, free water and Kapton film), besides analyzing several files and phases simultaneously [29]. Thus, using an adequate refinement strategy is essential due to two main reasons: (i) a good strategy improves the robustness of the analysis and reduces the chances of drifting; and (ii) a well-defined script improves the consistency of the analysis for different operators or for a sequence of patterns related to the same starting material (e.g., a time-dependent series) [30]. In this work, the contribution of C-S-H was considered by using the model proposed by Bergold et al. [31]; the diffuse contributions of the Kapton film and the free water were modeled using *hkl* phases with the space groups *P4/mmm* (n° 123) and $Fm\bar{3}$ (n° 202), respectively, as suggested by Scherb et al. [32]. The steps used for the free water and the Kapton film phase models creation and the refinement strategy conducted in this work are detailed in Ref. [14], while Figure 1 and Figure S1 illustrate fitted *in-situ* XRD patterns.

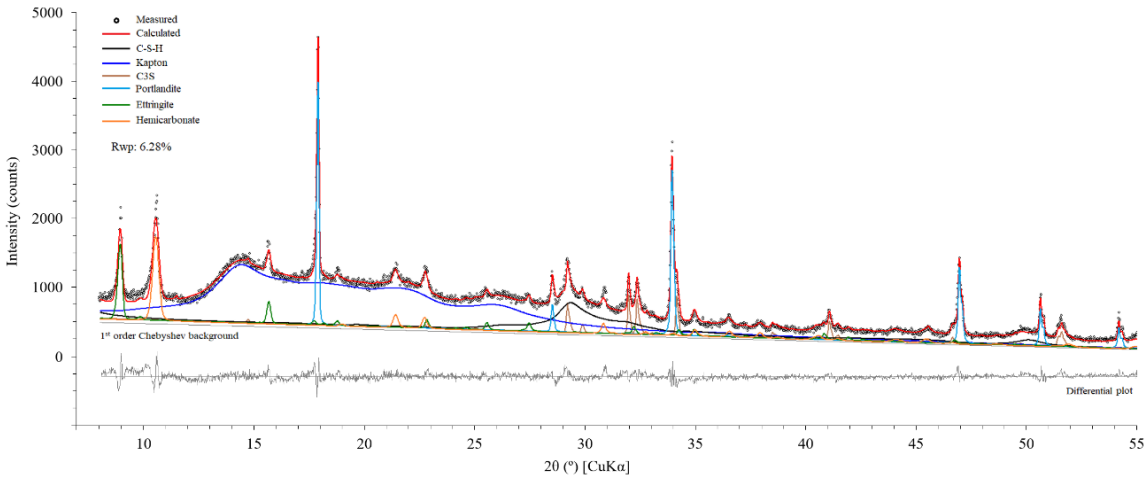

Figure 1 – Example of fitted *in-situ* XRD pattern (for Al-C_3S_cb-C_3A_GYP at 48 hours of hydration).

The absolute weight fraction of each crystalline phase was determined by the external standard method [33] using the G-factor approach (Eqs. 5-6) [34]. The corundum sample covered with Kapton was used as an external standard for this purpose. The mass absorption coefficient (MAC) of the paste was calculated from the chemical composition of the powder fraction and the water MAC.

$$W_i = S_i \frac{\rho_i V_i^2}{G} \mu^* \quad (5)$$

$$G = S_s \frac{\rho_s V_s^2 \mu_s}{W_s} \quad (6)$$

where W is the weight fraction of the phase (i) or the standard (s), in wt%; S is the refined scale factor of the phase (i) or the standard (s); ρ is the density of the phase (i) or the standard (s), V is the unit cell volume of the phase (i) or the standard (s) in Å³; and μ is the MAC of the sample (*) or the standard (s), in cm²/g. The density and unit cell volume of each phase are presented in Table 5, and the MAC of the raw materials and pastes are presented in the Supplementary Materials (Tables S1 and S3).

The weight fraction of C-S-H was calculated using the mass balance given by Eq. (7) [35,36] together with the factor F given by Eq. (8) [31]. Firstly, the expected amount of C-S-H formed after 48 hours was calculated from the amount of alite consumed at this age (i.e., the difference between the initial amount added and that determined by XRD after 48 hours) using Eq. (7). Then, factor F was determined using Eq. (5); by setting *Wi* equal to the C-S-H content yielded by the stoichiometric calculation and knowing the G and μ* terms, the only unknown part of Eq. (5) is $\rho \cdot V^2$, i.e., the factor F. The calibration

of factor F with the last measurement of each *in-situ* sample resulted in an F = 1.11 ± 0.03×10^{-45} g·cm³ (average ± standard deviation). It is stressed that the stoichiometry of C-S-H is not well defined, but since alite is the only silicate in the system, it seems reasonable to assume the mass balance of Eq. (7). The stoichiometry of C-S-H was considered as $C_{1.8}SH_{4.0}$, which is the average composition of C-S-H formed by the C_3S hydration according to Cuesta et al. [35,36]. It is worth highlighting that recent studies suggested the incorporation of sulfate anions into C-S-H [37], changing its stoichiometry, and this actual stoichiometry would depend on the sulfate availability and incorporation level. Thus, the absence of a well-defined stoichiometry for this case prevents us from using a more accurate model.

$$C_3S + 5.2\ H \rightarrow C_{1.8}SH_{4.0} + 1.2\ CH \quad (7)$$

$$F = \rho . V^2 \quad (8)$$

Table 5 – Crystallographic information files (CIFs) used for Rietveld QPA.

Phase	ICSD code	Unit cell volume (Å³)	Density (g/cm³)	Reference
C_3S T1	4331	2167.64	3.148	Golovastikov et al. [38]
C_3S M1	---	2175.02	3.138	de Noirfontaine et al. [39]
C_3A cubic	1841	3557.89	3.027	Mondal and Jeffery [40]
C_3A orthorhombic	1880	1790.35	3.018	Nishi and Takeuchi [41]
Portlandite	15471	54.49	2.260	Petch [42]
Ettringite	155395	2345.34	1.780	Goetz-Neunhoeffer and Neubauer [43]
Gypsum	151692	496.25	2.304	De la Torre et al. [44]
Bassanite (Hemihydrate)	69060	1060.51	2.727	Bezou et al. [45]
Hemicarbonate	263124	1410.15	1.900	Runčevski et al. [46]

Note.: The unit cell volume and density values for both C_3S and C_3A polymorphs, gypsum and bassanite were refined in dry samples, while those for portlandite, ettringite and hemicarbonate correspond to the theoretical values from the CIF files.

3 RESULTS

3.1 Isothermal calorimetry

3.1.1 Effect of the calcium sulfate source on C_3S and Al-C_3S hydration

Figure 2a and b show the heat flow and cumulative heat curves of the C_3S and Al-C_3S pastes, respectively, without calcium sulfate and with gypsum and hemihydrate (1.5 wt% SO_3), within the first 48 hours of hydration. Comparing the mixtures without calcium sulfate, C_3S hydrated much faster than the Al-C_3S, generating a higher heat flow peak and higher cumulative heat at 48 hours. These results agree well with previous studies [8–10] and are probably due to the effect of aluminum ions in solution leading to a delay and suppression of C_3S hydration. In addition, the larger particle size of Al-C_3S (see Table 1) probably contributed to the lower reactivity of this phase.

The addition of gypsum had similar effects in both C_3S and Al-C_3S hydration: a slight extension in the induction period but an enhancement in the hydration kinetics after its end, increasing the main heat flow peak. This agrees with previous studies which evaluated the hydration of C_3S in the presence of gypsum. The initial delay is probably related to the adsorption of sulfate ions in the C_3S surface, delaying its dissolution [17,47]. In turn, the enhancement in the main hydration peak may result from a change in the C-S-H morphology and the increase in the ionic strength of the pore solution [11].

The hemihydrate had a very similar effect than gypsum on both C_3S and Al-C_3S. Therefore, for the first time, it is observed that the faster dissolution of hemihydrate does not seem to impact differently than gypsum the C_3S hydration.

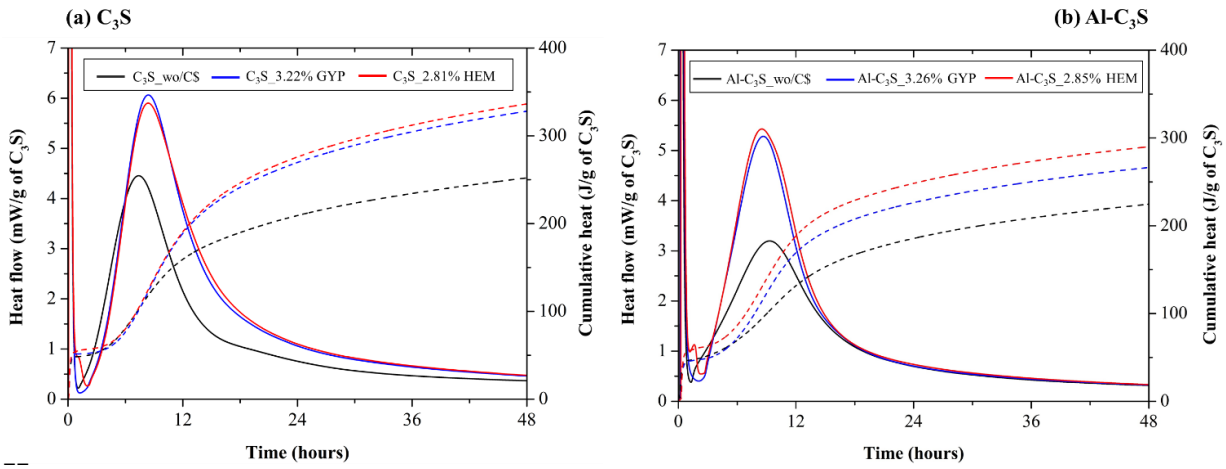

Figure 2 – Heat flow curves (solid lines) and cumulative heat curves (dashed lines) of the (A) C_3S and (B) Al-C_3S pastes during the first 48 hours of hydration.

3.1.2 Effect of the calcium sulfate source on cb-C_3A and ort-C_3A hydration

Figure 3a and b show the heat flow and cumulative heat curves of cub-C_3A and ort-C_3A, respectively, without calcium sulfate and with different levels of gypsum and hemihydrate (0.25, 0.50 and 1.00 wt% of SO_3) during the first 90 hours of hydration. For better visualization, Figure S2 presents the comparison of cb and ort-C_3A without and with 1.00 wt% of SO_3. Without calcium sulfate, cb-C_3A hydration results in a higher heat released in the first 48 hours than ort-C_3A. This behavior was also observed in previous studies [12,13,48].

The addition of calcium sulfate (gypsum or hemihydrate) delayed both cb- and ort-C_3A initial hydration, and this retarding effect was much stronger on the former. As for the cb-C_3A mixes, those with 5.9%, 11.6% and 21.4% of gypsum presented induction periods of 2.5, 3.2, and 9.6 h, respectively, while those with 5.2%, 10.3% and 19.2% of hemihydrate presented induction periods of 4.7, 5.4, and 12.9 h, respectively. In turn, the ort-C_3A mix with 21.4% of gypsum presented an induction period of 0.8 h (8.8 h less than the cb-C_3A mix with the corresponding amount of gypsum) and the ort-C_3A mix with 19.2% of hemihydrate presented an induction period of 2.7 h (10.2 h less than cb-C_3A mix with the corresponding amount of hemihydrate). Similar behaviors were observed by several authors [12–14,49]. The lower retarding effect of calcium sulfate in ort-C_3A hydration compared with the cb-C_3A hydration happens because the sodium-doping of ort-C_3A increases the solubility of $Al_6O_{18}^{18-}$, preventing the formation of the Al-rich leached layer on the C_3A particles, inhibiting the adsorption of SO_4^{2-} and/or Ca–SO_4 ion-pair that are responsible for the delay in cb-C_3A hydration [13,14].

Interestingly, the hemihydrate seems to be more effective in retarding the ort-C_3A hydration in the SO_3/C_3A ratios tested (while 21.4% of gypsum resulted in an induction period of 0.8 h, 19.2% of hemihydrate resulted in an induction period of 2.7 h). This is in contrary to what was observed by Andrade Neto et al. [14], in which the replacement of gypsum by hemihydrate led to an acceleration in the ort-C_3A hydration when using a much higher SO_3/C_3A ratio (0.29, i.e., gypsum content of 38.92% and hemihydrate content of 35.78%). The reasons for that are not clear yet and further studies are necessary.

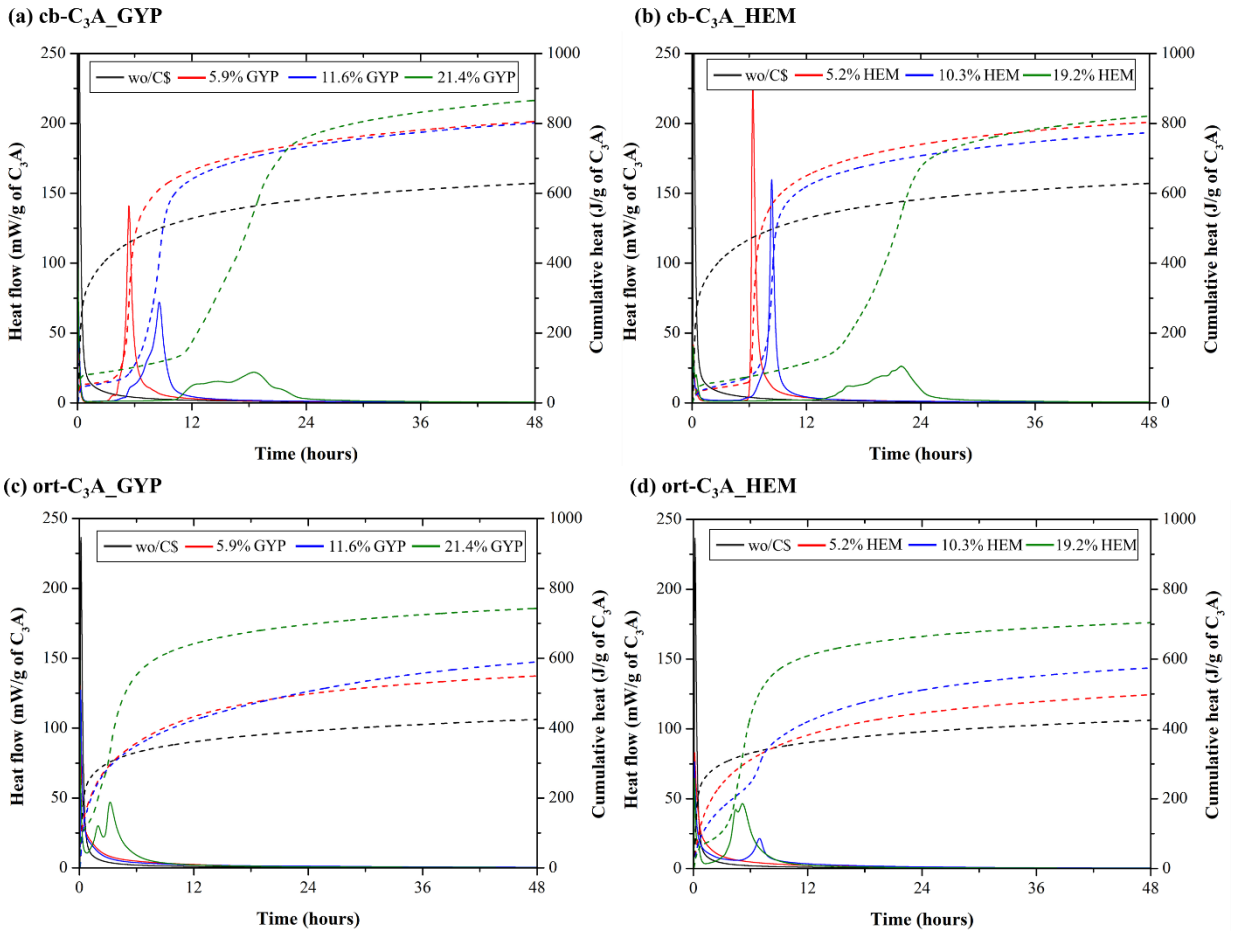

Figure 3 – Heat flow curves (solid lines) and cumulative heat curves (dashed lines) of the (a) cb-C_3A_GYP, (b) cb_C_3A-HEM, (c) ort-C_3A_GYP and (D) ort-C_3A_HEM pastes during the first 48 hours of hydration, the legend indicates the amount of gypsum or hemihydrate, which correspond to 0.25, 0.50 and 1.00 wt% of SO_3.

3.1.3 Effect of the SO_3 content on C_3S/C_3A systems

The heat flow curves of the C_3S/C_3A pastes with different contents of gypsum or hemihydrate are presented in Figure 4. The silicate and aluminate hydration heat flow peaks are indicated.

By comparing the hydration of the C_3S/C_3A/calcium sulfate systems (Figure 4) with the C_3S/calcium sulfate systems (Figure 2), it is possible to see that in undersulfated mixes (i.e., when the sulfate depletion and the renewed hydration of C_3A occur earlier than the main C_3S hydration peak), the hydration of both C_3S and Al-C_3S was retarded and suppressed. This agrees with previous results [7,24,50], and probably occurs due to the earlier C_3A dissolution, releasing a significant amount of aluminum into the solution. As discussed in Section 3.1.1, aluminum retards and suppresses the C_3S hydration – whether

due to the formation of alumino-silicate species on the C_3S surface, hindering its dissolution, or due to the C-A-S-H formation. In turn, in the proper sulfated mixes (i.e., when the sulfate depletion and the renewed hydration of C_3A happens after the main C_3S hydration peak), the C_3S and Al-C_3S hydration occurred as in the C_3S/calcium sulfate mixtures, with the maximum heat flow peak happening around 8 hours. In the proper sulfated mixes (> 0.50 wt% SO_3 for the C_3S mixes and 2.0 wt% SO_3 for the Al-C_3S mixes), the C_3A polymorphism does not seem to significantly influence the C_3S or Al-C_3S hydration rate. For these mixtures, regardless of the C_3A type, the induction period length and the silicate peak are very similar, indicating very similar C_3S hydration rates.

As for C_3A, the time for the renewed hydration of cb-C_3A occurred much earlier in the three-phase systems with the Al-C_3S (Figure 4) than in the C_3A pastes (Figure 3) even for the same SO_3/C_3A ratios. One can note that the time of occurrence of the aluminate peak (indicated as Ap) in Figure 4(c,d) is around 4-5 hours for the ternary mixes with 0.5 wt% SO_3 and around 8-10 hours for the ternary mixes with 1.0 wt% SO_3. In turn, for the cb-C_3A_(GYP, HEM) pastes (see Figure 3), the time for the aluminate peak is around 7-8 hours for the mixes with 11.6% of gypsum and those with 10.3% of hemihydrate and around 12-14 hours for the mixes with 21.4% of gypsum and those with 19.2% of hemihydrate -these C_3A pastes have the same SO_3/C_3A ratios of the three-phase systems with 0.5 wt% and 1.0 wt% of SO_3. This happens in the ternary mixes with Al-C_3S as the higher aluminum content in the solution (released from Al-C_3S dissolution) increases ettringite formation and, consequently, accelerates the sulfate depletion (as confirmed by *in-situ* XRD, see Section 3.2). Interestingly, the ort-C_3A presented slower hydration rate in C_3S/C_3A/calcium sulfates when compared to the ort-C_3A/calcium sulfates pastes. The ort-C_3A hydration is significantly influenced by the bulk composition of the pore solution [13], and the presence of C_3S seems to retard its reaction. Further analyses on this topic are necessary.

The type of C_3S was the major factor influencing the system's sulfate balance. For the ternary mixes with C_3S (Figure 4a-b), 0.5 wt%SO_3 was already enough to result in properly sulfated mixtures, i.e., that the renewed C_3A hydration occurred after the main C_3S hydration peak. In turn, for the ternary mixes with Al-C_3S (Figure 4c-d), 1.5-2.0 wt% SO_3 was required to reach the proper sulfate content. This happens because a higher concentration of aluminum into the pore solution is expected in the ternary mixes with

Al-C_3S, resulting in higher ettringite formation and sulfate consumption (as confirmed by *in-situ* XRD, see Section 3.2).

The C_3A polymorphism also influenced the sulfate balance of the system but to a less extent. The effect of C_3A polymorph on sulfate balance also depends on the wt% SO_3 content. On the one hand, for the ternary mixes with 0.25 and 0.5 wt% SO_3, the ternary mixes with cub-C_3A presented sulfate depletion and renewed hydration of C_3A earlier than those with ort-C_3A, increasing the sulfate demand of the system. On the other hand, for the ternary mixes with 1.0 wt% SO_3 or more, the opposite behavior was observed, i.e., the ternary mixes with ort-C_3A present earlier sulfate depletion and renewed hydration of C_3A. This apparent discrepancy might be due to the differences in cb-C_3A and ort-C_3A hydration, which depends on the sulfate level, as observed and discussed in Section 3.1.2. For sulfate-free solutions, cb-C_3A hydrates faster than the ort-C_3A. However, the addition of calcium (gypsum or hemihydrate) retards the C_3A hydration much more efficiently than the ort-C_3A hydration (see Figure 3). Therefore, for the ternary mixes with 0.25 and 0.50 wt% SO_3 (SO_3/C_3A ratio of 0.03 and 0.06, respectively), the very low sulfate content was not enough to retard the cb-C_3A hydration and make it slower than the ort-C_3A hydration. Finally, 1.0 wt% SO_3 (SO_3/C_3A ratio of 0.13) seems to be enough to make the cb-C_3A reaction slower than the ort-C_3A reaction.

Regarding the calcium sulfate source, the ternary mixes with hemihydrate presented earlier sulfate depletion and renewed hydration of C_3A than the ternary mixes with gypsum, which agrees with previous results [7]. This was expected since hemihydrate dissolves faster than gypsum [21,22], resulting in higher sulfate concentrations in the pore solution, which lead to higher ettringite formation (as confirmed by *in-situ* XRD, see Section 3.2) and anticipating the sulfate depletion. The calcium sulfate composition did not influence the C_3S and Al-C_3S hydration in the proper sulfated mixes, which corroborates the C_3S pastes results (Section 3.1.1) that showed that gypsum and hemihydrate led to very similar effects on C_3S and Al-C_3S hydrations.

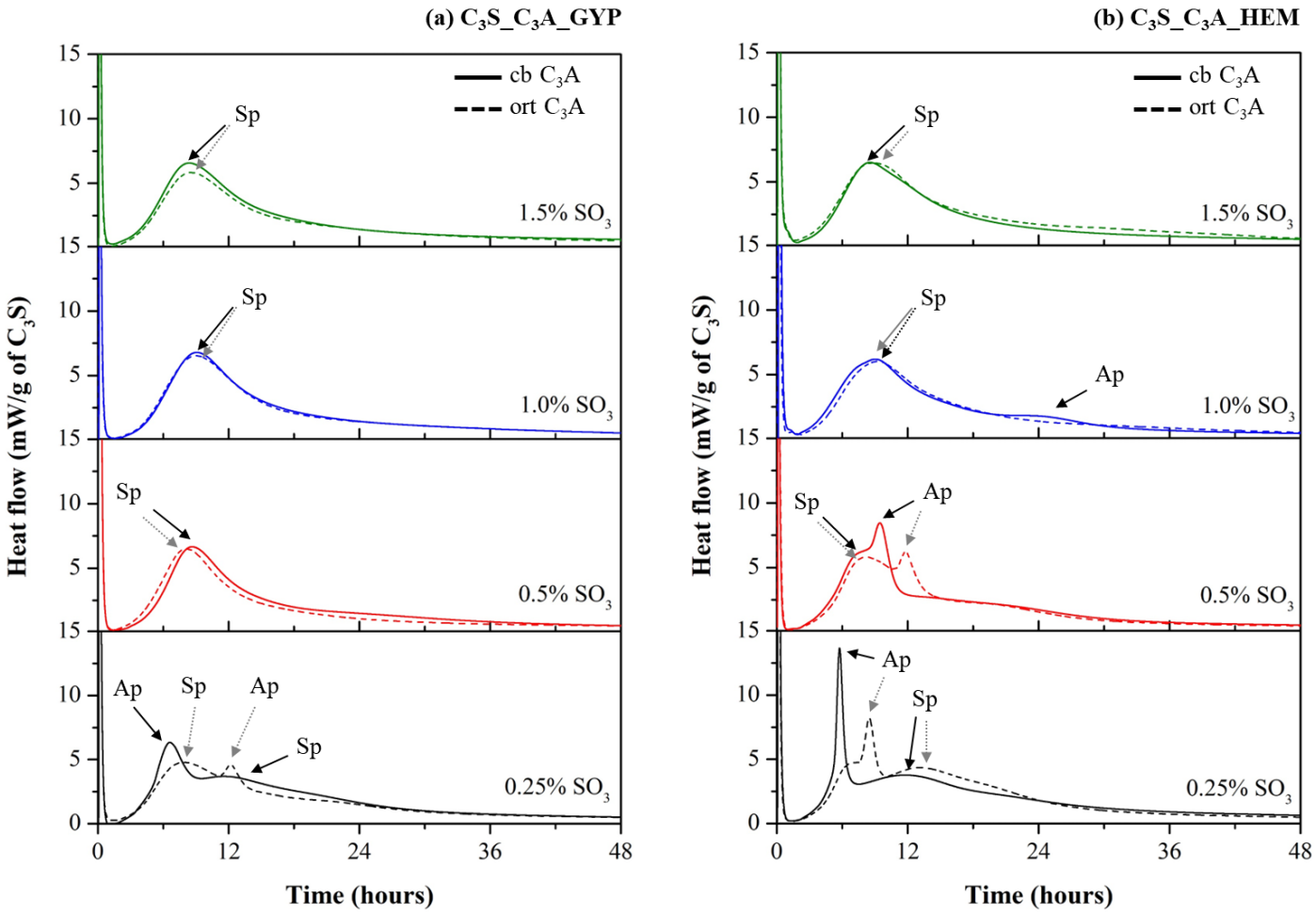
(a) C3S_C3A_GYP
(b) C3S_C3A_HEM
cb C3A
ort C3A
Sp
Ap
1.5% SO3
1.0% SO3
0.5% SO3
0.25% SO3
Heat flow (mW/g of C3S)
Time (hours)
0
12
24
36
48
0
5
10
15

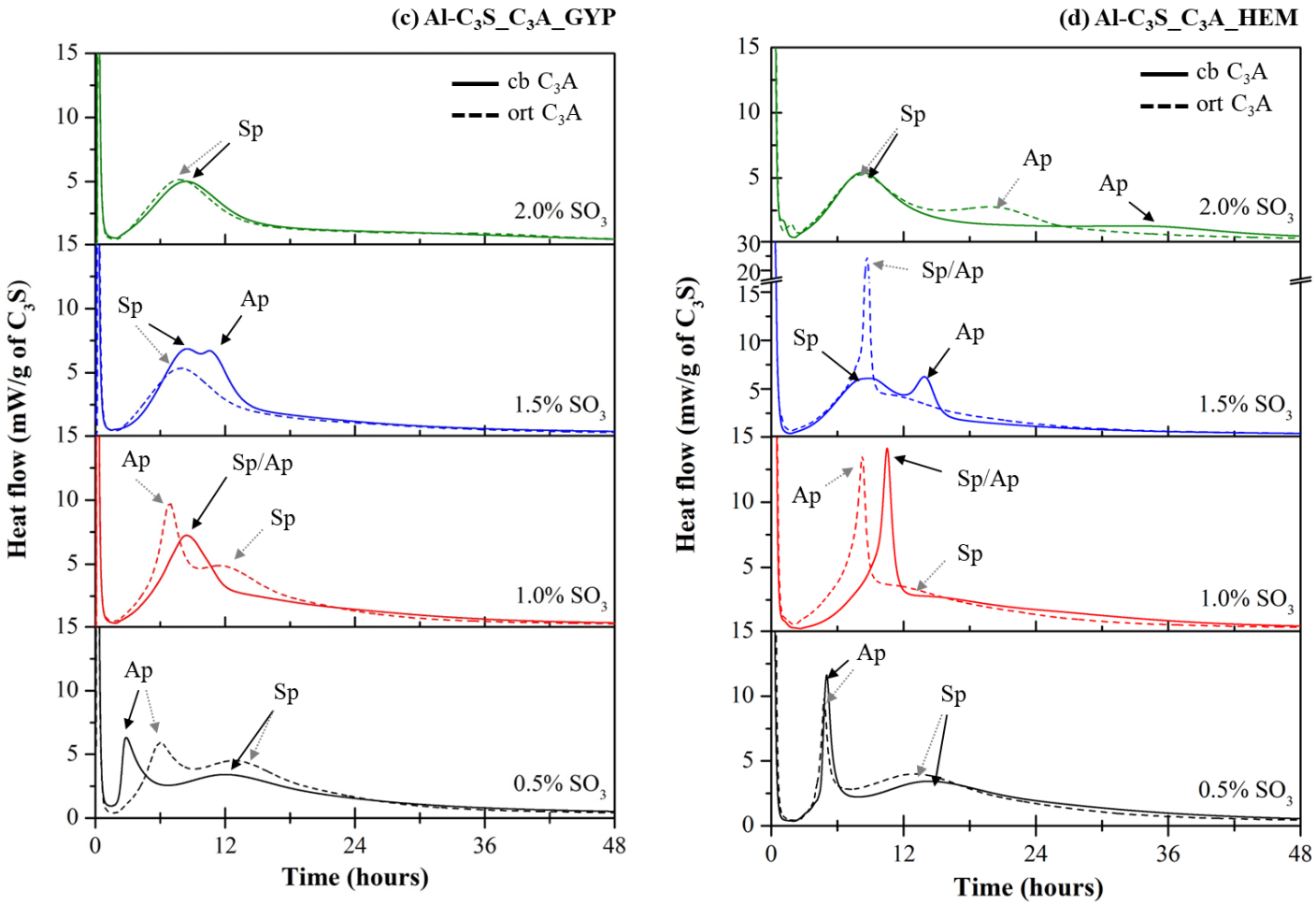

Figure 4 – Heat flow curves of the pastes with different gypsum and hemihydrate contents during the first 48 hours of hydration. The moment of the occurrence of the Aluminate peak (Ap) and Silicate peak (Sp) are indicated.

3.2 *In-situ* X-ray diffraction (XRD)

3.2.1 General trends

Figure 5 shows the XRD patterns of each mix at 0.5 and 48 hours of hydration. All the ternary mixes had 1.5 wt% SO_3 as according to the calorimetry results at this sulfate content, none of the ternary mixes was undersulfated (except for the Al-C_3S_ort-C_3A_HEM it was slightly undersulfated). No bassanite (i.e., crystalline hemihydrate) was found in hydrated pastes, indicating that it quickly converted into gypsum before the first XRD measurement, sooner than 30 minutes. This is in line with that reported by Jakob et al. [51], Jansen et al. [52], and García-Maté et al. [53], which observed this phenomenon before 10-20 minutes of hydration in Portland cement pastes and also supported by

Andrade Neto et al. [14] who observed the hydration of hemihydrate into gypsum in the first 30 minutes in C_3A pastes.

The ternary mixes with Al-C_3S (i.e., 3, 4, 7, and 8) showed ettringite peaks at 0.5 hours, especially at 9.1° 2θ. In addition, the Al-C_3S_(cb,ort)-C_3A_GYP mixes (i.e., 3 and 4) had virtually no gypsum traces at the first measurement, while the C_3S_(cb,ort)-C_3A_GYP mixes (i.e., 1 and 2) showed gypsum peak at 11.6° 2θ.

Regarding the hydration of the aluminates, the ternary mixes with C_3S (i.e., 1, 2, 5, and 6) showed evident C_3A peaks after 48 hours of hydration (at around 33° 2θ). The ternary mixes produced with cubic C_3A (i.e., 1 and 5) had practically no change on the relative intensity of such C_3A peak, indicating the low consumption of this phase along the first two days of hydration.

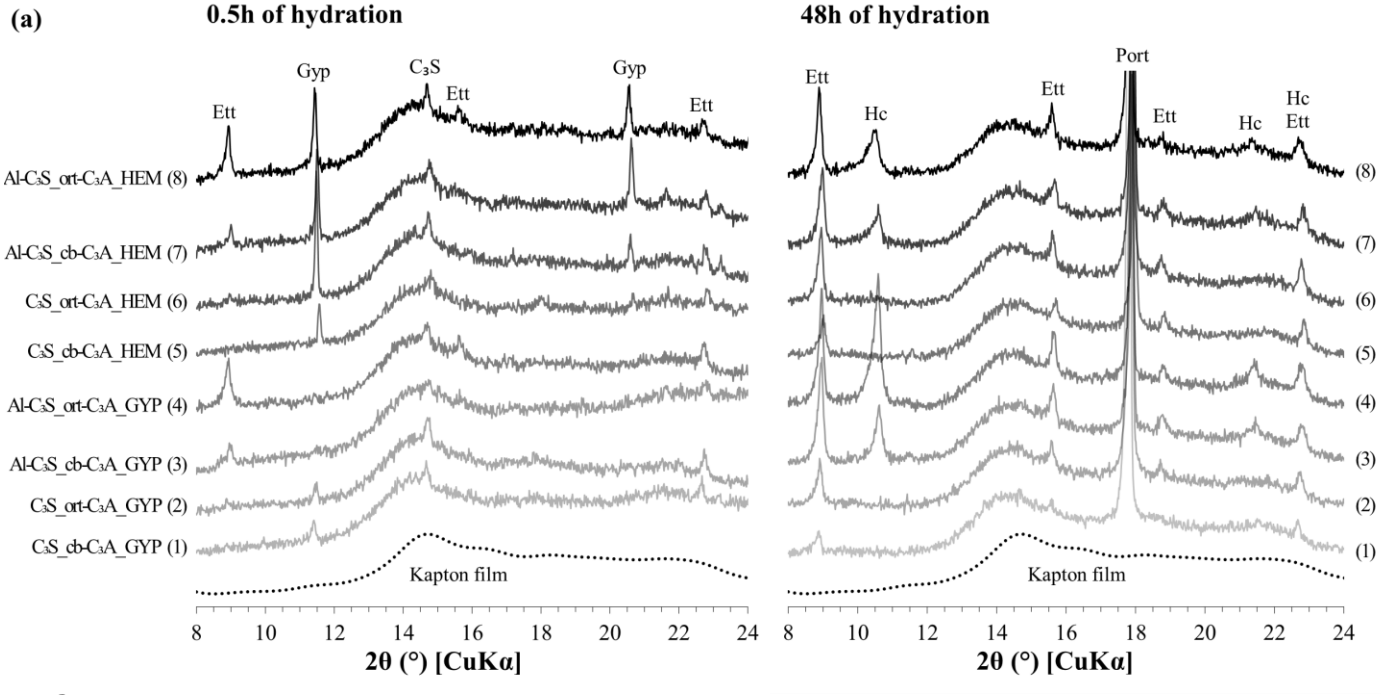

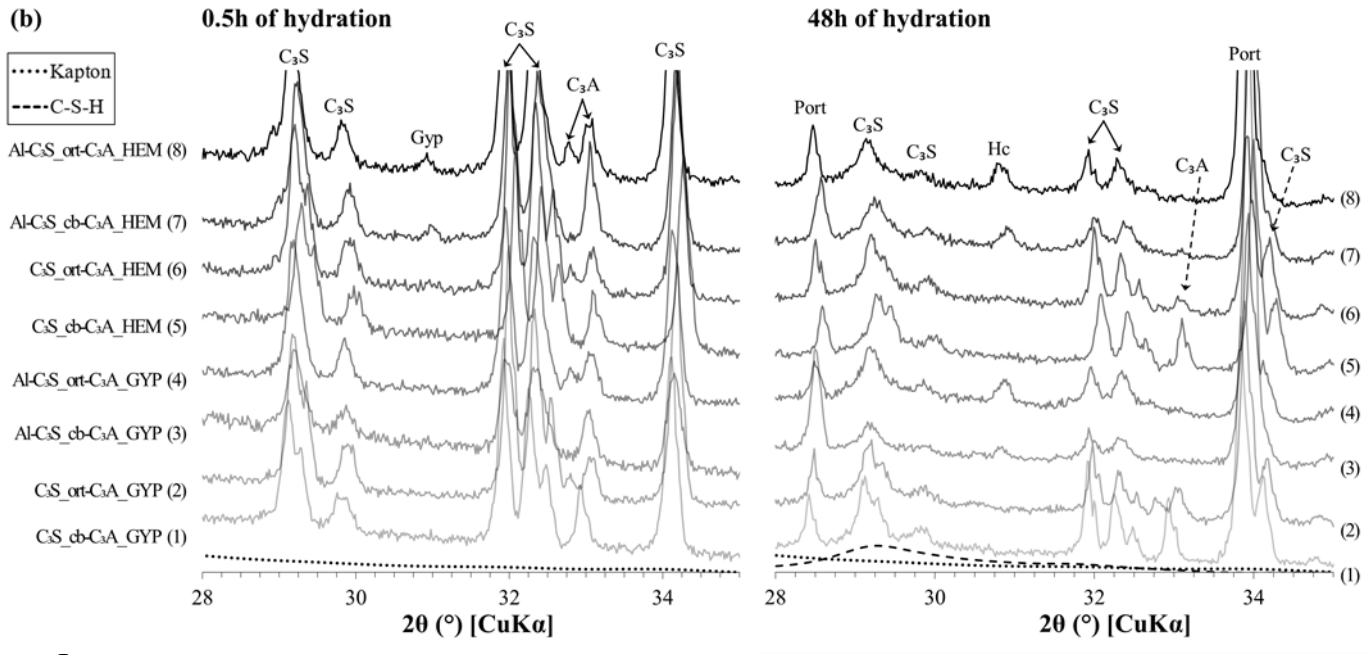

Figure 5 – Selected ranges of the XRD patterns of the ternary mixes at 0.5 and 48 hours of hydration. (a) 8-24° 2θ range; (b) 28-35° 2θ range. Ett: ettringite; Gyp: gypsum; Port: portlandite; Hc: hemicarbonate. Note: the patterns were vertically shifted for visualization, but the relative intensities (in linear scale) were not changed. The Kapton and C-S-H models are also shown as dotted and dashed lines, respectively.

Figure 6(a,b) exemplifies the phase content over time determined by XRD-Rietveld QPA and the heat flow within the first 48 hours of hydration for the C_3S_cb-C_3A_2.81% HEM and Al-C_3S_cb-C_3A_2.84% HEM pastes. The phases content over time of the other ternary mixes are presented in the Supplementary Information (Figure S3). Regarding silicates, all the mixtures showed very similar behavior. The C_3S content was approximately constant (considering the intrinsic deviations in Rietveld quantification) during the first ≈ 4 h, up to the end of the induction period. A supposed increase in the C_3S content was observed in some samples within this period (e.g., in Figure 6a), also observed in Refs [18,54]. However, this is most likely related to the variability in the XRD-Rietveld QPA, which can yield errors as high as 3 wt.% for the major cement phases [55]. At the beginning of the acceleration period, the C_3S contents start to reduce indicating its dissolution, while significant C-S-H and portlandite formation can be measured, in agreement with Refs. [51,52]. Previous works showed that C-S-H starts to precipitate shortly after mixing as primary particles of tens of nanometers in size [56,57], which are hardly detectable by XRD. After a few hours, these nanosized particles are converted into the known foil-like arrangement [57,58] detectable by XRD. The C_3S dissolution and the C-S-H and portlandite formation initially presented faster rates but

slowed down after the main heat flow peak. The lower C_3S dissolution rate can explain the decrease in heat release rate in IC curves.

As for the aluminates, for all the ternary mixes, it was observed an extremely fast initial C_3A dissolution (with approximately 50% of the C_3A dissolving within the first 30 minutes – before the first XRD measurement) and then its content remains virtually constant. Ettringite was formed in the first minutes (already detected in the first XRD scan), and its content kept increasing in the first hours, associated with gypsum dissolution. After 6-16 hours (varying from mix to mix), gypsum depletion is observed. From this point on, the ternary mixes with Al-C_3S presented very different behaviors when compared with the ternary mixes with C_3S. In the ternary mixes with Al-C_3S, a few hours after gypsum depletion, the C_3A started to dissolve again very quickly (Figures 6b and S3c,d,g,h). For those ternary mixes, the ettringite content initially increased fast up to a limit and then started to dissolve synchronously with the start of hemicarbonate formation. In turn, for the C_3S ternary mixes, the C_3A also starts to dissolve again after the sulfate depletion, but much slower than the mixtures with Al-C_3S. As a result, no AFm was detected in the C_3S-containing ternary mixes up to 48 hours, as observed in Figure 5a (see patterns 1, 2, 5, and 6) where the only reflection observed up to 12° 2θ was that from ettringite

The formation of hemicarboaluminate instead of monosulfate on Al-C_3S ternary mixes occurred due to the presence of calcite (0.5 wt%) and magnesite (0.9 wt%) on the Al-C_3S composition (see Section 2.1). In turn, for the C_3S ternary mixes, no ettringite dissolution and hemicarbonate or monosulfate formations were observed in the first 48 hours of hydration. Interestingly, the ternary mixes with ort-C_3A also formed hemicarbonate instead of U-phase ($4CaO \cdot 0.9Al_2O_3 \cdot 1.1SO_3 \cdot 0.5Na_2O \cdot 16H_2O$), which also belongs to the group of hexagonal or pseudo-hexagonal layered structures (AFm) and were observed in pure ort-C_3A pastes [14]. The U-phase is formed in the presence of SO_4^{2-} and Na^+ ions in a highly alkaline medium [59]. However, since the C_3S/C_3A/calcium sulfate mixes had much lower ort-C_3A amounts than pure C_3A pastes, the amount of Na^+ ions released was probably not enough to ensure the sufficiently high pH for the U-phase formation.

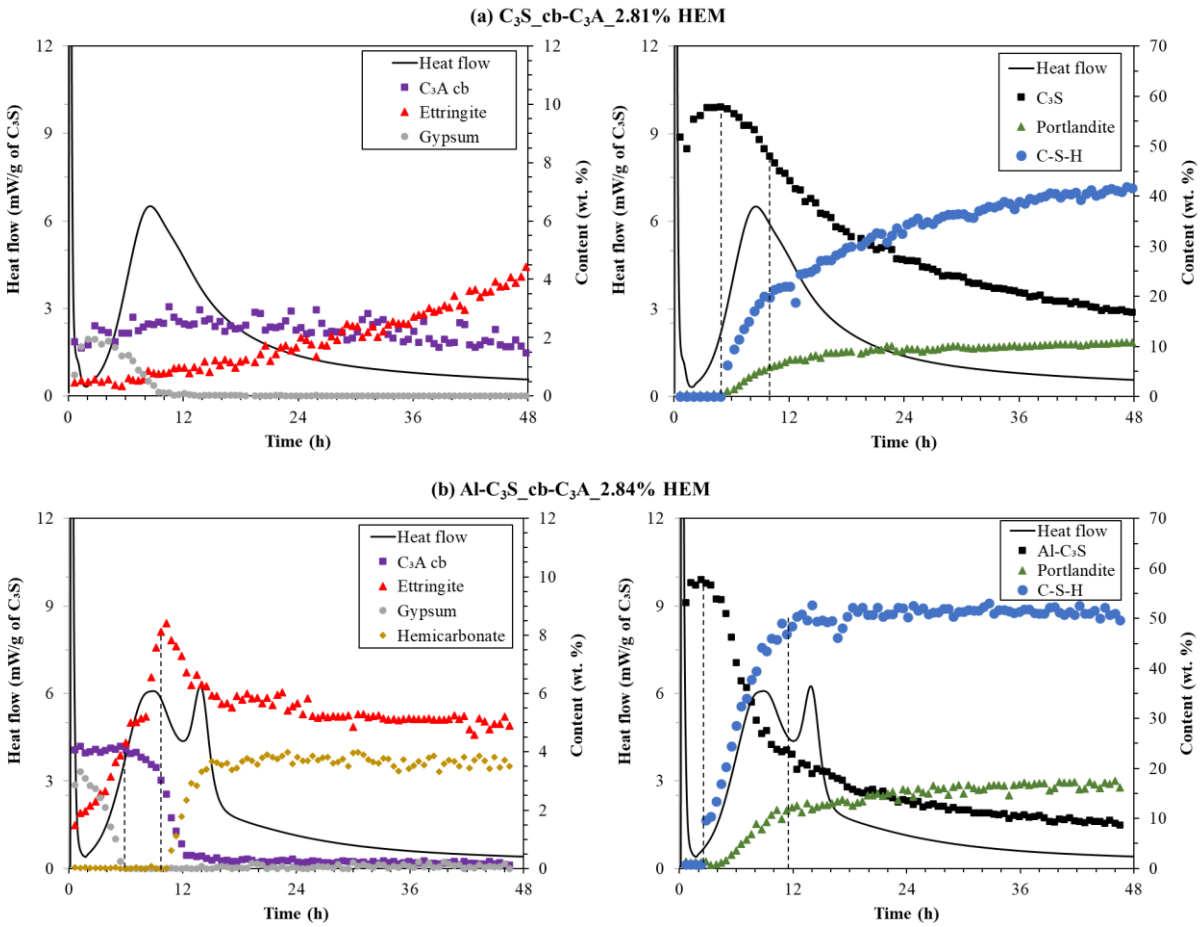

Figure 6 – Examples of heat flow curves and phase content (wt%) over the first 48 hours of hydration of (a) C_3S_cb-C_3A_2.81% HEM and (b) Al- C_3S_cb-C_3A_2.84% HEM.

3.2.2 Effect of C_3S and C_3A doping, and calcium sulfate source on the hydration of aluminate phases

Figure 7 presents the ettringite, hemicarbonate and C_3A contents of all samples measured by *in-situ* XRD during the first 48 hours. It was found that the C_3S type had the greatest influence on ettringite formation, and the Al-C_3S ternary mixes presented higher ettringite contents in the first hours compared with the respective ternary mixes containing pure C_3S. Consequently, the Al-C_3S ternary mixes showed hemicarbonate formation at 6.0-16.7 hours, while no significant formation of crystalline hemicarbonate was observed in the pure C_3S samples up to 48 hours. This can be associated with the higher aluminum content in the pore solution of the Al-C_3S pastes.

The C_3A type also influenced the amount of ettringite formed in the first hours. The ternary mixes with ort-C_3A generally presented higher ettringite contents when compared with the respective cb-C_3A ternary mixes. This result was expected due to the higher

reactivity of ort-C_3A, as discussed in Section 3.1.2. As a result of the higher ettringite formation and the faster sulfate consumption, the Al-C_3S_ort-C_3A_GYP paste presented earlier hemicarboaluminate formation (≈ 9.7 hours) compared to the Al-C_3S_cb-C_3A_GYP paste (≈ 16.7 hours).

Finally, the calcium sulfate type also influenced the ettringite formation rate. The ternary mixes with hemihydrate (Figure 7b) showed faster ettringite formation in the first hours, which agrees with Zunino and Scrivener [7] results. This was expected since the hemihydrate presents a faster dissolution when compared with gypsum [21,22], resulting in higher sulfate concentration in pore solution, leading to a faster ettringite formation. Finally, the replacement of gypsum by hemihydrate also influenced the beginning of hemicarbonate formation, anticipating it in 6.4 hours for the Al-C_3S_cb-C_3A pastes (from 16.7 hours for the mix with GYP to 10.3 hours for the mix with HEM) and in 3.7 hours for the Al-C_3S_ort-C_3A pastes (from 9.7 hours for the mix with GYP to 6.0 hours for the mix with HEM).

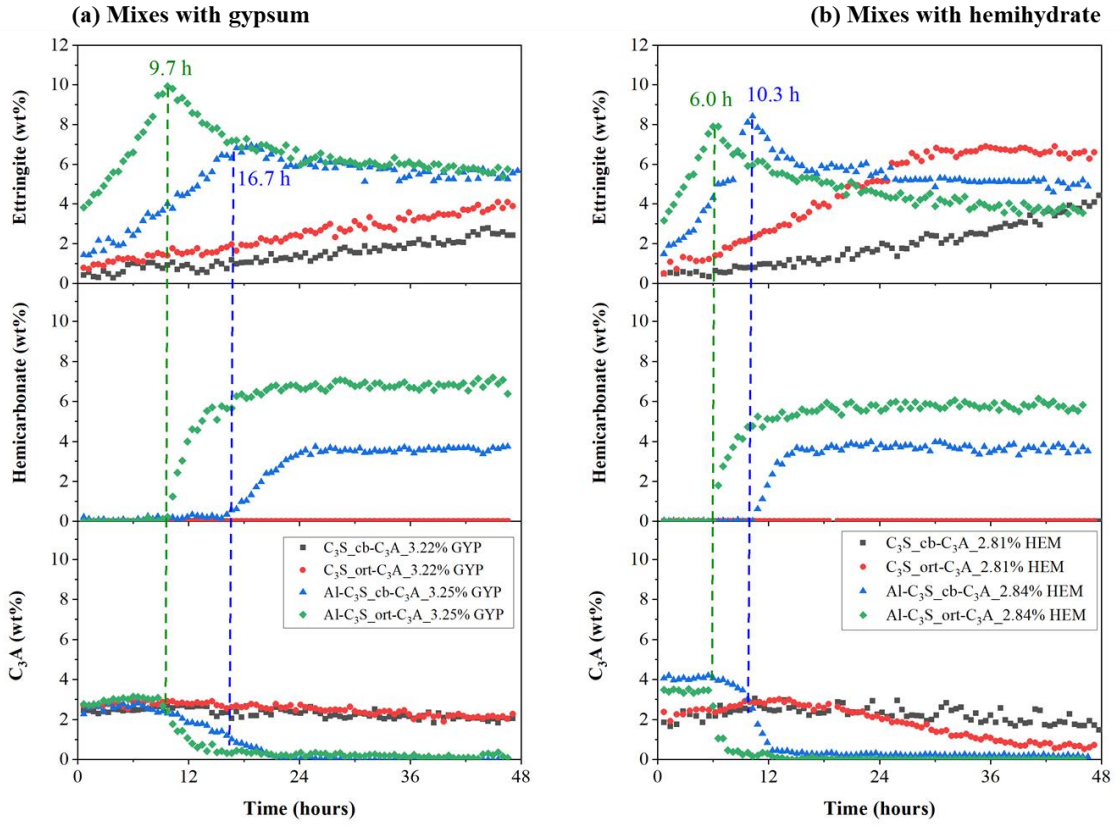

Figure 7 – Ettringite, hemicarbonate and C_3A content (wt%) in the C_3S/C_3A pastes with (a) gypsum and (b) hemihydrate over the first 48 hours.

3.3 Thermogravimetric analysis (TGA)

Figure 8 shows the DTG curves up to 300 °C of the C_3S/C_3A pastes with 1.5 wt% SO_3 (with gypsum or hemihydrate) at 8 hours, 1, 3, and 7 days of hydration. The complete DTG curves (up to 1000 °C) are presented in Supplementary materials (Figure S4). Peaks related to C-S-H (between 50 and 300 °C), ettringite (≈100 °C), gypsum (≈140 °C), AFm phases (≈ 55 °C), portlandite (between 400 and 500 °C), and carbonates (between 600 and 700 °C) were observed [27]. As expected, the peaks related to the hydrated phases' thermal decomposition increased with the hydration time, indicating higher amounts of hydrated phases and consequently a higher degree of hydration. In turn, the gypsum peaks were only observed in the mixtures with C_3S at 8 hours, which agrees with XRD-Rietveld results, showing that the sulfate depletion occurred after ≈10 hours of hydration for those samples, while occurred up to ≈6 hours for the ternary mixes with Al-C_3S.

The C_3S type had a remarkable influence on the moment of AFm formation. While the Al-C_3S pastes already presented the peaks related to AFm phases decomposition at 8 hours or 1 day, no AFm peaks are observed in the pure C_3S ternary mixes up to 3 days, being only observed at 7 days. This result also corroborates the XRD-Rietveld results, in which no AFm phases were observed in the first 48 hours for the pure C_3S ternary mixes while starting to form between 6.0 to 16.7 hours for the Al-C_3S pastes.

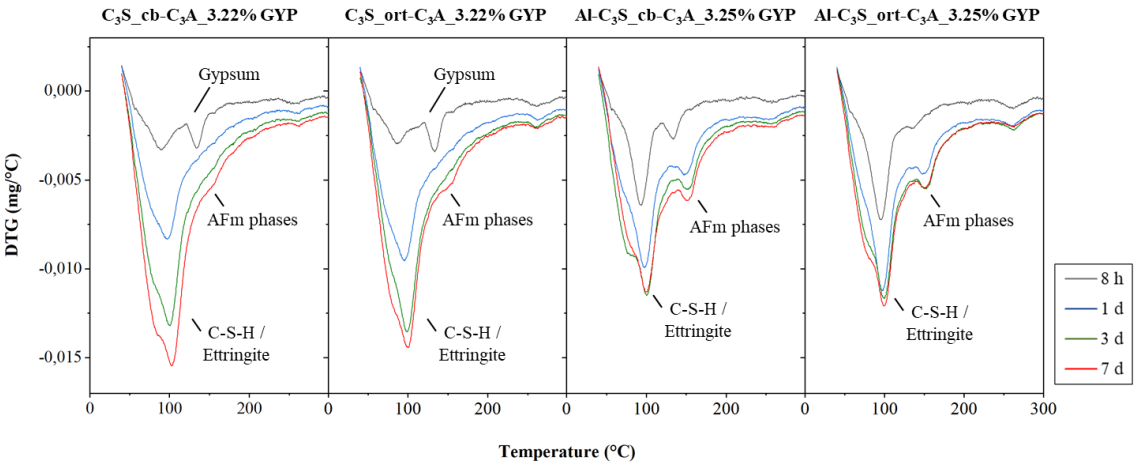

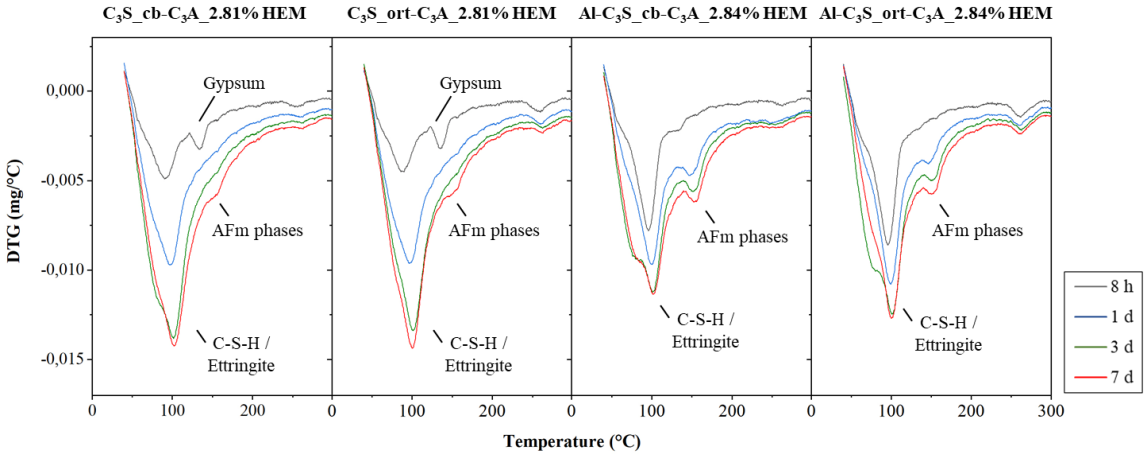

Figure 8 – DTG curves (up to 300 ºC) of the C_3S/C_3A pastes with gypsum and hemihydrate at 8 h, 1, 3, and 7 d of hydration.

The bound water content was calculated from the TGA results and is presented in Figure 9. The ternary mixes with pure C_3S presented higher bound water content than those with Al-C_3S. The bound water is related to the degree of hydration (DoH) of C_3S. As observed by isothermal calorimetry (see Section 3.1.1), pure C_3S was much more reactive than Al-C_3S, which explains the higher bound water content of the mixtures with pure C_3S. In turn, the C_3A and calcium sulfate types did not significantly influence the bound water content of the ternary mixes, which may be explained by their much lower content compared with C_3S.

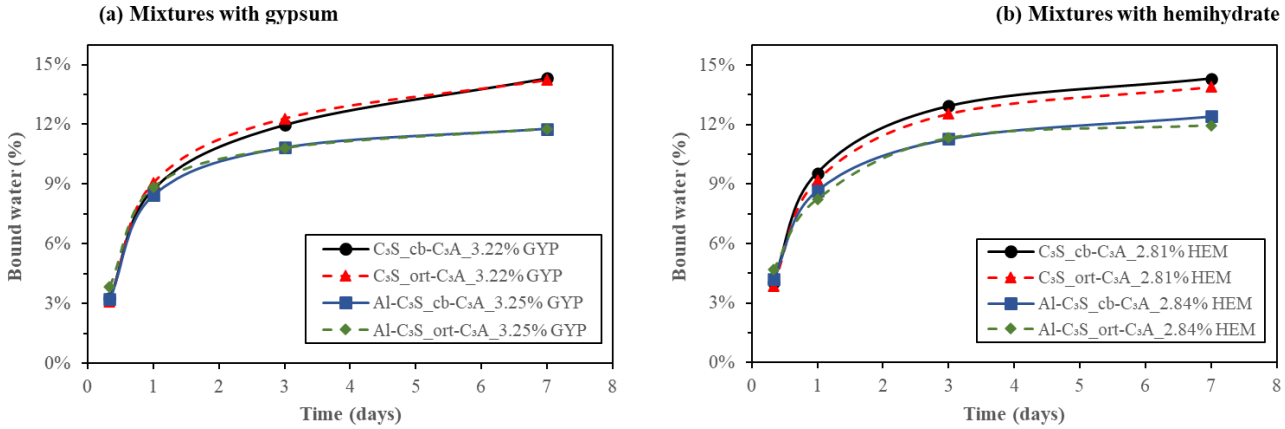

Figure 9 – Bound water (%) of the C_3S/C_3A pastes with (a) gypsum and (b) hemihydrate over the first 7 days of hydration.

Figure 10 presents the portlandite content (in g/100g of paste) of the C_3S/C_3A pastes with gypsum in (a) and hemihydrate in (b) during the first 7 days of hydration. The portlandite content showed the same trend observed for the bound water content: the C_3S type was

the only factor that significantly influenced the portlandite content, where the ternary mixes with pure C_3S presented higher portlandite content than the ternary mixes with Al-C_3S, which was expected since C_3S is more reactive than Al-C_3S.

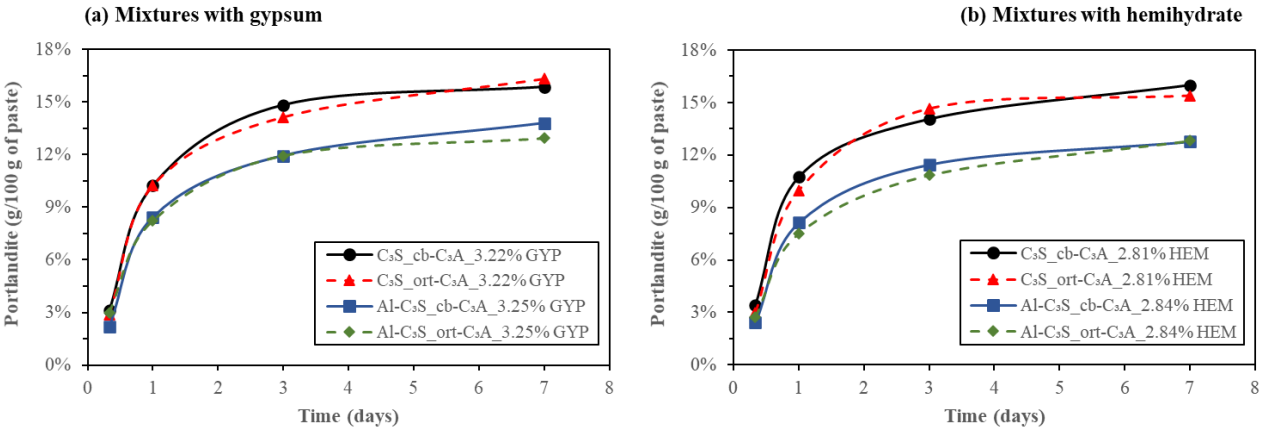

Figure 10 – Portlandite content (g/100 of paste), determined by TGA, of the C_3S/C_3A pastes with (a) gypsum and (b) hemihydrate over the first 7 days of hydration.

4 DISCUSSION

4.1 The impact of aluminum doping of C_3S on sulfate demand

Among the factors analyzed, the aluminum doping of C_3S had the most remarkable influence on the sulfate demand of the ternary systems. The beginning of ettringite decomposition and hemicarbonate formation occurred between 6.0 and 16.7 hours (depending on C_3A polymorph and calcium sulfate type used) in the ternary mixes with Al-C_3S (observed by *in-situ* XRD and confirmed by TGA), while only occurred between 3 and 7 days of hydration for the ternary mixes with C_3S (revealed by TGA).

Zunino and Scrivener [7] studied C_3S T_1/cb-C_3A/gypsum systems varying the C_3S fineness, finding that the higher the C_3S fineness, the earlier the sulfate depletion and the higher the sulfate demand. This occurs because the increase of the fineness of C_3S increases its reactivity and, consequently, increases the rate of C-S-H formation [7]. As mentioned early, the sulfates are physically adsorbed by the C-S-H due to charge affinity [60], consuming the sulfates from the solution. Therefore, the higher the amount of C-S-H formed in the first hours, the higher the amount of sulfates adsorbed on the C-S-H surface, and the earlier the sulfate depletion occurs.

Interestingly, the opposite behavior was observed here: the ternary systems with Al-C_3S, which presented lower reactivity when compared with pure C_3S (see Section 3.1), presented higher sulfate demand. For instance, the ternary mixes with Al-C_3S required 1.5-2.0 wt% SO_3 to be properly sulfated, while those with pure C_3S only required 0.5 wt% SO_3. This happens because of the impact of aluminum on sulfate consumption – the higher the aluminum content available in the pore solution, the higher the ettringite formation (observed here by *in-situ* XRD), and the faster the sulfate depletion.

We emphasize that Zunino and Scrivener [7] used the same C_3S used here (T_1, without aluminum) but with different fineness. Therefore, we can propose that not only the C_3S fineness and polymorph will influence the sulfate balance of the system (as observed by [7]) but also the aluminum content in the C_3S. In addition, the latter factor seems to have a greater impact on the sulfate demand than the former, since the ternary mixes with the coarser and less reactive Al-C_3S (with 0.8 wt% Al_2O_3) presented a higher sulfate demand than the ternary mixes with the finer and more reactive pure C_3S (without aluminum).

4.2 The impact of C_3A polymorphism on sulfate demand

The C_3A polymorphism also influenced the sulfate demand of the ternary mixes, although to a lesser extent than the aluminum doping of C_3S. The influence of the C_3A polymorphism on the sulfate demand depended on the percentage of SO_3 used. For the ternary mixes with low SO_3 contents (0.25 and 0.50 wt% SO_3), the systems with cb-C_3A presented earlier sulfate depletion and renewed hydration of C_3A than those mixes with ort-C_3A. However, for the ternary mixes with 1.00 wt% SO_3 or more, the opposite behavior was observed, i.e., the ternary mixes with ort-C_3A presented earlier sulfate depletion.

This behavior is due to the different impacts of calcium sulfates on cb-C_3A and ort-C_3A hydration. Without calcium sulfates, cubic C_3A hydrates faster than orthorhombic C_3A. Besides, the addition of calcium sulfates is much more efficient in delaying the cb-C_3A hydration than the ort-C_3A hydration (explained in Section 3.1.2 and consistent with other studies [12,13,61]). Therefore, when low amounts of calcium sulfate are used, the cb-C_3A hydration is not efficiently retarded to be slower than the ort-C_3A hydration.

4.3 The impact of calcium sulfate type on C_3S and C_3A hydration and sulfate demand

The addition of calcium sulfate slightly prolonged the induction period of both C_3S and Al-C_3S (see Section 3.1.1) but enhanced their hydration afterward, resulting in higher heat flow peaks and cumulative heat in the first 48 hours. The initial delay probably occurred due to the adsorption of sulfate ions on the C_3S surface [7,17,47], while the enhancement thereafter seems to be related to either the change in the C-S-H morphology due to the sulfate adsorption or to the increase in the ionic strength of the solution with the addition of calcium sulfate [11].

However, the calcium sulfate type did not significantly influence the hydration of pure C_3S and Al-C_3S. The C_3S-gypsum and the C_3S-hemihydrate pastes (with a 1.5 wt% SO_3) presented very close heat flow curves in the first 48 hours (Figure 4a,b), except for a small heat flow peak between 30 minutes and 2 hours associated with the hydration of hemihydrate and formation of gypsum crystals.

As for C_3A pastes, the presence of gypsum or hemihydrate retarded the reaction of both cb-C_3A and ort-C_3A, but the retarding effect was much less efficient for the latter. This occurs due to the higher solubility of $Al_6O_{18}^{18-}$ rings on the ort-C_3A, inhibiting the adsorption of SO_4^{2-} and/or Ca–SO_4 ion-pair responsible for the delay in cb-C_3A hydration [13,14]. The replacement of gypsum with hemihydrate leads to a substantial delay on both cb-C_3A and ort-C_3A. The faster dissolution of hemihydrate, which releases more sulfate ions into the pore solution in the first hours, might explain this. However, more studies on this matter are necessary to fully understand its mechanism.

The analysis of the effect of calcium sulfate type on the hydration of C_3S/C_3A/calcium sulfate systems showed that the use of hemihydrate resulted in earlier sulfate depletion and hemicarbonate formation (observed by calorimetry and *in-situ* XRD), consequently presenting a higher sulfate demand to obtain properly sulfated systems, which agrees with Zunino and Scrivener results [7]. This occurs due to the faster dissolution of hemihydrate compared with gypsum, resulting in higher sulfite concentrations in the pore solution in the first hours, increasing ettringite's formation (revealed by *in-situ* XRD).

4.4 Implications for PC production and PC concrete properties

As observed, the aluminum content in C_3S greatly impacts the sulfate balance of C_3S/C_3A/calcium sulfate systems, which usually correspond to about 70 wt% of ordinary Portland cement. Therefore, Portland clinkers with higher aluminum content (including the aluminum incorporated in the C_3S structure) will present higher sulfate demand, i.e., a higher amount of calcium sulfate will be required to obtain optimal fresh and mechanical properties.

The C_3A polymorph also affected the sulfate balance of the systems studied. For the ternary mixes with 1.0 wt% SO_3 or more, the ort-C_3A reacted faster than the cb-C_3A, leading to faster sulfate depletion (note that commercial PCs usually need 2.5-4.5 wt% SO_3 to be properly sulfated). Therefore, clinkers with ort-C_3A are likely to require more sulfate to reach optimum properties.

Finally, the presence of hemihydrate (which might occur in commercial PCs due to gypsum dehydration during milling) also increased the sulfate demand of the ternary mixes. Therefore, a higher sulfate content will be needed to optimize the properties of concrete produced with PC containing this type of sulfate source. Furthermore, the crystallization of gypsum and the higher ettringite formation in the presence of hemihydrate tends to decrease PC concrete workability and may result in a false setting [1,62,63].

Understanding how these parameters influence the sulfate demand of PC will help the cement industry control the amount and type of calcium sulfate that should be used. However, it stresses the need for further studies on this topic with commercial clinkers since pure phases have inherent differences compared with those present in the clinkers produced by the industry.

5 CONCLUSIONS

From our results, we can conclude that:

- Both gypsum and hemihydrate delayed the initial hydration of pure C_3S and Al-C_3S, prolonging the induction period but accelerating the reaction thereafter. The C_3S-gypsum and C_3S-hemihydrate pastes presented very similar behaviors for the same SO_3 content (1.5 wt% SO_3).

- Aluminum doping of C_3S greatly influenced the sulfate balance of C_3S/C_3A/calcium sulfate mixes. The ternary mixes with Al-C_3S presented faster and higher ettringite formation in the first hours, anticipating the sulfate depletion, the renewed hydration of C_3A, and the hemicarbonate formation.

- The impact of C_3A polymorphism on the sulfate demand of the C_3S/C_3A/calcium sulfate mixes varied with the SO_3 content used. For the systems with 0.25 and 0.50 wt% SO_3, the ternary mixes with cb-C_3A presented earlier sulfate depletion and renewed hydration of C_3A. However, for the systems with 1.0 wt% SO_3 or more, those with ort-C_3A presented earlier sulfate depletion and renewed dissolution of C_3A. In addition, the C_3A polymorphism does not seem to significantly influence the pure or Al-doped C_3S hydration rate in proper sulfated mixes.

- The replacement of gypsum with hemihydrate in the C_3S/C_3A/calcium sulfate mixes resulted in faster ettringite formation, anticipating the sulfate depletion and renewed hydration of C_3A. This happens due to the faster dissolution of hemihydrate when compared with gypsum. In addition, hemihydrate incorporation led to higher sulfate demand, which may require greater sulfate contents in commercial clinkers when this type of sulfate source is used.

6 Acknowledgments

JSAN and PRM thank the financial support of (Coordination for the Improvement of Higher Education Personnel). JSAN thanks the University of Malaga (Spain), where the experiments for the characterization of the raw materials were performed. JSAN also thanks the Spanish Junta de Andalucía [P18-RT-720 cofounded with ERDF] research project for the research stage at the University of Málaga (Spain) and the Graduate Program in Civil Engineering: Construction and Infrastructure (PPGCI) of the Federal University of Rio Grande do Sul (UFRGS), Brazil. APK acknowledge the financial support of CNPq (Brazilian National Council for Scientific and Technological Development). The staff of *Laboratório de Difração de Raios-X* (LDRX-UFSC) is acknowledged for the *in-situ* XRD data collection.

7 References

[1] J. da S. Andrade Neto, A.G. de la Torre, A.P. Kirchheim, Effects of sulfates on the hydration of Portland cement – A review, Construction and Building Materials. 279 (2021). https://doi.org/10.1016/j.conbuildmat.2021.122428.

[2] S. Adu-Amankwah, L. Black, J. Skocek, M. ben Haha, M. Zajac, Effect of sulfate additions on hydration and performance of ternary slag-limestone composite cements, Construction and Building Materials. 164 (2018) 451–462. https://doi.org/10.1016/j.conbuildmat.2017.12.165.

[3] S. Mohammed, O. Safiullah, Optimization of the SO3 content of an Algerian Portland cement: Study on the effect of various amounts of gypsum on cement properties, Construction and Building Materials. 164 (2018) 362–370. https://doi.org/10.1016/j.conbuildmat.2017.12.218.

[4] M. Zajac, J. Skocek, A. Müller, M. ben Haha, Effect of sulfate content on the porosity distribution and resulting performance of composite cements, Construction and Building Materials. 186 (2018) 912–919. https://doi.org/10.1016/j.conbuildmat.2018.07.247.

[5] K. Tosun, Effect of SO3 content and fineness on the rate of delayed ettringite formation in heat cured Portland cement mortars, Cement and Concrete Composites. 28 (2006) 761–772. https://doi.org/10.1016/j.cemconcomp.2006.06.003.

[6] A. Pavoine, X. Brunetaud, L. Divet, The impact of cement parameters on Delayed Ettringite Formation, Cement and Concrete Composites. 34 (2012) 521–528. https://doi.org/10.1016/j.cemconcomp.2011.11.012.

[7] F. Zunino, K. Scrivener, Factors influencing the sulfate balance in pure phase C3S/C3A systems, Cement and Concrete Research. 133 (2020) 106085. https://doi.org/10.1016/j.cemconres.2020.106085.

[8] D. Wagner, F. Bellmann, J. Neubauer, Influence of aluminium on the hydration of triclinic C3S with addition of KOH solution, Cement and Concrete Research. 137 (2020) 106198. https://doi.org/10.1016/j.cemconres.2020.106198.

[9] D. Stephan, S. Wistuba, Crystal structure refinement and hydration behaviour of 3CaO·SiO2 solid solutions with MgO, Al2 O3 and Fe2O3, J Eur Ceram Soc. 26 (2006) 141–148. https://doi.org/10.1016/j.jeurceramsoc.2004.10.031.

[10] F. Begarin, S. Garrault, A. Nonat, L. Nicoleau, Hydration of alite containing aluminium, Advances in Applied Ceramics. 110 (2011) 127–130. https://doi.org/10.1179/1743676110Y.0000000007.

[11] J.S. Andrade Neto, E.D. Rodríguez, P.J.M. Monteiro, A.G. de la Torre, A.P. Kirchheim, Hydration of C3S and Al-doped C3S in the presence of gypsum, Cement and Concrete Research. Submitted (2021).

[12] A.P. Kirchheim, E.D. Rodríguez, R.J. Myers, L.A. Gobbo, P.J.M. Monteiro, D.C.C. Dal Molin, R.B. de Souza, M.A. Cincotto, Effect of gypsum on the early hydration of cubic and Na-doped orthorhombic tricalcium aluminate, Materials. 11 (2018) 1–16. https://doi.org/10.3390/ma11040568.

[13] R.J. Myers, G. Geng, E.D. Rodriguez, P. da Rosa, A.P. Kirchheim, P.J.M. Monteiro, Solution chemistry of cubic and orthorhombic tricalcium aluminate hydration, Cement and Concrete Research. 100 (2017) 176–185. https://doi.org/10.1016/j.cemconres.2017.06.008.

[14] J.S. Andrade Neto, P.R. Matos, A.G. de la Torre, C.E.M. Campos, P.J.P. Gleize, P.J.M. Monteiro, A.P. Kirchheim, The role of sodium and sulfate sources on the rheology and hydration of C3A polymorphs, Cement and Concrete Research. 151 (2022) 106639. https://doi.org/10.1016/j.cemconres.2021.106639.

[15] E. Pustovgar, R.K. Mishra, M. Palacios, J.B. d'Espinose de Lacaillerie, T. Matschei, A.S. Andreev, H. Heinz, R. Verel, R.J. Flatt, Influence of aluminates on the hydration kinetics of tricalcium silicate, Cement and Concrete Research. 100 (2017) 245–262. https://doi.org/10.1016/j.cemconres.2017.06.006.

[16] S. Garrault, A. Nonat, Y. Sallier, L. Nicolaeau, On the Origin of the Dormant Period of Cement Hydration, in: 13th International Congress on the Chemistry of Cement., Madrid, 2011: pp. 1–7.

[17] L. Nicoleau, E. Schreiner, A. Nonat, Ion-specific effects influencing the dissolution of tricalcium silicate, Cement and Concrete Research. 59 (2014) 118–138. https://doi.org/10.1016/j.cemconres.2014.02.006.

[18] D. Jansen, Ch. Naber, D. Ectors, Z. Lu, X.-M. Kong, F. Goetz-Neunhoeffer, J. Neubauer, The early hydration of OPC investigated by in-situ XRD, heat flow calorimetry, pore water analysis and 1H NMR: Learning about adsorbed ions from a complete mass balance approach, Cement and Concrete Research. 109 (2018) 230–242. https://doi.org/10.1016/j.cemconres.2018.04.017.

[19] K. Fukuda, S. Inoue, H. Yoshida, Cationic substitution in tricalcium aluminate, Cement and Concrete Research. 33 (2003) 1771–1775. https://doi.org/10.1016/S0008-8846(03)00172-8.
[20] L. Gobbo, L. Sant'Agostino, L. Garcez, C3A polymorphs related to industrial clinker alkalies content, Cement and Concrete Research. 34 (2004) 657–664. https://doi.org/10.1016/j.cemconres.2003.10.020.
[21] V.H. Dodson, T.D. Hayden, Another look at the Portland cement/chemical admixture incompatibility problem, Cement, Concrete and Aggregates. 11 (1989) 52–56. https://doi.org/10.1520/cca10102j.
[22] S. Pourchet, L. Regnaud, J.P. Perez, A. Nonat, Early C3A hydration in the presence of different kinds of calcium sulfate, Cement and Concrete Research. 39 (2009) 989–996. https://doi.org/10.1016/j.cemconres.2009.07.019.
[23] M. Palacios, H. Kazemi-Kamyab, S. Mantellato, P. Bowen, Laser diffraction and gas adsorption techniques, in: K. Scrivener, R. Snellings, B. Lothenbach (Eds.), A Practical Guide to Microstructural Analysis of Cementitious Materials, 1st ed., CRC Press, 2016: pp. 445–480.
[24] A. Quennoz, K.L. Scrivener, Interactions between alite and C3A-gypsum hydrations in model cements, Cement and Concrete Research. 44 (2013) 46–54. https://doi.org/10.1016/j.cemconres.2012.10.018.
[25] L. Wadsö, Operational issues in isothermal calorimetry, Cement and Concrete Research. 40 (2010) 1129–1137. https://doi.org/10.1016/j.cemconres.2010.03.017.
[26] J.D. Zea-Garcia, A.G. de la Torre, M.A.G. Aranda, I. Santacruz, Processing and characterisation of standard and doped alite-belite-ye'elimite ecocement pastes and mortars, Cement and Concrete Research. 127 (2020). https://doi.org/10.1016/j.cemconres.2019.105911.
[27] B. Lothenbach, P.T. Durdziński, K. de Weerdt, Thermogravimetric analysis, in: K. Scrivener, R. Snellings, B. Lothenbach (Eds.), A Practical Guide to Microstructural Analysis of Cementitious Materials, 1st ed., CRC Press, 2016: pp. 177–212.
[28] A.A. Coelho, TOPAS and TOPAS-Academic: An optimization program integrating computer algebra and crystallographic objects written in C++: An, Journal of Applied Crystallography. 51 (2018) 210–218. https://doi.org/10.1107/S1600576718000183.
[29] P.R. de Matos, J.S. Andrade Neto, D. Jansen, Á.G. de la Torre, A.P. Kirchheim, C.E.M. Campos, In-situ laboratory X-ray diffraction applied to cement-based materials, Cement and Concrete Research (Under Review). (2022).
[30] R. Snellings, X-ray powder diffraction applied to cement, in: K. Scrivener, R. Snellings, B. Lothenbach (Eds.), A Practical Guide to Microstructural Analysis of Cementitious Materials, 1st ed., CRC Press, 2016: pp. 107–176.
[31] S.T. Bergold, F. Goetz-Neunhoeffer, J. Neubauer, Quantitative analysis of C-S-H in hydrating alite pastes by in-situ XRD, Cement and Concrete Research. 53 (2013) 119–126. https://doi.org/10.1016/j.cemconres.2013.06.001.
[32] S. Scherb, N. Beuntner, K.C. Thienel, J. Neubauer, Quantitative X-ray diffraction of free, not chemically bound water with the PONKCS method, Journal of Applied Crystallography. 51 (2018) 1535–1543. https://doi.org/10.1107/S1600576718012888.
[33] B.H. O'Connor, M.D. Raven, Application of the Rietveld Refinement Procedure in Assaying Powdered Mixtures, Powder Diffraction. 3 (1988) 2–6. https://doi.org/10.1017/S0885715600013026.
[34] D. Jansen, F. Goetz-Neunhoeffer, C. Stabler, J. Neubauer, A remastered external standard method applied to the quantification of early OPC hydration, Cement and Concrete Research. 41 (2011) 602–608. https://doi.org/10.1016/j.cemconres.2011.03.004.
[35] A. Cuesta, J.D. Zea-Garcia, D. Londono-Zuluaga, A.G. de La Torre, I. Santacruz, O. Vallcorba, M. Dapiaggi, S.G. Sanfélix, M.A.G. Aranda, Multiscale understanding of tricalcium silicate hydration reactions, Scientific Reports. 8 (2018) 1–11. https://doi.org/10.1038/s41598-018-26943-y.
[36] A. Cuesta, Á.G. de La Torre, I. Santacruz, A. Diaz, P. Trtik, M. Holler, B. Lothenbach, M.A.G. Aranda, Quantitative disentanglement of nanocrystalline phases in cement pastes by synchrotron ptychographic X-ray tomography, IUCrJ. 6 (2019) 473–491. https://doi.org/10.1107/S2052252519003774.
[37] L. Valentini, M.C. Dalconi, M. Favero, G. Artioli, G. Ferrari, In-Situ XRD measurement and quantitative analysis of hydrating cement: Implications for sulfate incorporation in C-S-H, Journal of the American Ceramic Society. 98 (2015) 1259–1264. https://doi.org/10.1111/jace.13401.
[38] N.I. Golovastikov, R.G. Matveeva, N. v. Belov, Crystal structure of the tricalcium silicate 3CaO SiO2 = C3S, Soviet Physics - Crystallography. 20 (1975) 441–445.

[39] M.N. de Noirfontaine, M. Courtial, F. Dunstetter, G. Gasecki, M. Signes-Frehel, Tricalcium silicate Ca3SiO5 superstructure analysis: A route towards the structure of the M1 polymorph, Zeitschrift Fur Kristallographie. 227 (2012) 102–112. https://doi.org/10.1524/zkri.2012.1425.
[40] P. Mondal, J.W. Jeffery, The Crystal Structure of Triealeium Aluminate, Ca3Al2O6, Acta Crystallographica. (1975) 689.
[41] F. Nishi, Y. Takeuchi, The A16018 Rings of Tetrahedra in the Structure of Cas.sNaA16O18, Acta Crystallographica Section B Structural Crystallography and Crystal Chemistry. 31 (1975) 1169–1173.
[42] H.E. Petch, The hydrogen positions in portlandite, Ca(OH)2, as indicated by the electron distribution, Acta Crystallographica. 14 (1961) 950–957. https://doi.org/10.1107/s0365110x61002771.
[43] F. Goetz-Neunhoeffer, J. Neubauer, Refined ettringite (Ca 6 Al 2 (SO 4) 3 (OH) 12 ·26H 2 O) structure for quantitative X-ray diffraction analysis , Powder Diffraction. 21 (2006) 4–11. https://doi.org/10.1154/1.2146207.
[44] Á.G. de la Torre, M.-G. López-Olmo, C. Álvarez-Rua, S. García-Granda, Miguel.A.G. Aranda, Structure and microstructure of gypsum and its relevance to Rietveld quantitative phase analyses, Powder Diffraction. 19 (2004) 240–246. https://doi.org/10.1154/1.1725254.
[45] C. Bezou, A. Nonat, J.C. Mutin, A. Nørlund Christensen, M.S. Lehmann, Investigation of the crystal structure of γ-CaSO4, CaSO4 · 0.5 H2O, and CaSO4 · 0.6 H2O by powder diffraction methods, Journal of Solid State Chemistry. 117 (1995) 165–176. https://doi.org/10.1006/jssc.1995.1260.
[46] T. Runčevski, R.E. Dinnebier, O. v. Magdysyuk, H. Pöllmann, Crystal structures of calcium hemicarboaluminate and carbonated calcium hemicarboaluminate from synchrotron powder diffraction data, Acta Crystallographica Section B: Structural Science. 68 (2012) 493–500. https://doi.org/10.1107/S010876811203042X.
[47] P. Juilland, L. Nicoleau, R.S. Arvidson, E. Gallucci, Advances in dissolution understanding and their implications for cement hydration, RILEM Technical Letters. 2 (2017) 90. https://doi.org/10.21809/rilemtechlett.2017.47.
[48] F.P. Glasser, M.B. Marinho, Early stages of the hydration of tricalcium aluminate and its sodium-cotaining solid solutions, Proceedings of the British Ceramic Society. 35 (1984) 221–236.
[49] A.P. Kirchheim, V. Fernàndez-Altable, P.J.M. Monteiro, D.C.C. Dal Molin, I. Casanova, Analysis of cubic and orthorhombic C3A hydration in presence of gypsum and lime, Journal of Materials Science. 44 (2009) 2038–2045. https://doi.org/10.1007/s10853-009-3292-3.
[50] S.T. Bergold, F. Goetz-Neunhoeffer, J. Neubauer, Interaction of silicate and aluminate reaction in a synthetic cement system: Implications for the process of alite hydration, Cement and Concrete Research. 93 (2017) 32–44. https://doi.org/10.1016/j.cemconres.2016.12.006.
[51] C. Jakob, D. Jansen, N. Ukrainczyk, E. Koenders, U. Pott, D. Stephan, J. Neubauer, Relating ettringite formation and rheological changes during the initial cement hydration: A comparative study applying XRD analysis, rheological measurements and modeling, Materials. 12 (2019). https://doi.org/10.3390/ma12182957.
[52] D. Jansen, J. Neubauer, F. Goetz-Neunhoeffer, R. Haerzschel, W.D. Hergeth, Change in reaction kinetics of a Portland cement caused by a superplasticizer - Calculation of heat flow curves from XRD data, Cement and Concrete Research. 42 (2012) 327–332. https://doi.org/10.1016/j.cemconres.2011.10.005.
[53] M. García-Maté, A.G. de La Torre, L. León-Reina, E.R. Losilla, M.A.G. Aranda, I. Santacruz, Effect of calcium sulfate source on the hydration of calcium sulfoaluminate eco-cement, Cement and Concrete Composites. 55 (2015) 53–61. https://doi.org/10.1016/j.cemconcomp.2014.08.003.
[54] X. Kong, J. Pakusch, D. Jansen, S. Emmerling, J. Neubauer, F. Goetz-Neuhoeffer, Effect of polymer latexes with cleaned serum on the phase development of hydrating cement pastes, Cement and Concrete Research. 84 (2016) 30–40. https://doi.org/10.1016/j.cemconres.2016.02.013.
[55] P.R. de Matos, J. Andrade Neto, R. Sakata, A.P. Kirchheim, E.D. Rodríguez, C. Campos, Strategies for XRD quantitative phase analysis of blended Portland cements, Cement and Concrete Research. Under revi (2022) 104571. https://doi.org/10.1016/j.cemconcomp.2022.104571.
[56] J.W. Bullard, H.M. Jennings, R.A. Livingston, A. Nonat, G.W. Scherer, J.S. Schweitzer, K.L. Scrivener, J.J. Thomas, Mechanisms of cement hydration, Cement and Concrete Research. 41 (2011) 1208–1223. https://doi.org/10.1016/B978-0-08-100693-1.00008-4.

[57] L. Huang, L. Tang, H. Gu, Z. Li, Z. Yang, New insights into the reaction of tricalcium silicate (C3S) with solutions to the end of the induction period, Cement and Concrete Research. 152 (2022) 106688. https://doi.org/10.1016/j.cemconres.2021.106688.
[58] J. Plank, M. Schönlein, V. Kanchanason, Study on the early crystallization of calcium silicate hydrate (C-S-H) in the presence of polycarboxylate superplasticizers, Journal of Organometallic Chemistry. 869 (2018) 227–232. https://doi.org/10.1016/j.jorganchem.2018.02.005.
[59] M.J. Sánchez-Herrero, A. Fernández-Jiménez, A. Palomo, C4A3Š hydration in different alkaline media, Cement and Concrete Research. 46 (2013) 41–49. https://doi.org/10.1016/j.cemconres.2013.01.008.
[60] B. Mota, T. Matschei, K. Scrivener, The influence of sodium salts and gypsum on alite hydration, Cement and Concrete Research. 75 (2015) 53–65. https://doi.org/10.1016/j.cemconres.2015.04.015.
[61] M.M. Alonso, F. Puertas, Adsorption of PCE and PNS superplasticisers on cubic and orthorhombic C3A. Effect of sulfate, Construction and Building Materials. 78 (2015) 324–332. https://doi.org/10.1016/j.conbuildmat.2014.12.050.
[62] C.W. Chung, P. Suraneni, J.S. Popovics, L.J. Struble, Using ultrasonic wave reflection to monitor false set of cement paste, Cement and Concrete Composites. 84 (2017) 10–18. https://doi.org/10.1016/j.cemconcomp.2017.08.010.
[63] R.M. Mota, A.S. Silva, V.H.S. Ramos, J.C.T. Rezende, E. de Jesus, Effects of storage temperature and time on false setting behavior of CPI-S Portland cement, Ceramica. 66 (2020) 321–329. https://doi.org/10.1590/0366-69132020663792842.

Hydration and interactions between pure and doped C_3S and C_3A in the presence of different calcium sulfates

José S. Andrade Neto[1,a*], Paulo R. de Matos[2,b], Angeles G. De la Torre[3,c], Carlos E. M. Campos[4,d], Sandro M. Torres[5,e], Paulo J. M. Monteiro[6,f], Ana Paula Kirchheim[1,g]

[1] Programa de Pós-Graduação em Engenharia Civil: Construção e Infraestrutura / Universidade Federal do Rio Grande do Sul (UFRGS) – Av. Osvaldo Aranha 99, Centro Histórico, 90035-190, Porto Alegre/RS, Brazil

[2] Universidade Federal de Santa Maria (UFSM).

[3] Departamento de Química Inorgánica, Cristalografía y Mineralogía, Universidad de Malaga, Campus Teatinos s/n., 29071 Málaga, Spain

[4] Laboratório de Difração de raios-X, Departamento de Física, Universidade Federal de Santa Catarina (UFSC)

[5] Departamento de Engenharia Mecânica, Universidade Federal da Paraíba (UFRB)

[6] Department of Civil and Environmental Engineering, University of California, Berkeley, CA 94720, USA

[a]jose.andrade@ufrgs.br, [b]paulo.matos@ufsm.br, [c]mgd@uma.es, [d]carlos.campos@ufsc.br, [e]sandromardentorres@yahoo.co.uk, [f]monteiro@ce.berkeley.edu, [g]anapaula.k@ufrgs.br

*Corresponding author.

ABSTRACT

This research studied the hydration of C_3S-C_3A-calcium sulfate systems made of combinations of two C_3S (pure triclinic and Al-doped monoclinic), two C_3A (pure cubic C_3A and Na-doped orthorhombic), and two calcium sulfates (gypsum and hemihydrate). For each system, the hydration of four different SO_3 contents (0.25-2.0 wt%) was assessed by calorimetry. The optimum SO_3 content was fixed from calorimetry results, and the mixtures were evaluated by *in-situ* XRD and TGA. The type of C_3S was the factor that most affected the sulfate balance of the systems. The mixes with Al-C_3S produced a higher amount of ettringite in the first hours, resulting in much earlier sulfate depletions when compared to the mixes with pure C_3S. The mixes with ort-C_3A also showed faster sulfate depletion due to its higher reactivity compared with cb-C_3A. Finally, the replacement of gypsum by hemihydrate resulted in faster sulfate depletion caused by the faster hemihydrate dissolution.

Keywords: C_3S; C_3A; Calcium sulfate; Polymorphism; Hydration.

1 INTRODUCTION

Calcium sulfate, such as gypsum and/or anhydrite, is added to the Portland clinker to control the C_3A[§] hydration and prevent flash set [1]. In addition, the amount of calcium sulfate added needs to be enough to delay the renewed hydration of C_3A until after the main C_3S hydration peak. Otherwise, the C_3S hydration is hindered, negatively affecting the early strength of Portland cement (PC) concrete [1]. However, if an excess of sulfate is used, the mechanical strength decreases [1–4], and durability problems with delayed ettringite formation (DEF) in pastes cured at high temperatures may occur [5,6]. Thus, there is an optimum sulfate content in which the mixture presents the lowest shrinkage and highest compressive strength without causing quick setting and DEF problems. In a properly sulfated cement, the calcium sulfate depletion and the renewed hydration of C_3A occur after the main C_3S hydration. Therefore, factors interfering in sulfate's supply or consumption will affect the optimum sulfate content [1,7]. Sulfate ions are mainly supplied by calcium and alkaline sulfates dissolution and consumed by the ettringite formation and C-S-H adsorption [1].

Zunino and Scrivener [7] showed that increasing C_3S and C_3A fineness – and consequently their reactivities – increases the C-S-H and ettringite formation and increases the optimum amount of calcium sulfate. In addition to their fineness, the polymorphism and ion doping of C_3S and C_3A also change their reactivities [1,8–14]. However, to the best of the authors' knowledge, no systematic study regarding the aluminum doping of C_3S and C_3A polymorphism on the optimum sulfate content was reported. The correct understanding of the influence of polymorphism or ion doping on the optimization of sulfates is essential to ensure that the cements meet performance requirements.

The incorporation of aluminum in C_3S decreases its reactivity [8–11]. With aluminum-doped C_3S (Al-C_3S) dissolution, the aluminum ions are released in the solution, which is known to retard C_3S hydration [10,15–17]. The reason for that is not clear, but it may be related to the formation of C-A-S-H, which according to some authors [10,16] is not a good substrate for the C-S-H growth as the C-S-H nuclei itself, or it may be related to the condensation of aluminum-silicate species at C_3S surface [15,17]. Either way, the delay in the C_3S hydration decreases the amount of C-S-H formed in the first days and tends to

[§] C = CaO; S = SiO_2; A = Al_2O_3; H = H_2O.

reduce the amount of sulfate consumption due to adsorption by C-S-H. However, the aluminum coming from Al-C_3S dissolution may contribute to ettringite formation. Although, as pointed out by Jansen et al. [18], it is not yet clear if the aluminum coming from the alite/Al-C_3S plays a role in the sulfate demand or not. Therefore, the incorporation of aluminum in C_3S may change the optimum sulfate content of cement, but which phenomenon is predominant (i.e., lower sulfate adsorption by C-S-H or higher sulfate consumption by ettringite formation) is still not known.

Regarding the aluminates, the polymorphism of C_3A depends on the sulfate/alkali balance during clinker production and therefore the alkali content incorporated in the C_3A structure. In industrial Portland clinkers, the C_3A may be present as cubic (cb-C_3A) and/or orthorhombic (ort-C_3A) polymorphs [19,20], depending on the raw materials and fuel used. Despite forming the same hydration products (ettringite and AFm phases), ort-C_3A reacts much faster than cb-C_3A in the presence of calcium sulfate [12–14]. This will probably influence the sulfate balance in the PC hydration, but no study regarding this has been published to date, and there is a gap on this topic.

Finally, during cement milling, gypsum ($CaSO_4 \cdot 2H_2O$) may dehydrate into hemihydrate ($CaSO_4 \cdot 1/2H_2O$) and/or soluble anhydrite ($CaSO_4$), which dissolves faster than gypsum or natural anhydrite [21,22]. As shown by previous studies, gypsum delays the initial hydration of C_3S, prolonging the induction period, but enhances afterward, resulting in higher main heat flow peaks. However, no studies regarding the effect of hemihydrate on C_3S have been conducted yet. In relation to C_3A, as showed by Andrade Neto et al. [14], gypsum replacement with hemihydrate did not significantly influence cb-C_3A but accelerated ort-C_3A reaction. The authors used only one sulfate/C_3A ratio, and the effect of different gypsum/hemihydrate content on the cb- and ort-C_3A hydration needs further studies to understand better its impact on the sulfate balance of Portland cements.

Zunino and Scrivener [7] studied the T1-C_3S/cb-C_3A systems and reported that the use of hemihydrate instead of gypsum resulted in higher ettringite precipitation until the renewed hydration of C_3A. This occurs due to the faster dissolution rate of hemihydrate than gypsum, resulting in more sulfate ions in the pore solutions [7]. The higher ettringite precipitation leads to an earlier sulfate depletion, increasing the sulfate demand of the mixtures. However, how this change in sulfate source will influence the sulfate balance

of systems with Al-C_3S or with ort-C_3A, which have quite different reactivities than C_3S and cb-C_3A, is an important question to answer.

This study aims to evaluate the influence of the aluminum doping C_3S, the C_3A polymorph, and the calcium sulfate type on the hydration and sulfate demand of the system and their interactions. Additionally, the effect of calcium sulfate composition (gypsum/hemihydrate) on the C_3S and Al-C_3S hydration and the effect of different gypsum/hemihydrate contents on the cb-C_3A and ort-C_3A hydrations were studied. First, the hydration of the C_3S and C_3A polymorphs (alone and in the presence of gypsum or hemihydrate) was evaluated separately through isothermal calorimetry. Then, ternary mixes of both types of C_3S and C_3A in a constant C_3S/C_3A ratio of 92/8 were produced with four different contents of gypsum or hemihydrate and were evaluated by calorimetry. Finally, an optimum SO_3 content was fixed from these results, and the hydration of the ternary mixes was evaluated by *in-situ* XRD and TGA.

2 MATERIALS AND METHODS

2.1 Materials

Powder samples of C_3S, aluminum-doped C_3S (Al-C_3S), cubic C_3A (cb-C_3A), and orthorhombic C_3A (ort-C_3A) were acquired from Mineral Research Processing Cie (MRPC, France). The C_3S and Al-C_3S were synthesized at MRPC by heating a stoichiometric mixture of reagent grade $CaCO_3$ and SiO_2 at around 1450°C. Cb-C_3A and ort-C_3A were synthesized by heating twice at 1350°C, a stoichiometric mixture of calcium carbonate ($CaCO_3$) and alumina (Al_2O_3). For the ort-C_3A, sodium carbonate ($NaCO_3$) was also used. High purity (>96 wt%) natural gypsum ($CaSO_4{\cdot}2H_2O$) and hemihydrate ($CaSO_4{\cdot}1/2H_2O$) were used as calcium sulfate sources. Hemihydrate was prepared by heating the gypsum at 100 °C for 48 hours. Details about elemental composition and mineralogy have been reported elsewhere [11,14] and are presented in the Supplementary Materials (Tables S1 and S2). The C_3S mainly consists of triclinic (T_1) C_3S (95.7 wt%), while the Al-C_3S has 98.7 wt% of monoclinic (M_1) C_3S. The C_3S does not have aluminum in its composition, while Al-C_3S has 0.8 wt%. Cub-C_3A has 96.9 wt% of cubic C_3A, while ort-C_3A has 94.4 wt% of orthorhombic C_3A and 5.6 wt% of cubic C_3A. Finally, the gypsum contains 96.1 wt% of $CaSO_4{\cdot}(H_2O)_2$, and the hemihydrate contains 97.2 wt% of bassanite (crystalline $CaSO_4{\cdot}(H_2O)_{0.5}$).

The particle size distribution was determined by laser diffraction, using a PSA 1090 equipment from Anton Paar (Graz, Austria), using isopropanol as the dispersant, and considering Mie theory [23]. The BET surface area was determined using an ASAP 2420 equipment from Micromeritics (Georgia, USA). The physical characterization results of the raw materials are presented in Table 1.

Table 1 – Physical characterization of the raw materials.

Property	**C_3S**	**Al-C_3S**	**cub-C_3A**	**orth-C_3A**	**Gypsum**	**Hemihydrate**
BET surface area (m^2/g)	1.14	1.08	1.42	1.13	1.33	1.38
D_v 90 (μm)	16.9	32.4	30.8	28.7	51.8	40.8
D_v 50 (μm)	6.7	11.6	7.5	7.6	16.9	14.8
D_v 10 (μm)	1.5	1.7	1.6	1.8	3.6	3.5

2.2 Methods

2.2.1 *Mixture proportions and sample preparation*

Firstly, the hydration of C_3S and Al-C_3S alone and in the presence of gypsum or hemihydrate were evaluated by isothermal calorimetry (IC) (see Section 2.2.2). Table 2 presents the mix proportions of the C_3S pastes evaluated. For this purpose, a water-to-solid ratio of 0.50 by mass was used. In the mixes with gypsum or hemihydrate, the C_3S was replaced with the amount of calcium sulfate to result in an SO_3 content of 1.5 wt% (≈ 3.22-3.26 wt% of gypsum or ≈ 2.81-2.85 wt% of hemihydrate). This SO_3 content was chosen because it resulted in properly sulfated C_3S/C_3A mixes (see Section 3.1.2) and was used to analyze the ternary systems. For this purpose, the SO_3 present in C_3S and Al-C_3S were also considered, so the amounts weighed were slightly different.

Table 2 – Mix proportions of the C_3S pastes.

Id	C_3S type	Calcium sulfate type	C_3S (wt%)	Calcium sulfate (wt%)	SO_3 (wt%)	w/s ratio	Tests performed
C_3S_wo/C$	C_3S	-	100	0	0	0.5	IC
C_3S_3.22% GYP	C_3S	Gypsum	96.78	3.22	1.5		
C_3S_2.81% HEM	C_3S	Hemihydrate	97.19	2.81	1.5		
Al-C_3S_wo/C$	Al-C_3S	-	100	0	0		
Al-C_3S_3.26% GYP	Al-C_3S	Gypsum	96.74	3.26	1.5		
Al-C_3S_2.85% HEM	Al-C_3S	Hemihydrate	97.15	2.85	1.5		

The hydration of cb-C_3A and ort-C_3A, alone and in the presence of gypsum or hemihydrate, were also assessed by calorimetry. Table 3 presents the mix design of the C_3A pastes evaluated. A water-to-solid ratio of 1.0 by mass was used for these mixes because it is enough to hydrate the C_3A fully and provide good workability. Different amounts of calcium sulfate were used, resulting in mixtures with SO_3-to-C_3A ratios of 0, 0.03, 0.06 and 0.12 by weight (≈ 0, 5.9, 11.6, and 21.4 wt% of gypsum or ≈ 0, 5.2, 10.3, 19.2 wt% of hemihydrate). These values were chosen as it corresponds to the SO_3-to-C_3A ratios of the ternary mixes (see Table 4) with 0.25, 0.50 and 1.00 wt% of SO_3, respectively.

Table 3 – Mix proportions of the C_3A pastes.

Id	C_3A type	Calcium sulfate type	C_3A (wt%)	Calcium sulfate (wt%)	SO_3/ C_3A	w/s ratio	Tests performed
cb-C_3A_wo/C$	cb-C_3A	-	100	0	0	1.0	IC
cb-C_3A_5.9% GYP	cb-C_3A	Gypsum	94.1	5.9	0.03		
cb-C_3A_11.6% GYP	cb-C_3A	Gypsum	88.4	11.6	0.06		
cb-C_3A_21.4% GYP	cb-C_3A	Gypsum	78.6	21.4	0.12		
cb-C_3A_5.2% HEM	cb-C_3A	Hemihydrate	94.8	5.2	0.03		
cb-C_3A_10.3% HEM	cb-C_3A	Hemihydrate	89.7	10.3	0.06		
cb-C_3A_19.2% HEM	cb-C_3A	Hemihydrate	80.8	19.2	0.12		
ort-C_3A_wo/C$	ort-C_3A	-	100	0	0		
ort-C_3A_5.9% GYP	ort-C_3A	Gypsum	94.1	5.9	0.03		
ort-C_3A_11.6% GYP	ort-C_3A	Gypsum	88.4	11.6	0.06		
ort-C_3A_21.4% GYP	ort-C_3A	Gypsum	78.6	21.4	0.12		
ort-C_3A_5.2% HEM	ort-C_3A	Hemihydrate	94.8	5.2	0.03		
ort-C_3A_10.3% HEM	ort-C_3A	Hemihydrate	89.7	10.3	0.06		
ort-C_3A_19.2% HEM	ort-C_3A	Hemihydrate	80.8	19.2	0.12		

Mixtures of C_3S (pure C_3S or Al-C_3S) with C_3A (cb-C_3A or ort-C_3A) and different amounts of gypsum or hemihydrate were evaluated, as presented in Table 4. The C_3S/C_3A ratio was fixed at 92/8 by weight, which is the same ratio used by Zunino and Scrivener [7] and Quennoz and Scrivener [24] and is similar to the ratio usually found in Portland cement clinkers. The water/solid ratio of all mixtures was kept at 0.50 by weight. Firstly, the hydration of C_3S/C_3A pastes was evaluated by isothermal calorimetry in systems with four different contents of calcium sulfate (gypsum or hemihydrate): 0.25, 0.50, 1.00 and 1.50 wt% for the systems with C_3S and 0.50, 1.00, 1.50 and 2.00 wt% of SO_3 for the systems with Al-C_3S. These SO_3 content considered the SO_3 from C_3S, C_3A and calcium sulfate. From these results, 1.5 wt% SO_3 content was fixed for all the mixtures for the other analysis, i.e., *in situ* XRD and TGA (see sections 2.2.3, 2.2.4, and 2.2.5, respectively). This content was chosen since none of the C_3S/C_3A systems was undersulfated on this level of sulfates (for more details, see section 3.1.3).

1 Table 4 – Mix proportions of the C_3S-C_3A pastes.

Id	C_3S type	C_3A type	Calcium sulfate type	C_3S (wt%)	C_3A (wt%)	Calcium sulfate (wt%)	SO_3 (wt%)	w/s ratio	Tests performed
C_3S_(cb, ort)-C_3A_0.50% GYP	C_3S	(cb, ort)-C_3A	Gypsum	91.54	7.96	0.50	**0.25**	0.50	IC
C_3S_(cb, ort)-C_3A_1.04% GYP	C_3S	(cb, ort)-C_3A	Gypsum	91.04	7.92	1.04	**0.50**	0.50	IC
C_3S_(cb, ort)-C_3A_2.13% GYP	C_3S	(cb, ort)-C_3A	Gypsum	90.04	7.83	2.13	**1.00**	0.50	IC
C_3S_(cb, ort)-C_3A_3.22% GYP	C_3S	(cb, ort)-C_3A	Gypsum	89.04	7.74	3.22	**1.50**	0.50	IC, *in-situ* XRD, TGA
C_3S_(cb, ort)-C_3A_0.44% HEM	C_3S	(cb, ort)-C_3A	Hemihydrate	91.60	7.97	0.44	**0.25**	0.50	IC
C_3S_(cb, ort)-C_3A_0.91% HEM	C_3S	(cb, ort)-C_3A	Hemihydrate	91.16	7.93	0.91	**0.50**	0.50	IC
C_3S_(cb, ort)-C_3A_1.86% HEM	C_3S	(cb, ort)-C_3A	Hemihydrate	90.29	7.85	1.86	**1.00**	0.50	IC
C_3S_(cb, ort)-C_3A_2.81% HEM	C_3S	(cb, ort)-C_3A	Hemihydrate	89.41	7.78	2.81	**1.50**	0.50	IC, *in-situ* XRD, TGA
Al-C_3S_(cb, ort)-C_3A_1.08% GYP	Al-C_3S	(cb, ort)-C_3A	Gypsum	91.01	7.91	1.08	**0.50**	0.50	IC
Al-C_3S_(cb, ort)-C_3A_2.17% GYP	Al-C_3S	(cb, ort)-C_3A	Gypsum	90.01	7.83	2.17	**1.00**	0.50	IC
Al-C_3S_(cb, ort)-C_3A_3.25% GYP	Al-C_3S	(cb, ort)-C_3A	Gypsum	89.01	7.74	3.25	**1.50**	0.50	IC, *in-situ* XRD, TGA
Al-C_3S_(cb, ort)-C_3A_4.34% GYP	Al-C_3S	(cb, ort)-C_3A	Gypsum	88.01	7.65	4.34	**2.00**	0.50	IC
Al-C_3S_(cb, ort)-C_3A_0.94% HEM	Al-C_3S	(cb, ort)-C_3A	Hemihydrate	91.13	7.92	0.94	**0.50**	0.50	IC
Al-C_3S_(cb, ort)-C_3A_1.89% HEM	Al-C_3S	(cb, ort)-C_3A	Hemihydrate	90.26	7.85	1.89	**1.00**	0.50	IC
Al-C_3S_(cb, ort)-C_3A_2.84% HEM	Al-C_3S	(cb, ort)-C_3A	Hemihydrate	89.38	7.77	2.84	**1.50**	0.50	IC, *in-situ* XRD, TGA
Al-C_3S_(cb, ort)-C_3A_3.79% HEM	Al-C_3S	(cb, ort)-C_3A	Hemihydrate	88.51	7.70	3.79	**2.00**	0.50	IC

2

For paste preparation, 2 g of anhydrous materials (C_3S, C_3A, and calcium sulfate) were previously manually mixed in an agate mortar for 10 minutes, subsequently mixed with distilled water at 350 rpm for 2 minutes using a rotational mixer. For the calorimetry analysis, the mixing procedure was conducted in the glass ampoule used in the test. The plastic rod was left inside the glass ampoule to minimize material loss during mixing. The mixing procedure and insertion of glass ampoule in the calorimetry took less than 3 minutes after the initial contact with the water. For the TGA and *in-situ* XRD tests, the mixes were prepared in plastic vessels. For the TGA analysis, the paste remained inside the hermetically closed vessels until the hydration stoppage.

The hydration of the pastes was stopped at 8 hours, 1, 3, and 7 days for the TGA. The pastes were first ground to a fine powder using an agate mortar. Then, ~0.5 g of each paste was mixed with 25 ml of isopropanol for 30 minutes while stirring. In the sequence, the sample was filtered at a low vacuum through a nylon filter with a 15 µm opening for 10 minutes and dried in an oven at 40°C for another 10 minutes.

2.2.2 *Isothermal calorimetry (IC)*

For the IC analyses, an eight-channel Thermal Activity Monitor of Tam Air, TA Instruments (New Castle, DE, USA) was used. The pastes were mixed *ex-situ* but inside the glass ampoule, as described in item 2.2.1. A glass ampoule with distilled water was used as the reference. The amount of distilled water was defined according to Wadsö [25] to obtain a similar heat capacity of C_3S/C_3A pastes. The heat flow and the cumulative heat were recorded for 48 hours at 22 °C for all the pastes.

2.2.3 *Thermogravimetry analysis (TGA)*

The TGA of the pastes at 8 hours, 1, 3, and 7 days were performed in a TGA 2 analyzer from Mettler Toledo (Columbus, Ohio, USA). The samples were placed in open alumina crucibles under airflow, and the temperature varied between room temperature (RT) and 1000°C with a heating rate of 20 °C/min.

From TGA results, the bound water and the portlandite contents were determined. After stopping the hydration, the bound water of the pastes after stopping hydration content was assigned to the weighed loss from RT to 550°C. Eq. 1 calculates the actual bounded water and Eq. 2 determines the amount of free water [26].

$$\mathrm{BW} = \frac{\mathrm{BW_{ATD}} \cdot \mathrm{CM}}{100 - \mathrm{BW_{ATD}}} \quad (1)$$

$$\mathrm{FW} = \mathrm{TW} - \mathrm{BW} \quad (2)$$

Where BW corresponds to actual chemically bound water content; BW_{ATD} is the mass loss measured between RT and 550ºC from TGA curves; CM is the cement (C_3S + C_3A + calcium sulfate) content; TW is the total water content added (all the numbers in weight percentages).

Also, the portlandite content was determined by Eq. 3 [27].

$$Ca(\mathrm{OH})_{2,\mathrm{measured}} = \mathrm{WL}_{\mathrm{Ca(OH)_2}} \cdot \frac{\mathrm{m}_{\mathrm{Ca(OH)_2}}}{\mathrm{m}_{\mathrm{H_2O}}} \quad (3)$$

Where $\mathrm{WL}_{\mathrm{Ca(OH)_2}}$ is the weight loss due to the evaporation of water, obtained by the integration of DTG peak located in the temperature range from ~400 to ~500 ºC using the tangential method [27]; $\mathrm{m}_{\mathrm{Ca(OH)_2}}$ is the molecular mass of portlandite (74 g/mol); and $\mathrm{m}_{\mathrm{H_2O}}$ is the molecular mass of water (18 g/mol).

The total mass of solids increases with C_3S/C_3A hydration progress, as free water is bound into hydration products. Therefore, the portlandite content obtained by TGA was normalized per 100 g of paste according to Eq. 4.

$$Ca(\mathrm{OH})_{2,\mathrm{rescaled}} = Ca(\mathrm{OH})_{2,\mathrm{measured}} \cdot \frac{(100 - \mathrm{FW})}{100} \quad (4)$$

Where $Ca(\mathrm{OH})_{2,\mathrm{rescaled}}$ is the portlandite content in g/100 g of paste; $Ca(\mathrm{OH})_{2,\mathrm{measured}}$ is the portlandite content obtained by TGA; and FW is the free water content determined by TGA according to Eq. 2.

2.2.4 *In-situ X-ray diffraction (In-situ XRD)*

In-situ XRD was conducted using an X'Pert Pro (PANalytical) diffractometer operating at 45 kV and 40 mA, equipped with an X'Celerator detector with an active length of 2.122°. The following experimental setup was used: Bragg–Brentano θ-2θ geometry with a 240 mm radius goniometer; CuKα radiation with a wavelength of 1.5418 Å; a 0.04 rad Soller slit, a 10 mm beam mask, a 1° fixed anti-scatter slit, and a 1/2° fixed divergence

slit on the incident beam; a 5.0 mm fixed anti-scatter slit, a 0.04 rad Soller slit, and a 0.020 mm Ni filter on the diffracted beam; and knife-edge at the first division.

For this analysis, scans were recorded at the range from 7 to 55° 2θ with a counting time of 24.76 seconds per step, totaling about 10 minutes per scan. The fresh sample was placed on the sample holder and immediately covered with a Kapton film to prevent water loss and carbonation. The measurements started 30 minutes after the first contact between the water and the dry materials and were recorded for 48 hours. Three samples were tested alternatively, placed at an X-ray beam automatically by a robotic arm, providing an XRD pattern for each sample every 30 minutes. Immediately before each 48-hour measurement set, a corundum (α-Al_2O_3) sample covered with Kapton was measured in the same testing conditions to be used as an external standard.

Rietveld quantitative phase analysis (QPA) was conducted using TOPAS v.5 software [28], and the crystallographic information files used are detailed in Table 5. All the XRD patterns of each mix were refined together, and the same refinement steps were applied for each group of patterns (i.e., for each mix). The refinement of *in-situ* XRD data is somehow delicate since it deals with simultaneous amorphous contributions (e.g., C-S-H, free water and Kapton film), besides analyzing several files and phases simultaneously [29]. Thus, using an adequate refinement strategy is essential due to two main reasons: (i) a good strategy improves the robustness of the analysis and reduces the chances of drifting; and (ii) a well-defined script improves the consistency of the analysis for different operators or for a sequence of patterns related to the same starting material (e.g., a time-dependent series) [30]. In this work, the contribution of C-S-H was considered by using the model proposed by Bergold et al. [31]; the diffuse contributions of the Kapton film and the free water were modeled using *hkl* phases with the space groups *P4/mmm* (n° 123) and $Fm\bar{3}$ (n° 202), respectively, as suggested by Scherb et al. [32]. The steps used for the free water and the Kapton film phase models creation and the refinement strategy conducted in this work are detailed in Ref. [14], while Figure 1 and Figure S1 illustrate fitted *in-situ* XRD patterns.

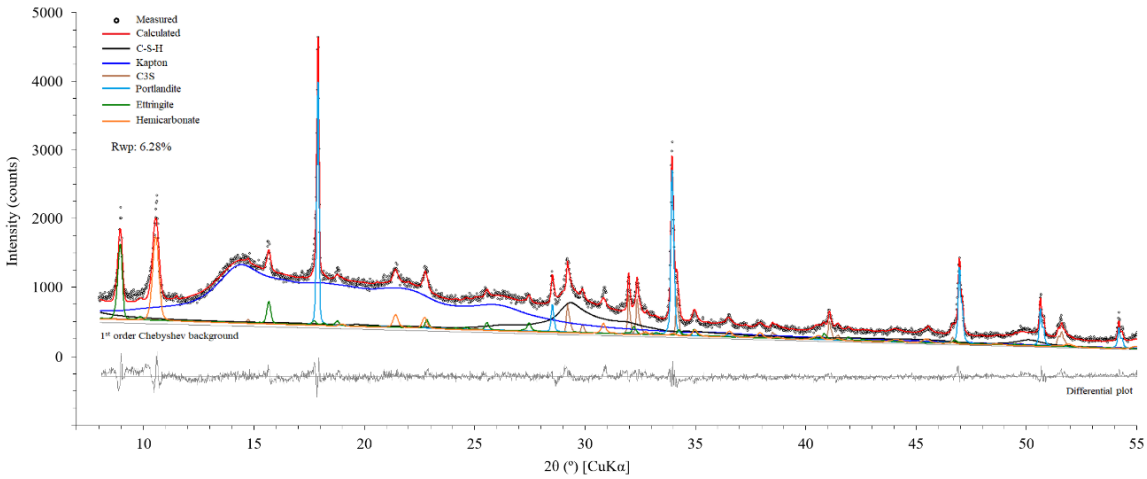

Figure 1 – Example of fitted *in-situ* XRD pattern (for Al-C_3S_cb-C_3A_GYP at 48 hours of hydration).

The absolute weight fraction of each crystalline phase was determined by the external standard method [33] using the G-factor approach (Eqs. 5-6) [34]. The corundum sample covered with Kapton was used as an external standard for this purpose. The mass absorption coefficient (MAC) of the paste was calculated from the chemical composition of the powder fraction and the water MAC.

$$W_i = S_i \frac{\rho_i V_i^2}{G} \mu^* \quad (5)$$

$$G = S_s \frac{\rho_s V_s^2 \mu_s}{W_s} \quad (6)$$

where W is the weight fraction of the phase (i) or the standard (s), in wt%; S is the refined scale factor of the phase (i) or the standard (s); ρ is the density of the phase (i) or the standard (s), V is the unit cell volume of the phase (i) or the standard (s) in Å³; and μ is the MAC of the sample (*) or the standard (s), in cm²/g. The density and unit cell volume of each phase are presented in Table 5, and the MAC of the raw materials and pastes are presented in the Supplementary Materials (Tables S1 and S3).

The weight fraction of C-S-H was calculated using the mass balance given by Eq. (7) [35,36] together with the factor F given by Eq. (8) [31]. Firstly, the expected amount of C-S-H formed after 48 hours was calculated from the amount of alite consumed at this age (i.e., the difference between the initial amount added and that determined by XRD after 48 hours) using Eq. (7). Then, factor F was determined using Eq. (5); by setting *Wi* equal to the C-S-H content yielded by the stoichiometric calculation and knowing the G and μ* terms, the only unknown part of Eq. (5) is $\rho \cdot V^2$, i.e., the factor F. The calibration

of factor F with the last measurement of each *in-situ* sample resulted in an F = 1.11 ± 0.03×10^{-45} g·cm³ (average ± standard deviation). It is stressed that the stoichiometry of C-S-H is not well defined, but since alite is the only silicate in the system, it seems reasonable to assume the mass balance of Eq. (7). The stoichiometry of C-S-H was considered as $C_{1.8}SH_{4.0}$, which is the average composition of C-S-H formed by the C_3S hydration according to Cuesta et al. [35,36]. It is worth highlighting that recent studies suggested the incorporation of sulfate anions into C-S-H [37], changing its stoichiometry, and this actual stoichiometry would depend on the sulfate availability and incorporation level. Thus, the absence of a well-defined stoichiometry for this case prevents us from using a more accurate model.

$$C_3S + 5.2\ H \rightarrow C_{1.8}SH_{4.0} + 1.2\ CH \quad (7)$$

$$F = \rho.V^2 \quad (8)$$

Table 5 – Crystallographic information files (CIFs) used for Rietveld QPA.

Phase	ICSD code	Unit cell volume (Å³)	Density (g/cm³)	Reference
C_3S T1	4331	2167.64	3.148	Golovastikov et al. [38]
C_3S M1	---	2175.02	3.138	de Noirfontaine et al. [39]
C_3A cubic	1841	3557.89	3.027	Mondal and Jeffery [40]
C_3A orthorhombic	1880	1790.35	3.018	Nishi and Takeuchi [41]
Portlandite	15471	54.49	2.260	Petch [42]
Ettringite	155395	2345.34	1.780	Goetz-Neunhoeffer and Neubauer [43]
Gypsum	151692	496.25	2.304	De la Torre et al. [44]
Bassanite (Hemihydrate)	69060	1060.51	2.727	Bezou et al. [45]
Hemicarbonate	263124	1410.15	1.900	Runčevski et al. [46]

Note.: The unit cell volume and density values for both C_3S and C_3A polymorphs, gypsum and bassanite were refined in dry samples, while those for portlandite, ettringite and hemicarbonate correspond to the theoretical values from the CIF files.

3 RESULTS

3.1 Isothermal calorimetry

3.1.1 Effect of the calcium sulfate source on C_3S and Al-C_3S hydration

Figure 2a and b show the heat flow and cumulative heat curves of the C_3S and Al-C_3S pastes, respectively, without calcium sulfate and with gypsum and hemihydrate (1.5 wt% SO_3), within the first 48 hours of hydration. Comparing the mixtures without calcium sulfate, C_3S hydrated much faster than the Al-C_3S, generating a higher heat flow peak and higher cumulative heat at 48 hours. These results agree well with previous studies [8–10] and are probably due to the effect of aluminum ions in solution leading to a delay and suppression of C_3S hydration. In addition, the larger particle size of Al-C_3S (see Table 1) probably contributed to the lower reactivity of this phase.

The addition of gypsum had similar effects in both C_3S and Al-C_3S hydration: a slight extension in the induction period but an enhancement in the hydration kinetics after its end, increasing the main heat flow peak. This agrees with previous studies which evaluated the hydration of C_3S in the presence of gypsum. The initial delay is probably related to the adsorption of sulfate ions in the C_3S surface, delaying its dissolution [17,47]. In turn, the enhancement in the main hydration peak may result from a change in the C-S-H morphology and the increase in the ionic strength of the pore solution [11].

The hemihydrate had a very similar effect than gypsum on both C_3S and Al-C_3S. Therefore, for the first time, it is observed that the faster dissolution of hemihydrate does not seem to impact differently than gypsum the C_3S hydration.

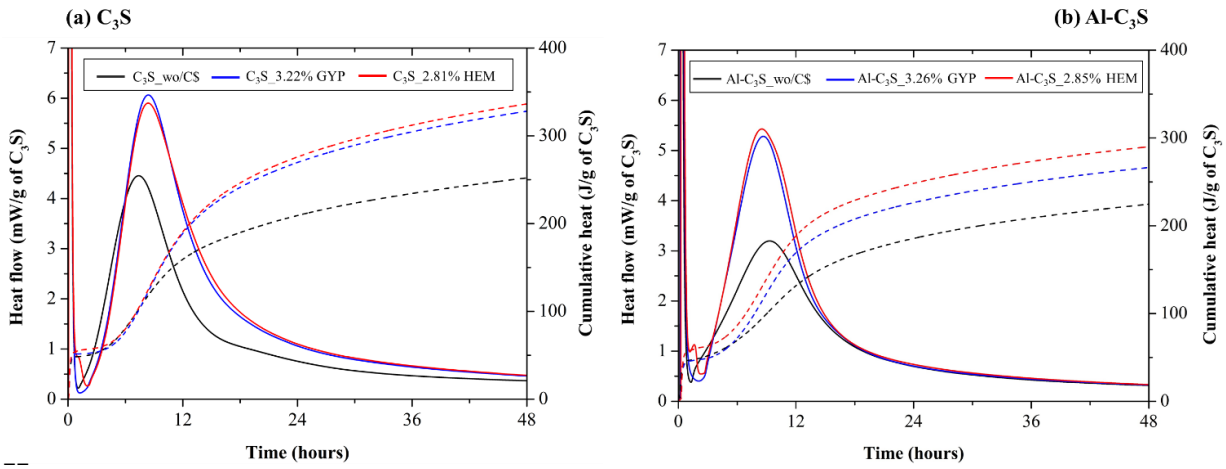

Figure 2 – Heat flow curves (solid lines) and cumulative heat curves (dashed lines) of the (A) C_3S and (B) Al-C_3S pastes during the first 48 hours of hydration.

3.1.2 Effect of the calcium sulfate source on cb-C_3A and ort-C_3A hydration

Figure 3a and b show the heat flow and cumulative heat curves of cub-C_3A and ort-C_3A, respectively, without calcium sulfate and with different levels of gypsum and hemihydrate (0.25, 0.50 and 1.00 wt% of SO_3) during the first 90 hours of hydration. For better visualization, Figure S2 presents the comparison of cb and ort-C_3A without and with 1.00 wt% of SO_3. Without calcium sulfate, cb-C_3A hydration results in a higher heat released in the first 48 hours than ort-C_3A. This behavior was also observed in previous studies [12,13,48].

The addition of calcium sulfate (gypsum or hemihydrate) delayed both cb- and ort-C_3A initial hydration, and this retarding effect was much stronger on the former. As for the cb-C_3A mixes, those with 5.9%, 11.6% and 21.4% of gypsum presented induction periods of 2.5, 3.2, and 9.6 h, respectively, while those with 5.2%, 10.3% and 19.2% of hemihydrate presented induction periods of 4.7, 5.4, and 12.9 h, respectively. In turn, the ort-C_3A mix with 21.4% of gypsum presented an induction period of 0.8 h (8.8 h less than the cb-C_3A mix with the corresponding amount of gypsum) and the ort-C_3A mix with 19.2% of hemihydrate presented an induction period of 2.7 h (10.2 h less than cb-C_3A mix with the corresponding amount of hemihydrate). Similar behaviors were observed by several authors [12–14,49]. The lower retarding effect of calcium sulfate in ort-C_3A hydration compared with the cb-C_3A hydration happens because the sodium-doping of ort-C_3A increases the solubility of $Al_6O_{18}^{18-}$, preventing the formation of the Al-rich leached layer on the C_3A particles, inhibiting the adsorption of SO_4^{2-} and/or Ca–SO_4 ion-pair that are responsible for the delay in cb-C_3A hydration [13,14].

Interestingly, the hemihydrate seems to be more effective in retarding the ort-C_3A hydration in the SO_3/C_3A ratios tested (while 21.4% of gypsum resulted in an induction period of 0.8 h, 19.2% of hemihydrate resulted in an induction period of 2.7 h). This is in contrary to what was observed by Andrade Neto et al. [14], in which the replacement of gypsum by hemihydrate led to an acceleration in the ort-C_3A hydration when using a much higher SO_3/C_3A ratio (0.29, i.e., gypsum content of 38.92% and hemihydrate content of 35.78%). The reasons for that are not clear yet and further studies are necessary.

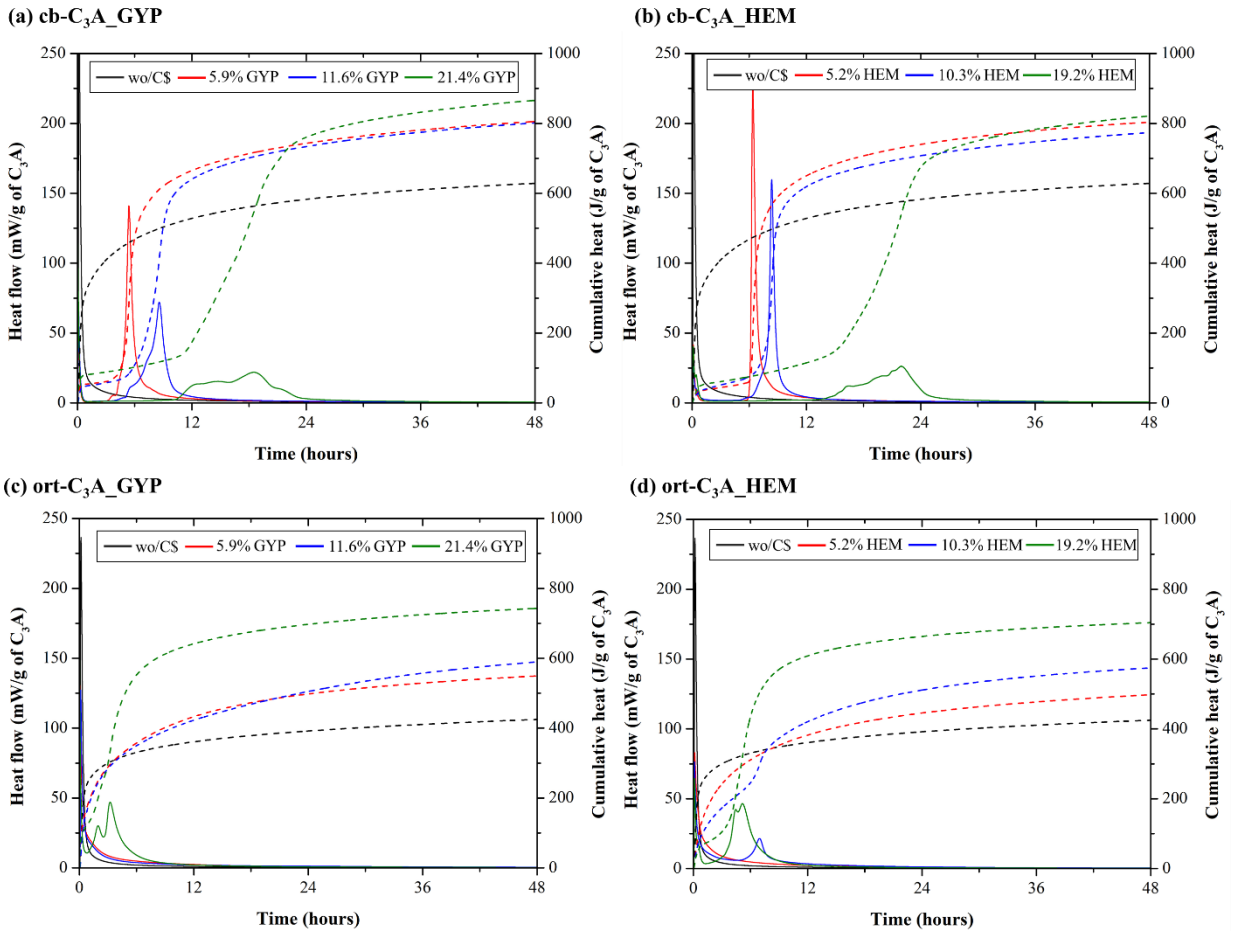

Figure 3 – Heat flow curves (solid lines) and cumulative heat curves (dashed lines) of the (a) cb-C_3A_GYP, (b) cb_C_3A-HEM, (c) ort-C_3A_GYP and (D) ort-C_3A_HEM pastes during the first 48 hours of hydration, the legend indicates the amount of gypsum or hemihydrate, which correspond to 0.25, 0.50 and 1.00 wt% of SO_3.

3.1.3 Effect of the SO_3 content on C_3S/C_3A systems

The heat flow curves of the C_3S/C_3A pastes with different contents of gypsum or hemihydrate are presented in Figure 4. The silicate and aluminate hydration heat flow peaks are indicated.

By comparing the hydration of the C_3S/C_3A/calcium sulfate systems (Figure 4) with the C_3S/calcium sulfate systems (Figure 2), it is possible to see that in undersulfated mixes (i.e., when the sulfate depletion and the renewed hydration of C_3A occur earlier than the main C_3S hydration peak), the hydration of both C_3S and Al-C_3S was retarded and suppressed. This agrees with previous results [7,24,50], and probably occurs due to the earlier C_3A dissolution, releasing a significant amount of aluminum into the solution. As discussed in Section 3.1.1, aluminum retards and suppresses the C_3S hydration – whether

due to the formation of alumino-silicate species on the C_3S surface, hindering its dissolution, or due to the C-A-S-H formation. In turn, in the proper sulfated mixes (i.e., when the sulfate depletion and the renewed hydration of C_3A happens after the main C_3S hydration peak), the C_3S and Al-C_3S hydration occurred as in the C_3S/calcium sulfate mixtures, with the maximum heat flow peak happening around 8 hours. In the proper sulfated mixes (> 0.50 wt% SO_3 for the C_3S mixes and 2.0 wt% SO_3 for the Al-C_3S mixes), the C_3A polymorphism does not seem to significantly influence the C_3S or Al-C_3S hydration rate. For these mixtures, regardless of the C_3A type, the induction period length and the silicate peak are very similar, indicating very similar C_3S hydration rates.

As for C_3A, the time for the renewed hydration of cb-C_3A occurred much earlier in the three-phase systems with the Al-C_3S (Figure 4) than in the C_3A pastes (Figure 3) even for the same SO_3/C_3A ratios. One can note that the time of occurrence of the aluminate peak (indicated as Ap) in Figure 4(c,d) is around 4-5 hours for the ternary mixes with 0.5 wt% SO_3 and around 8-10 hours for the ternary mixes with 1.0 wt% SO_3. In turn, for the cb-C_3A_(GYP, HEM) pastes (see Figure 3), the time for the aluminate peak is around 7-8 hours for the mixes with 11.6% of gypsum and those with 10.3% of hemihydrate and around 12-14 hours for the mixes with 21.4% of gypsum and those with 19.2% of hemihydrate -these C_3A pastes have the same SO_3/C_3A ratios of the three-phase systems with 0.5 wt% and 1.0 wt% of SO_3. This happens in the ternary mixes with Al-C_3S as the higher aluminum content in the solution (released from Al-C_3S dissolution) increases ettringite formation and, consequently, accelerates the sulfate depletion (as confirmed by *in-situ* XRD, see Section 3.2). Interestingly, the ort-C_3A presented slower hydration rate in C_3S/C_3A/calcium sulfates when compared to the ort-C_3A/calcium sulfates pastes. The ort-C_3A hydration is significantly influenced by the bulk composition of the pore solution [13], and the presence of C_3S seems to retard its reaction. Further analyses on this topic are necessary.

The type of C_3S was the major factor influencing the system's sulfate balance. For the ternary mixes with C_3S (Figure 4a-b), 0.5 wt%SO_3 was already enough to result in properly sulfated mixtures, i.e., that the renewed C_3A hydration occurred after the main C_3S hydration peak. In turn, for the ternary mixes with Al-C_3S (Figure 4c-d), 1.5-2.0 wt% SO_3 was required to reach the proper sulfate content. This happens because a higher concentration of aluminum into the pore solution is expected in the ternary mixes with

Al-C_3S, resulting in higher ettringite formation and sulfate consumption (as confirmed by *in-situ* XRD, see Section 3.2).

The C_3A polymorphism also influenced the sulfate balance of the system but to a less extent. The effect of C_3A polymorph on sulfate balance also depends on the wt% SO_3 content. On the one hand, for the ternary mixes with 0.25 and 0.5 wt% SO_3, the ternary mixes with cub-C_3A presented sulfate depletion and renewed hydration of C_3A earlier than those with ort-C_3A, increasing the sulfate demand of the system. On the other hand, for the ternary mixes with 1.0 wt% SO_3 or more, the opposite behavior was observed, i.e., the ternary mixes with ort-C_3A present earlier sulfate depletion and renewed hydration of C_3A. This apparent discrepancy might be due to the differences in cb-C_3A and ort-C_3A hydration, which depends on the sulfate level, as observed and discussed in Section 3.1.2. For sulfate-free solutions, cb-C_3A hydrates faster than the ort-C_3A. However, the addition of calcium (gypsum or hemihydrate) retards the C_3A hydration much more efficiently than the ort-C_3A hydration (see Figure 3). Therefore, for the ternary mixes with 0.25 and 0.50 wt% SO_3 (SO_3/C_3A ratio of 0.03 and 0.06, respectively), the very low sulfate content was not enough to retard the cb-C_3A hydration and make it slower than the ort-C_3A hydration. Finally, 1.0 wt% SO_3 (SO_3/C_3A ratio of 0.13) seems to be enough to make the cb-C_3A reaction slower than the ort-C_3A reaction.

Regarding the calcium sulfate source, the ternary mixes with hemihydrate presented earlier sulfate depletion and renewed hydration of C_3A than the ternary mixes with gypsum, which agrees with previous results [7]. This was expected since hemihydrate dissolves faster than gypsum [21,22], resulting in higher sulfate concentrations in the pore solution, which lead to higher ettringite formation (as confirmed by *in-situ* XRD, see Section 3.2) and anticipating the sulfate depletion. The calcium sulfate composition did not influence the C_3S and Al-C_3S hydration in the proper sulfated mixes, which corroborates the C_3S pastes results (Section 3.1.1) that showed that gypsum and hemihydrate led to very similar effects on C_3S and Al-C_3S hydrations.

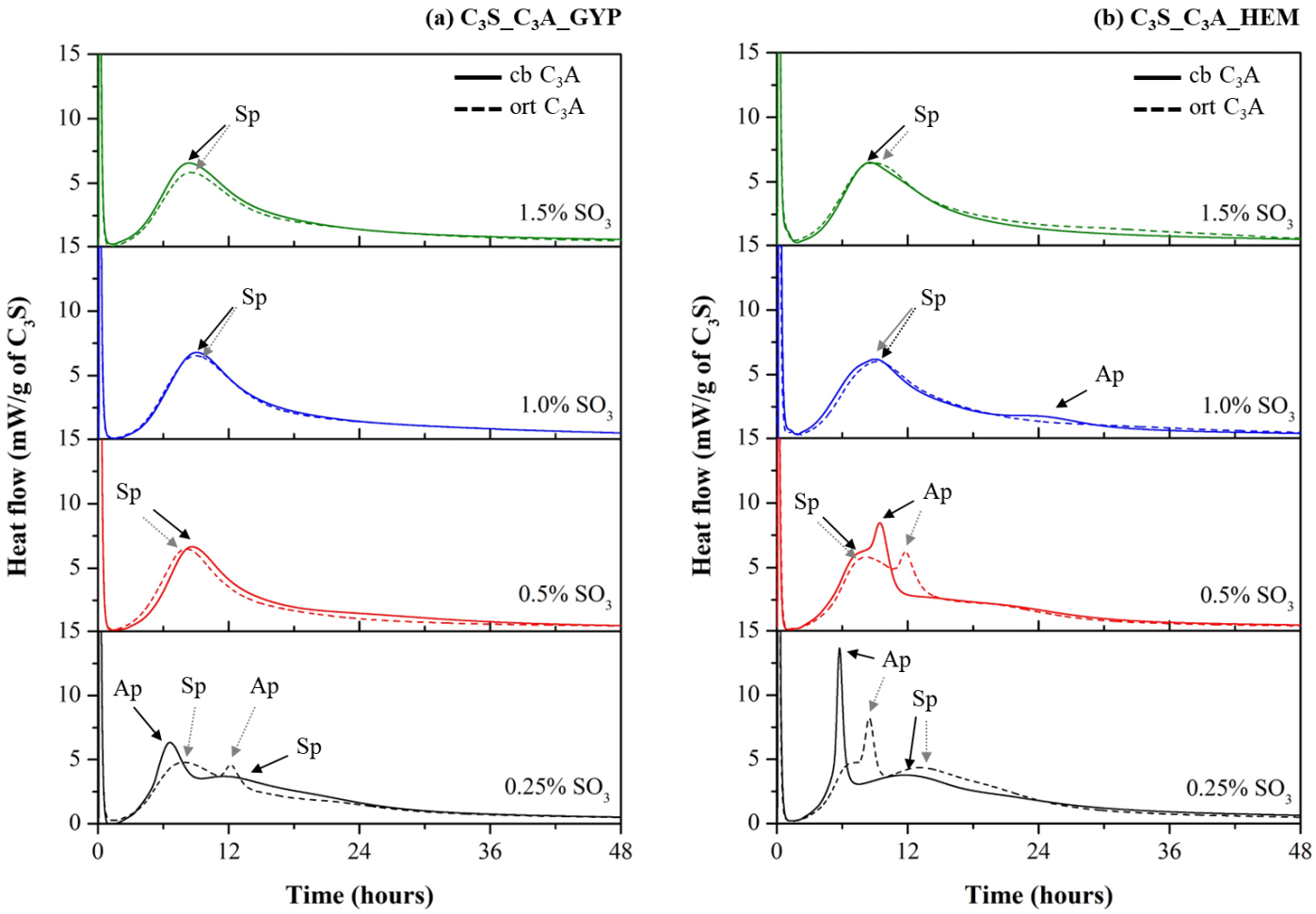
(a) C3S_C3A_GYP
(b) C3S_C3A_HEM
cb C3A
ort C3A
Sp
Ap
1.5% SO3
1.0% SO3
0.5% SO3
0.25% SO3
Heat flow (mW/g of C3S)
Time (hours)
0
12
24
36
48
0
5
10
15

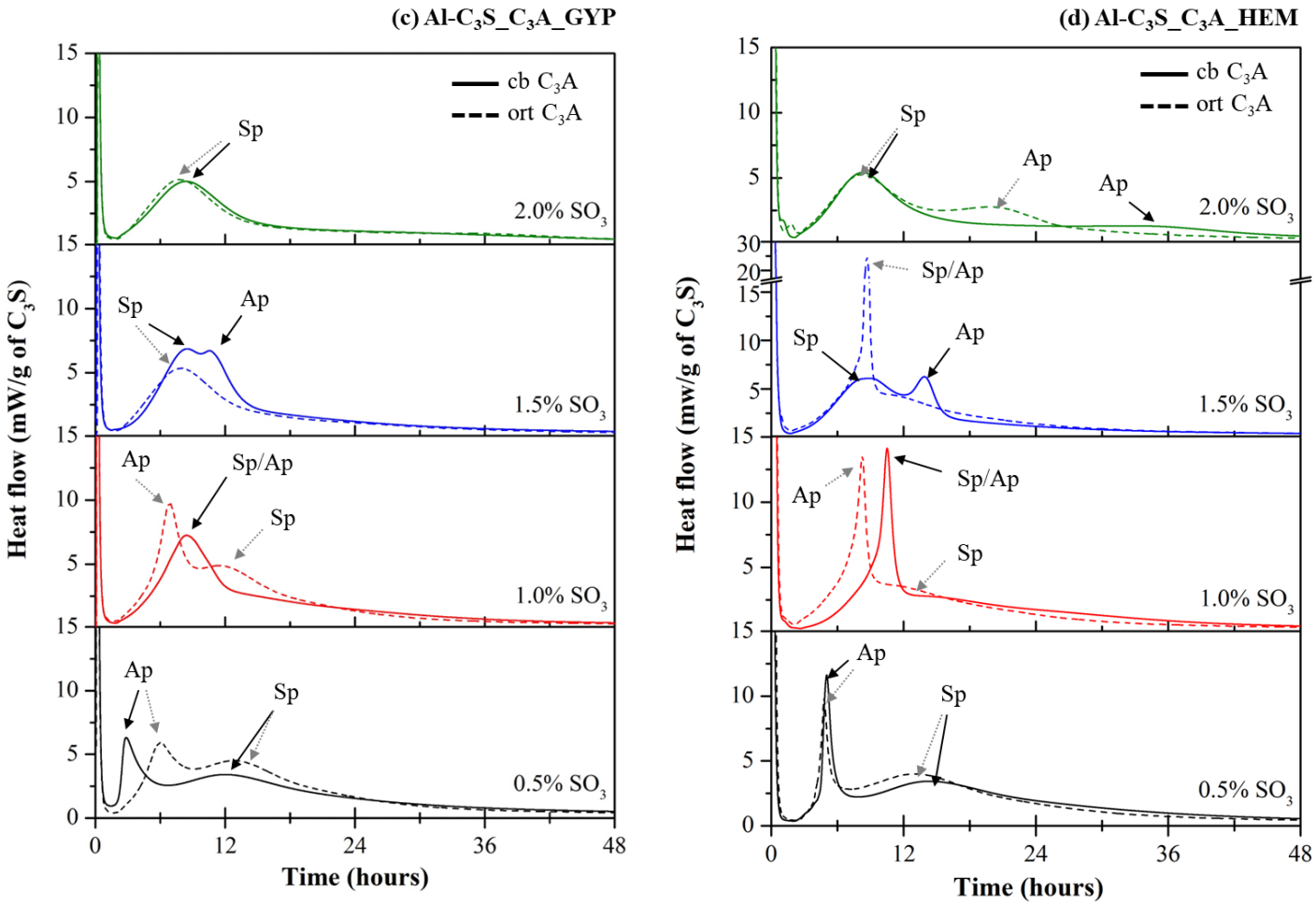

Figure 4 – Heat flow curves of the pastes with different gypsum and hemihydrate contents during the first 48 hours of hydration. The moment of the occurrence of the Aluminate peak (Ap) and Silicate peak (Sp) are indicated.

3.2 *In-situ* X-ray diffraction (XRD)

3.2.1 General trends

Figure 5 shows the XRD patterns of each mix at 0.5 and 48 hours of hydration. All the ternary mixes had 1.5 wt% SO_3 as according to the calorimetry results at this sulfate content, none of the ternary mixes was undersulfated (except for the Al-C_3S_ort-C_3A_HEM it was slightly undersulfated). No bassanite (i.e., crystalline hemihydrate) was found in hydrated pastes, indicating that it quickly converted into gypsum before the first XRD measurement, sooner than 30 minutes. This is in line with that reported by Jakob et al. [51], Jansen et al. [52], and García-Maté et al. [53], which observed this phenomenon before 10-20 minutes of hydration in Portland cement pastes and also supported by

Andrade Neto et al. [14] who observed the hydration of hemihydrate into gypsum in the first 30 minutes in C_3A pastes.

The ternary mixes with Al-C_3S (i.e., 3, 4, 7, and 8) showed ettringite peaks at 0.5 hours, especially at 9.1° 2θ. In addition, the Al-C_3S_(cb,ort)-C_3A_GYP mixes (i.e., 3 and 4) had virtually no gypsum traces at the first measurement, while the C_3S_(cb,ort)-C_3A_GYP mixes (i.e., 1 and 2) showed gypsum peak at 11.6° 2θ.

Regarding the hydration of the aluminates, the ternary mixes with C_3S (i.e., 1, 2, 5, and 6) showed evident C_3A peaks after 48 hours of hydration (at around 33° 2θ). The ternary mixes produced with cubic C_3A (i.e., 1 and 5) had practically no change on the relative intensity of such C_3A peak, indicating the low consumption of this phase along the first two days of hydration.

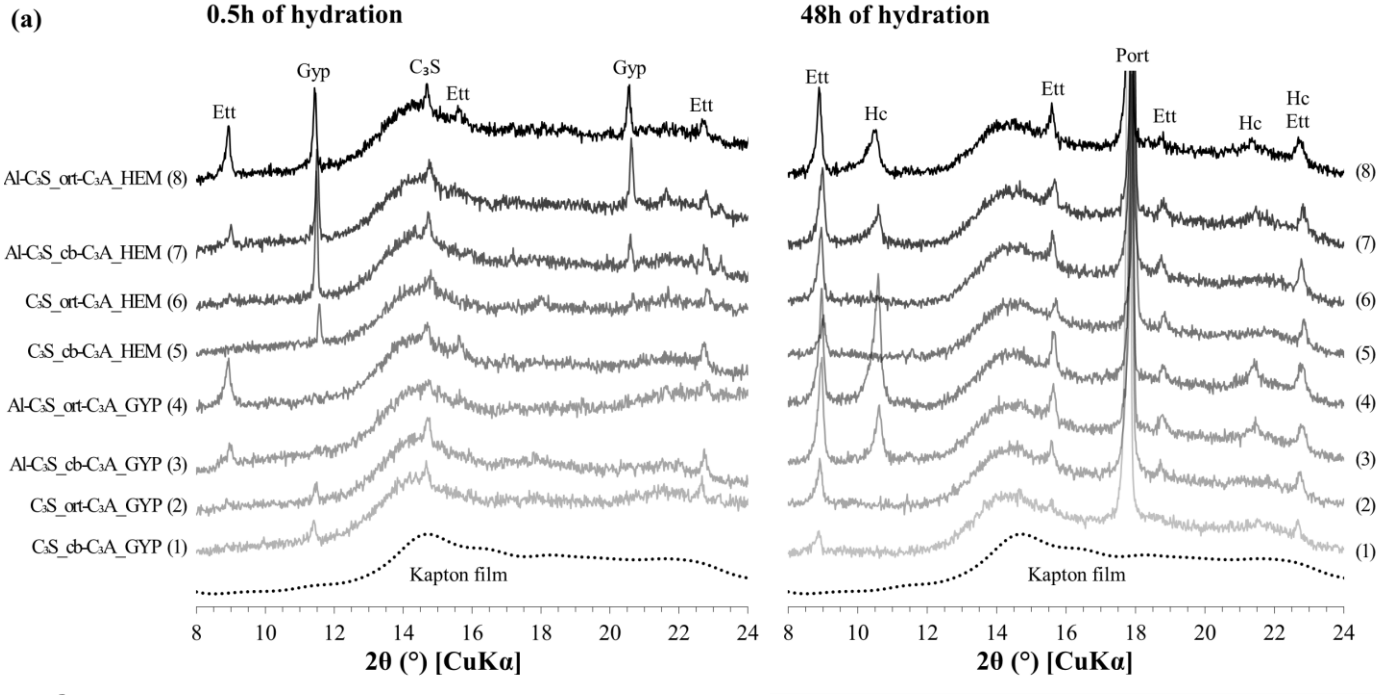

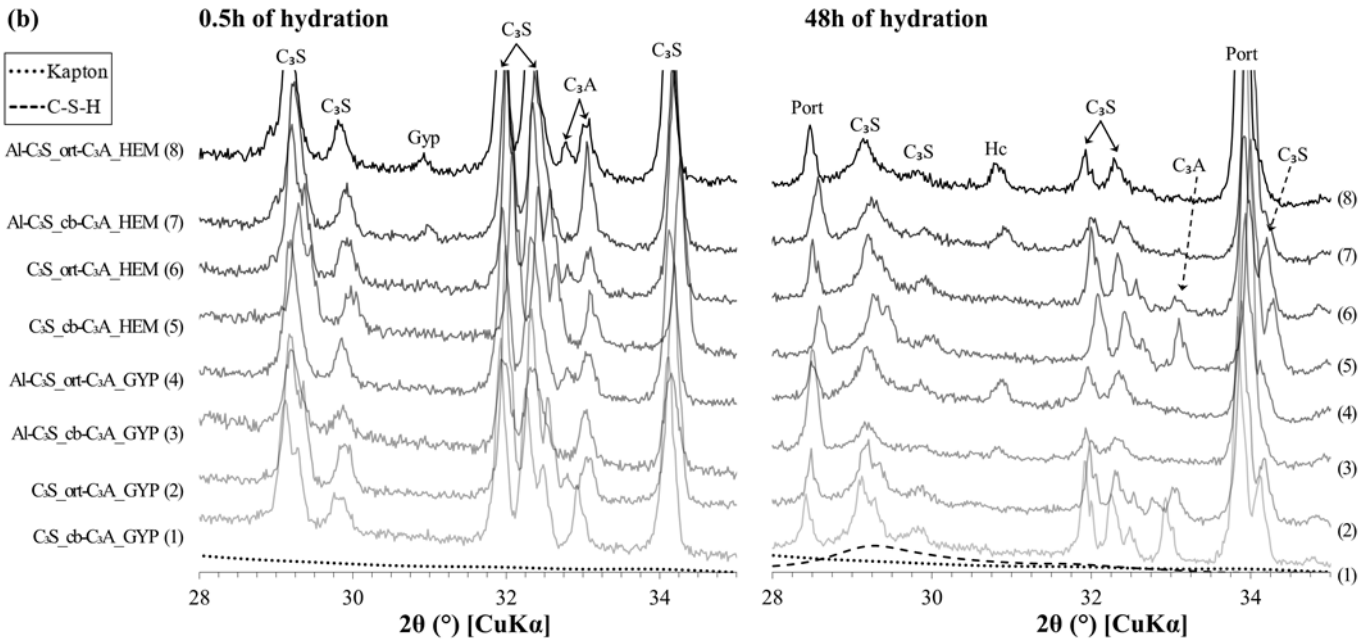

Figure 5 – Selected ranges of the XRD patterns of the ternary mixes at 0.5 and 48 hours of hydration. (a) 8-24° 2θ range; (b) 28-35° 2θ range. Ett: ettringite; Gyp: gypsum; Port: portlandite; Hc: hemicarbonate. Note: the patterns were vertically shifted for visualization, but the relative intensities (in linear scale) were not changed. The Kapton and C-S-H models are also shown as dotted and dashed lines, respectively.

Figure 6(a,b) exemplifies the phase content over time determined by XRD-Rietveld QPA and the heat flow within the first 48 hours of hydration for the C_3S_cb-C_3A_2.81% HEM and Al-C_3S_cb-C_3A_2.84% HEM pastes. The phases content over time of the other ternary mixes are presented in the Supplementary Information (Figure S3). Regarding silicates, all the mixtures showed very similar behavior. The C_3S content was approximately constant (considering the intrinsic deviations in Rietveld quantification) during the first ≈ 4 h, up to the end of the induction period. A supposed increase in the C_3S content was observed in some samples within this period (e.g., in Figure 6a), also observed in Refs [18,54]. However, this is most likely related to the variability in the XRD-Rietveld QPA, which can yield errors as high as 3 wt.% for the major cement phases [55]. At the beginning of the acceleration period, the C_3S contents start to reduce indicating its dissolution, while significant C-S-H and portlandite formation can be measured, in agreement with Refs. [51,52]. Previous works showed that C-S-H starts to precipitate shortly after mixing as primary particles of tens of nanometers in size [56,57], which are hardly detectable by XRD. After a few hours, these nanosized particles are converted into the known foil-like arrangement [57,58] detectable by XRD. The C_3S dissolution and the C-S-H and portlandite formation initially presented faster rates but

slowed down after the main heat flow peak. The lower C_3S dissolution rate can explain the decrease in heat release rate in IC curves.

As for the aluminates, for all the ternary mixes, it was observed an extremely fast initial C_3A dissolution (with approximately 50% of the C_3A dissolving within the first 30 minutes – before the first XRD measurement) and then its content remains virtually constant. Ettringite was formed in the first minutes (already detected in the first XRD scan), and its content kept increasing in the first hours, associated with gypsum dissolution. After 6-16 hours (varying from mix to mix), gypsum depletion is observed. From this point on, the ternary mixes with Al-C_3S presented very different behaviors when compared with the ternary mixes with C_3S. In the ternary mixes with Al-C_3S, a few hours after gypsum depletion, the C_3A started to dissolve again very quickly (Figures 6b and S3c,d,g,h). For those ternary mixes, the ettringite content initially increased fast up to a limit and then started to dissolve synchronously with the start of hemicarbonate formation. In turn, for the C_3S ternary mixes, the C_3A also starts to dissolve again after the sulfate depletion, but much slower than the mixtures with Al-C_3S. As a result, no AFm was detected in the C_3S-containing ternary mixes up to 48 hours, as observed in Figure 5a (see patterns 1, 2, 5, and 6) where the only reflection observed up to 12° 2θ was that from ettringite

The formation of hemicarboaluminate instead of monosulfate on Al-C_3S ternary mixes occurred due to the presence of calcite (0.5 wt%) and magnesite (0.9 wt%) on the Al-C_3S composition (see Section 2.1). In turn, for the C_3S ternary mixes, no ettringite dissolution and hemicarbonate or monosulfate formations were observed in the first 48 hours of hydration. Interestingly, the ternary mixes with ort-C_3A also formed hemicarbonate instead of U-phase ($4CaO \cdot 0.9Al_2O_3 \cdot 1.1SO_3 \cdot 0.5Na_2O \cdot 16H_2O$), which also belongs to the group of hexagonal or pseudo-hexagonal layered structures (AFm) and were observed in pure ort-C_3A pastes [14]. The U-phase is formed in the presence of SO_4^{2-} and Na^+ ions in a highly alkaline medium [59]. However, since the C_3S/C_3A/calcium sulfate mixes had much lower ort-C_3A amounts than pure C_3A pastes, the amount of Na^+ ions released was probably not enough to ensure the sufficiently high pH for the U-phase formation.

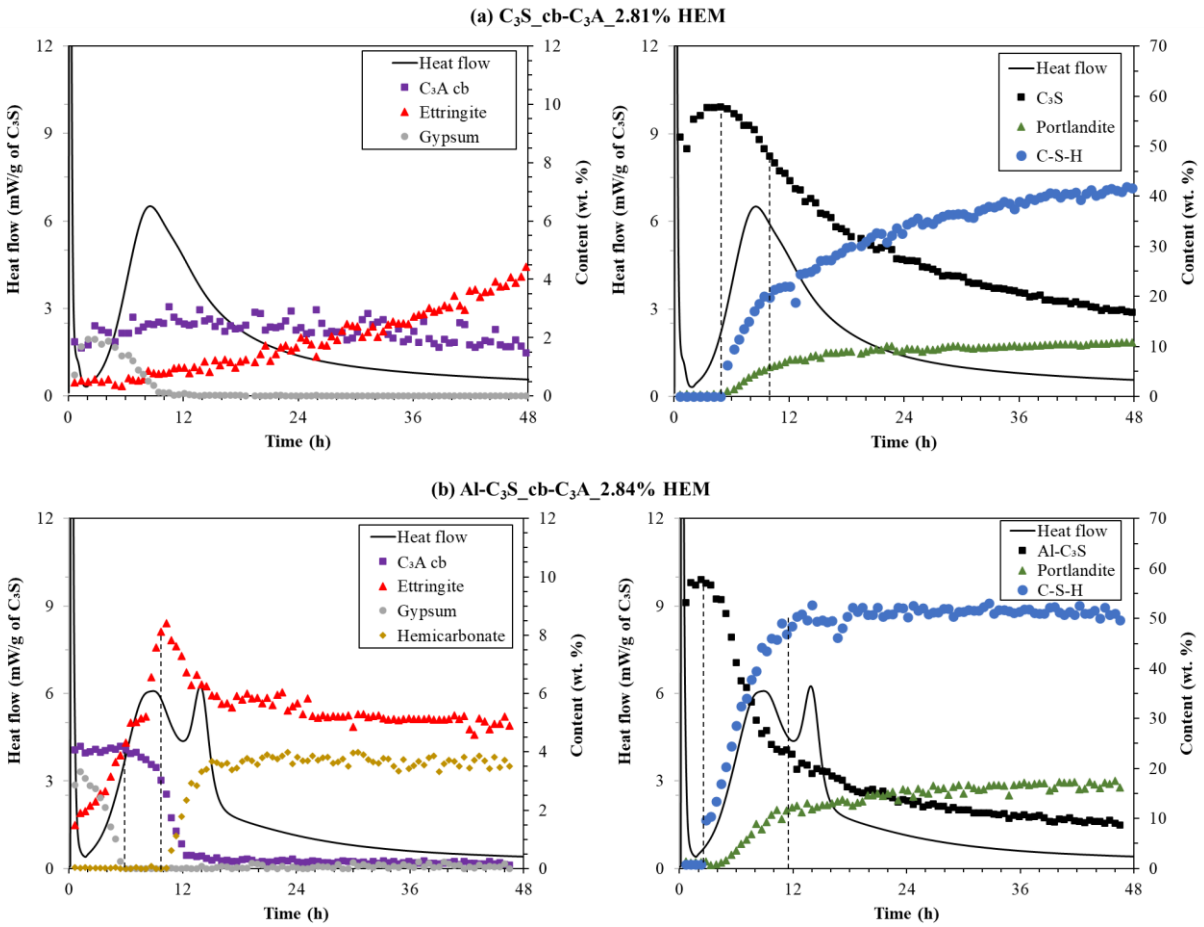

Figure 6 – Examples of heat flow curves and phase content (wt%) over the first 48 hours of hydration of (a) C_3S_cb-C_3A_2.81% HEM and (b) Al- C_3S_cb-C_3A_2.84% HEM.

3.2.2 Effect of C_3S and C_3A doping, and calcium sulfate source on the hydration of aluminate phases

Figure 7 presents the ettringite, hemicarbonate and C_3A contents of all samples measured by *in-situ* XRD during the first 48 hours. It was found that the C_3S type had the greatest influence on ettringite formation, and the Al-C_3S ternary mixes presented higher ettringite contents in the first hours compared with the respective ternary mixes containing pure C_3S. Consequently, the Al-C_3S ternary mixes showed hemicarbonate formation at 6.0-16.7 hours, while no significant formation of crystalline hemicarbonate was observed in the pure C_3S samples up to 48 hours. This can be associated with the higher aluminum content in the pore solution of the Al-C_3S pastes.

The C_3A type also influenced the amount of ettringite formed in the first hours. The ternary mixes with ort-C_3A generally presented higher ettringite contents when compared with the respective cb-C_3A ternary mixes. This result was expected due to the higher

reactivity of ort-C_3A, as discussed in Section 3.1.2. As a result of the higher ettringite formation and the faster sulfate consumption, the Al-C_3S_ort-C_3A_GYP paste presented earlier hemicarboaluminate formation (≈ 9.7 hours) compared to the Al-C_3S_cb-C_3A_GYP paste (≈ 16.7 hours).

Finally, the calcium sulfate type also influenced the ettringite formation rate. The ternary mixes with hemihydrate (Figure 7b) showed faster ettringite formation in the first hours, which agrees with Zunino and Scrivener [7] results. This was expected since the hemihydrate presents a faster dissolution when compared with gypsum [21,22], resulting in higher sulfate concentration in pore solution, leading to a faster ettringite formation. Finally, the replacement of gypsum by hemihydrate also influenced the beginning of hemicarbonate formation, anticipating it in 6.4 hours for the Al-C_3S_cb-C_3A pastes (from 16.7 hours for the mix with GYP to 10.3 hours for the mix with HEM) and in 3.7 hours for the Al-C_3S_ort-C_3A pastes (from 9.7 hours for the mix with GYP to 6.0 hours for the mix with HEM).

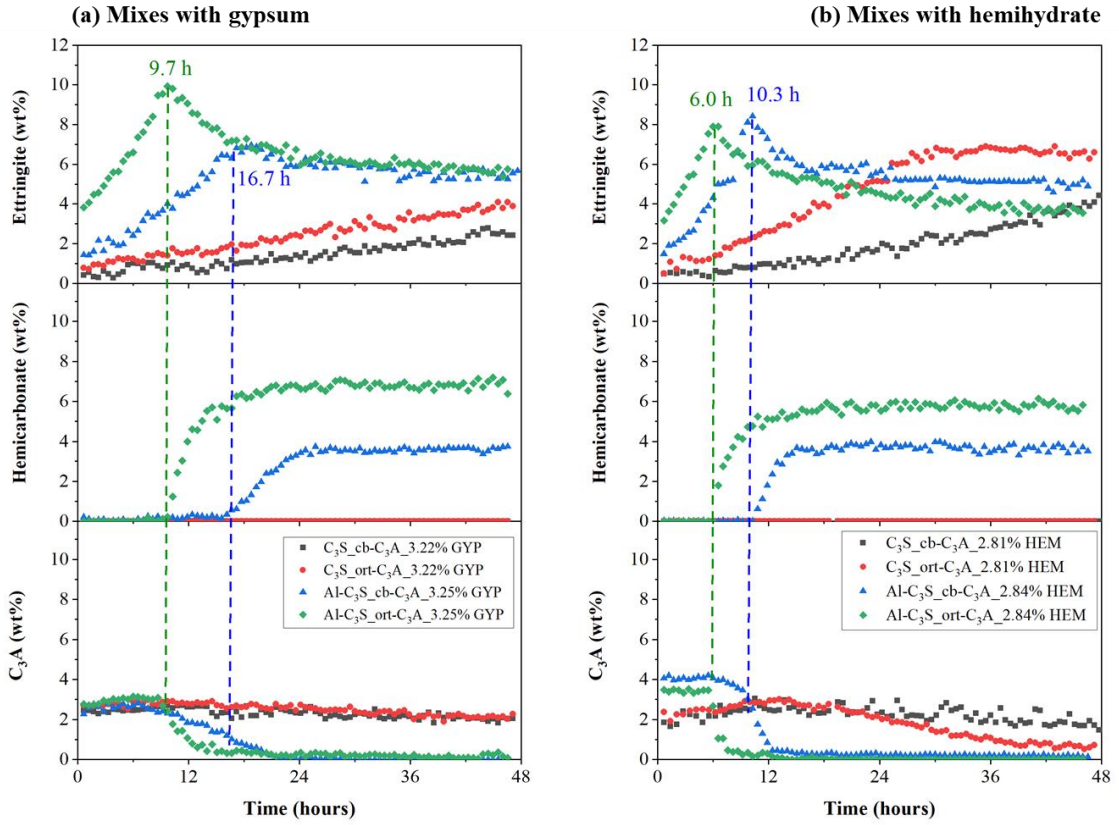

Figure 7 – Ettringite, hemicarbonate and C_3A content (wt%) in the C_3S/C_3A pastes with (a) gypsum and (b) hemihydrate over the first 48 hours.

3.3 Thermogravimetric analysis (TGA)

Figure 8 shows the DTG curves up to 300 °C of the C_3S/C_3A pastes with 1.5 wt% SO_3 (with gypsum or hemihydrate) at 8 hours, 1, 3, and 7 days of hydration. The complete DTG curves (up to 1000 °C) are presented in Supplementary materials (Figure S4). Peaks related to C-S-H (between 50 and 300 °C), ettringite (≈100 °C), gypsum (≈140 °C), AFm phases (≈ 55 °C), portlandite (between 400 and 500 °C), and carbonates (between 600 and 700 °C) were observed [27]. As expected, the peaks related to the hydrated phases' thermal decomposition increased with the hydration time, indicating higher amounts of hydrated phases and consequently a higher degree of hydration. In turn, the gypsum peaks were only observed in the mixtures with C_3S at 8 hours, which agrees with XRD-Rietveld results, showing that the sulfate depletion occurred after ≈10 hours of hydration for those samples, while occurred up to ≈6 hours for the ternary mixes with Al-C_3S.

The C_3S type had a remarkable influence on the moment of AFm formation. While the Al-C_3S pastes already presented the peaks related to AFm phases decomposition at 8 hours or 1 day, no AFm peaks are observed in the pure C_3S ternary mixes up to 3 days, being only observed at 7 days. This result also corroborates the XRD-Rietveld results, in which no AFm phases were observed in the first 48 hours for the pure C_3S ternary mixes while starting to form between 6.0 to 16.7 hours for the Al-C_3S pastes.

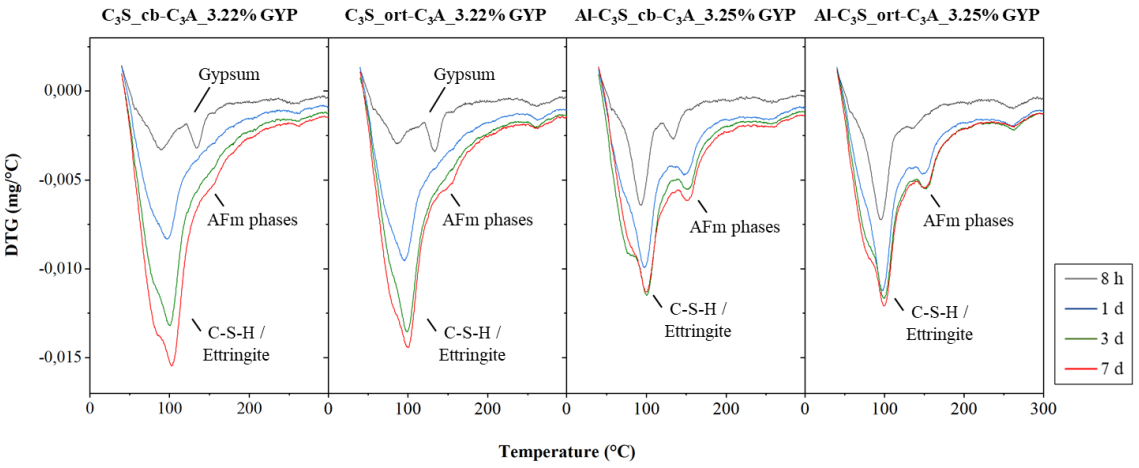

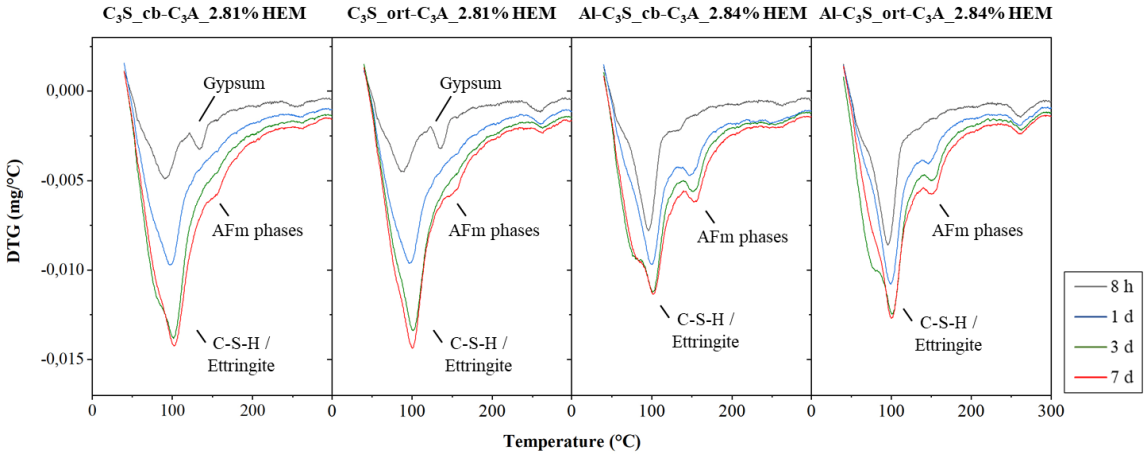

Figure 8 – DTG curves (up to 300 ºC) of the C_3S/C_3A pastes with gypsum and hemihydrate at 8 h, 1, 3, and 7 d of hydration.

The bound water content was calculated from the TGA results and is presented in Figure 9. The ternary mixes with pure C_3S presented higher bound water content than those with Al-C_3S. The bound water is related to the degree of hydration (DoH) of C_3S. As observed by isothermal calorimetry (see Section 3.1.1), pure C_3S was much more reactive than Al-C_3S, which explains the higher bound water content of the mixtures with pure C_3S. In turn, the C_3A and calcium sulfate types did not significantly influence the bound water content of the ternary mixes, which may be explained by their much lower content compared with C_3S.

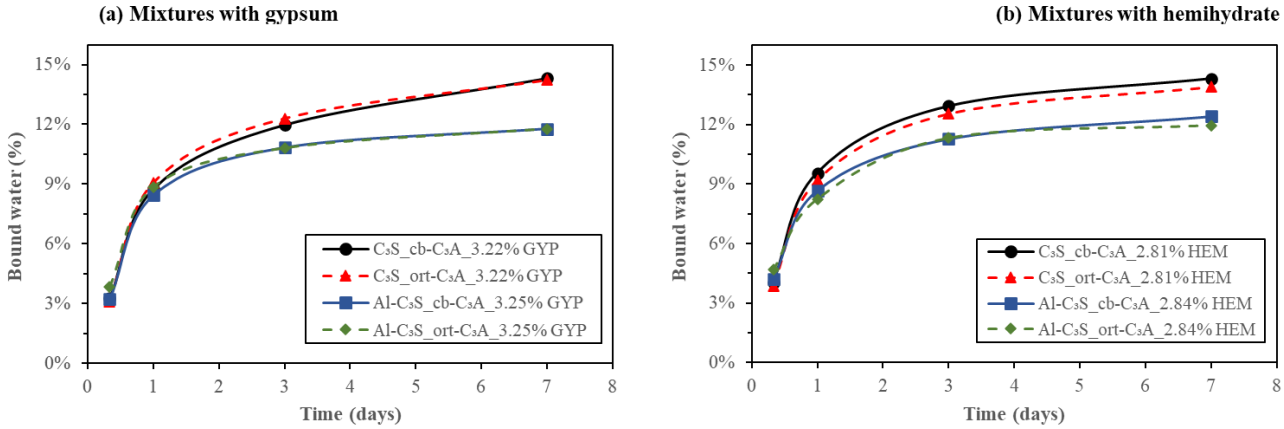

Figure 9 – Bound water (%) of the C_3S/C_3A pastes with (a) gypsum and (b) hemihydrate over the first 7 days of hydration.

Figure 10 presents the portlandite content (in g/100g of paste) of the C_3S/C_3A pastes with gypsum in (a) and hemihydrate in (b) during the first 7 days of hydration. The portlandite content showed the same trend observed for the bound water content: the C_3S type was

the only factor that significantly influenced the portlandite content, where the ternary mixes with pure C_3S presented higher portlandite content than the ternary mixes with Al-C_3S, which was expected since C_3S is more reactive than Al-C_3S.

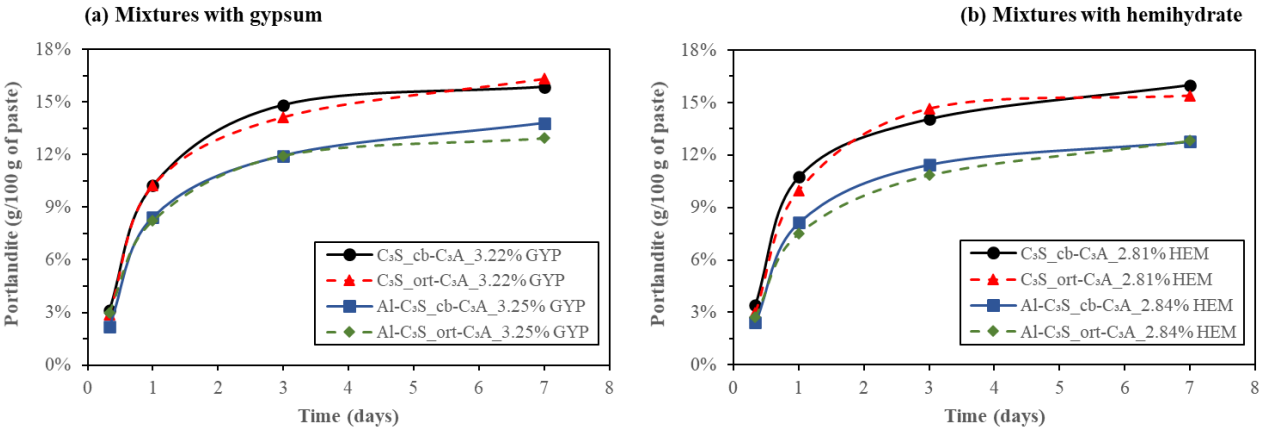

Figure 10 – Portlandite content (g/100 of paste), determined by TGA, of the C_3S/C_3A pastes with (a) gypsum and (b) hemihydrate over the first 7 days of hydration.

4 DISCUSSION

4.1 The impact of aluminum doping of C_3S on sulfate demand

Among the factors analyzed, the aluminum doping of C_3S had the most remarkable influence on the sulfate demand of the ternary systems. The beginning of ettringite decomposition and hemicarbonate formation occurred between 6.0 and 16.7 hours (depending on C_3A polymorph and calcium sulfate type used) in the ternary mixes with Al-C_3S (observed by *in-situ* XRD and confirmed by TGA), while only occurred between 3 and 7 days of hydration for the ternary mixes with C_3S (revealed by TGA).

Zunino and Scrivener [7] studied C_3S T_1/cb-C_3A/gypsum systems varying the C_3S fineness, finding that the higher the C_3S fineness, the earlier the sulfate depletion and the higher the sulfate demand. This occurs because the increase of the fineness of C_3S increases its reactivity and, consequently, increases the rate of C-S-H formation [7]. As mentioned early, the sulfates are physically adsorbed by the C-S-H due to charge affinity [60], consuming the sulfates from the solution. Therefore, the higher the amount of C-S-H formed in the first hours, the higher the amount of sulfates adsorbed on the C-S-H surface, and the earlier the sulfate depletion occurs.

Interestingly, the opposite behavior was observed here: the ternary systems with Al-C_3S, which presented lower reactivity when compared with pure C_3S (see Section 3.1), presented higher sulfate demand. For instance, the ternary mixes with Al-C_3S required 1.5-2.0 wt% SO_3 to be properly sulfated, while those with pure C_3S only required 0.5 wt% SO_3. This happens because of the impact of aluminum on sulfate consumption – the higher the aluminum content available in the pore solution, the higher the ettringite formation (observed here by *in-situ* XRD), and the faster the sulfate depletion.

We emphasize that Zunino and Scrivener [7] used the same C_3S used here (T_1, without aluminum) but with different fineness. Therefore, we can propose that not only the C_3S fineness and polymorph will influence the sulfate balance of the system (as observed by [7]) but also the aluminum content in the C_3S. In addition, the latter factor seems to have a greater impact on the sulfate demand than the former, since the ternary mixes with the coarser and less reactive Al-C_3S (with 0.8 wt% Al_2O_3) presented a higher sulfate demand than the ternary mixes with the finer and more reactive pure C_3S (without aluminum).

4.2 The impact of C_3A polymorphism on sulfate demand

The C_3A polymorphism also influenced the sulfate demand of the ternary mixes, although to a lesser extent than the aluminum doping of C_3S. The influence of the C_3A polymorphism on the sulfate demand depended on the percentage of SO_3 used. For the ternary mixes with low SO_3 contents (0.25 and 0.50 wt% SO_3), the systems with cb-C_3A presented earlier sulfate depletion and renewed hydration of C_3A than those mixes with ort-C_3A. However, for the ternary mixes with 1.00 wt% SO_3 or more, the opposite behavior was observed, i.e., the ternary mixes with ort-C_3A presented earlier sulfate depletion.

This behavior is due to the different impacts of calcium sulfates on cb-C_3A and ort-C_3A hydration. Without calcium sulfates, cubic C_3A hydrates faster than orthorhombic C_3A. Besides, the addition of calcium sulfates is much more efficient in delaying the cb-C_3A hydration than the ort-C_3A hydration (explained in Section 3.1.2 and consistent with other studies [12,13,61]). Therefore, when low amounts of calcium sulfate are used, the cb-C_3A hydration is not efficiently retarded to be slower than the ort-C_3A hydration.

4.3 The impact of calcium sulfate type on C_3S and C_3A hydration and sulfate demand

The addition of calcium sulfate slightly prolonged the induction period of both C_3S and Al-C_3S (see Section 3.1.1) but enhanced their hydration afterward, resulting in higher heat flow peaks and cumulative heat in the first 48 hours. The initial delay probably occurred due to the adsorption of sulfate ions on the C_3S surface [7,17,47], while the enhancement thereafter seems to be related to either the change in the C-S-H morphology due to the sulfate adsorption or to the increase in the ionic strength of the solution with the addition of calcium sulfate [11].

However, the calcium sulfate type did not significantly influence the hydration of pure C_3S and Al-C_3S. The C_3S-gypsum and the C_3S-hemihydrate pastes (with a 1.5 wt% SO_3) presented very close heat flow curves in the first 48 hours (Figure 4a,b), except for a small heat flow peak between 30 minutes and 2 hours associated with the hydration of hemihydrate and formation of gypsum crystals.

As for C_3A pastes, the presence of gypsum or hemihydrate retarded the reaction of both cb-C_3A and ort-C_3A, but the retarding effect was much less efficient for the latter. This occurs due to the higher solubility of $Al_6O_{18}^{18-}$ rings on the ort-C_3A, inhibiting the adsorption of SO_4^{2-} and/or Ca–SO_4 ion-pair responsible for the delay in cb-C_3A hydration [13,14]. The replacement of gypsum with hemihydrate leads to a substantial delay on both cb-C_3A and ort-C_3A. The faster dissolution of hemihydrate, which releases more sulfate ions into the pore solution in the first hours, might explain this. However, more studies on this matter are necessary to fully understand its mechanism.

The analysis of the effect of calcium sulfate type on the hydration of C_3S/C_3A/calcium sulfate systems showed that the use of hemihydrate resulted in earlier sulfate depletion and hemicarbonate formation (observed by calorimetry and *in-situ* XRD), consequently presenting a higher sulfate demand to obtain properly sulfated systems, which agrees with Zunino and Scrivener results [7]. This occurs due to the faster dissolution of hemihydrate compared with gypsum, resulting in higher sulfite concentrations in the pore solution in the first hours, increasing ettringite's formation (revealed by *in-situ* XRD).

4.4 Implications for PC production and PC concrete properties

As observed, the aluminum content in C_3S greatly impacts the sulfate balance of C_3S/C_3A/calcium sulfate systems, which usually correspond to about 70 wt% of ordinary Portland cement. Therefore, Portland clinkers with higher aluminum content (including the aluminum incorporated in the C_3S structure) will present higher sulfate demand, i.e., a higher amount of calcium sulfate will be required to obtain optimal fresh and mechanical properties.

The C_3A polymorph also affected the sulfate balance of the systems studied. For the ternary mixes with 1.0 wt% SO_3 or more, the ort-C_3A reacted faster than the cb-C_3A, leading to faster sulfate depletion (note that commercial PCs usually need 2.5-4.5 wt% SO_3 to be properly sulfated). Therefore, clinkers with ort-C_3A are likely to require more sulfate to reach optimum properties.

Finally, the presence of hemihydrate (which might occur in commercial PCs due to gypsum dehydration during milling) also increased the sulfate demand of the ternary mixes. Therefore, a higher sulfate content will be needed to optimize the properties of concrete produced with PC containing this type of sulfate source. Furthermore, the crystallization of gypsum and the higher ettringite formation in the presence of hemihydrate tends to decrease PC concrete workability and may result in a false setting [1,62,63].

Understanding how these parameters influence the sulfate demand of PC will help the cement industry control the amount and type of calcium sulfate that should be used. However, it stresses the need for further studies on this topic with commercial clinkers since pure phases have inherent differences compared with those present in the clinkers produced by the industry.

5 CONCLUSIONS

From our results, we can conclude that:

- Both gypsum and hemihydrate delayed the initial hydration of pure C_3S and Al-C_3S, prolonging the induction period but accelerating the reaction thereafter. The C_3S-gypsum and C_3S-hemihydrate pastes presented very similar behaviors for the same SO_3 content (1.5 wt% SO_3).

- Aluminum doping of C_3S greatly influenced the sulfate balance of C_3S/C_3A/calcium sulfate mixes. The ternary mixes with Al-C_3S presented faster and higher ettringite formation in the first hours, anticipating the sulfate depletion, the renewed hydration of C_3A, and the hemicarbonate formation.

- The impact of C_3A polymorphism on the sulfate demand of the C_3S/C_3A/calcium sulfate mixes varied with the SO_3 content used. For the systems with 0.25 and 0.50 wt% SO_3, the ternary mixes with cb-C_3A presented earlier sulfate depletion and renewed hydration of C_3A. However, for the systems with 1.0 wt% SO_3 or more, those with ort-C_3A presented earlier sulfate depletion and renewed dissolution of C_3A. In addition, the C_3A polymorphism does not seem to significantly influence the pure or Al-doped C_3S hydration rate in proper sulfated mixes.

- The replacement of gypsum with hemihydrate in the C_3S/C_3A/calcium sulfate mixes resulted in faster ettringite formation, anticipating the sulfate depletion and renewed hydration of C_3A. This happens due to the faster dissolution of hemihydrate when compared with gypsum. In addition, hemihydrate incorporation led to higher sulfate demand, which may require greater sulfate contents in commercial clinkers when this type of sulfate source is used.

6 Acknowledgments

JSAN and PRM thank the financial support of (Coordination for the Improvement of Higher Education Personnel). JSAN thanks the University of Malaga (Spain), where the experiments for the characterization of the raw materials were performed. JSAN also thanks the Spanish Junta de Andalucía [P18-RT-720 cofounded with ERDF] research project for the research stage at the University of Málaga (Spain) and the Graduate Program in Civil Engineering: Construction and Infrastructure (PPGCI) of the Federal University of Rio Grande do Sul (UFRGS), Brazil. APK acknowledge the financial support of CNPq (Brazilian National Council for Scientific and Technological Development). The staff of *Laboratório de Difração de Raios-X* (LDRX-UFSC) is acknowledged for the *in-situ* XRD data collection.

7 References

[1] J. da S. Andrade Neto, A.G. de la Torre, A.P. Kirchheim, Effects of sulfates on the hydration of Portland cement – A review, Construction and Building Materials. 279 (2021). https://doi.org/10.1016/j.conbuildmat.2021.122428.

[2] S. Adu-Amankwah, L. Black, J. Skocek, M. ben Haha, M. Zajac, Effect of sulfate additions on hydration and performance of ternary slag-limestone composite cements, Construction and Building Materials. 164 (2018) 451–462. https://doi.org/10.1016/j.conbuildmat.2017.12.165.

[3] S. Mohammed, O. Safiullah, Optimization of the SO3 content of an Algerian Portland cement: Study on the effect of various amounts of gypsum on cement properties, Construction and Building Materials. 164 (2018) 362–370. https://doi.org/10.1016/j.conbuildmat.2017.12.218.

[4] M. Zajac, J. Skocek, A. Müller, M. ben Haha, Effect of sulfate content on the porosity distribution and resulting performance of composite cements, Construction and Building Materials. 186 (2018) 912–919. https://doi.org/10.1016/j.conbuildmat.2018.07.247.

[5] K. Tosun, Effect of SO3 content and fineness on the rate of delayed ettringite formation in heat cured Portland cement mortars, Cement and Concrete Composites. 28 (2006) 761–772. https://doi.org/10.1016/j.cemconcomp.2006.06.003.

[6] A. Pavoine, X. Brunetaud, L. Divet, The impact of cement parameters on Delayed Ettringite Formation, Cement and Concrete Composites. 34 (2012) 521–528. https://doi.org/10.1016/j.cemconcomp.2011.11.012.

[7] F. Zunino, K. Scrivener, Factors influencing the sulfate balance in pure phase C3S/C3A systems, Cement and Concrete Research. 133 (2020) 106085. https://doi.org/10.1016/j.cemconres.2020.106085.

[8] D. Wagner, F. Bellmann, J. Neubauer, Influence of aluminium on the hydration of triclinic C3S with addition of KOH solution, Cement and Concrete Research. 137 (2020) 106198. https://doi.org/10.1016/j.cemconres.2020.106198.

[9] D. Stephan, S. Wistuba, Crystal structure refinement and hydration behaviour of 3CaO·SiO2 solid solutions with MgO, Al2 O3 and Fe2O3, J Eur Ceram Soc. 26 (2006) 141–148. https://doi.org/10.1016/j.jeurceramsoc.2004.10.031.

[10] F. Begarin, S. Garrault, A. Nonat, L. Nicoleau, Hydration of alite containing aluminium, Advances in Applied Ceramics. 110 (2011) 127–130. https://doi.org/10.1179/1743676110Y.0000000007.

[11] J.S. Andrade Neto, E.D. Rodríguez, P.J.M. Monteiro, A.G. de la Torre, A.P. Kirchheim, Hydration of C3S and Al-doped C3S in the presence of gypsum, Cement and Concrete Research. Submitted (2021).

[12] A.P. Kirchheim, E.D. Rodríguez, R.J. Myers, L.A. Gobbo, P.J.M. Monteiro, D.C.C. Dal Molin, R.B. de Souza, M.A. Cincotto, Effect of gypsum on the early hydration of cubic and Na-doped orthorhombic tricalcium aluminate, Materials. 11 (2018) 1–16. https://doi.org/10.3390/ma11040568.

[13] R.J. Myers, G. Geng, E.D. Rodriguez, P. da Rosa, A.P. Kirchheim, P.J.M. Monteiro, Solution chemistry of cubic and orthorhombic tricalcium aluminate hydration, Cement and Concrete Research. 100 (2017) 176–185. https://doi.org/10.1016/j.cemconres.2017.06.008.

[14] J.S. Andrade Neto, P.R. Matos, A.G. de la Torre, C.E.M. Campos, P.J.P. Gleize, P.J.M. Monteiro, A.P. Kirchheim, The role of sodium and sulfate sources on the rheology and hydration of C3A polymorphs, Cement and Concrete Research. 151 (2022) 106639. https://doi.org/10.1016/j.cemconres.2021.106639.

[15] E. Pustovgar, R.K. Mishra, M. Palacios, J.B. d'Espinose de Lacaillerie, T. Matschei, A.S. Andreev, H. Heinz, R. Verel, R.J. Flatt, Influence of aluminates on the hydration kinetics of tricalcium silicate, Cement and Concrete Research. 100 (2017) 245–262. https://doi.org/10.1016/j.cemconres.2017.06.006.

[16] S. Garrault, A. Nonat, Y. Sallier, L. Nicolaeau, On the Origin of the Dormant Period of Cement Hydration, in: 13th International Congress on the Chemistry of Cement., Madrid, 2011: pp. 1–7.

[17] L. Nicoleau, E. Schreiner, A. Nonat, Ion-specific effects influencing the dissolution of tricalcium silicate, Cement and Concrete Research. 59 (2014) 118–138. https://doi.org/10.1016/j.cemconres.2014.02.006.

[18] D. Jansen, Ch. Naber, D. Ectors, Z. Lu, X.-M. Kong, F. Goetz-Neunhoeffer, J. Neubauer, The early hydration of OPC investigated by in-situ XRD, heat flow calorimetry, pore water analysis and 1H NMR: Learning about adsorbed ions from a complete mass balance approach, Cement and Concrete Research. 109 (2018) 230–242. https://doi.org/10.1016/j.cemconres.2018.04.017.

[19] K. Fukuda, S. Inoue, H. Yoshida, Cationic substitution in tricalcium aluminate, Cement and Concrete Research. 33 (2003) 1771–1775. https://doi.org/10.1016/S0008-8846(03)00172-8.
[20] L. Gobbo, L. Sant'Agostino, L. Garcez, C3A polymorphs related to industrial clinker alkalies content, Cement and Concrete Research. 34 (2004) 657–664. https://doi.org/10.1016/j.cemconres.2003.10.020.
[21] V.H. Dodson, T.D. Hayden, Another look at the Portland cement/chemical admixture incompatibility problem, Cement, Concrete and Aggregates. 11 (1989) 52–56. https://doi.org/10.1520/cca10102j.
[22] S. Pourchet, L. Regnaud, J.P. Perez, A. Nonat, Early C3A hydration in the presence of different kinds of calcium sulfate, Cement and Concrete Research. 39 (2009) 989–996. https://doi.org/10.1016/j.cemconres.2009.07.019.
[23] M. Palacios, H. Kazemi-Kamyab, S. Mantellato, P. Bowen, Laser diffraction and gas adsorption techniques, in: K. Scrivener, R. Snellings, B. Lothenbach (Eds.), A Practical Guide to Microstructural Analysis of Cementitious Materials, 1st ed., CRC Press, 2016: pp. 445–480.
[24] A. Quennoz, K.L. Scrivener, Interactions between alite and C3A-gypsum hydrations in model cements, Cement and Concrete Research. 44 (2013) 46–54. https://doi.org/10.1016/j.cemconres.2012.10.018.
[25] L. Wadsö, Operational issues in isothermal calorimetry, Cement and Concrete Research. 40 (2010) 1129–1137. https://doi.org/10.1016/j.cemconres.2010.03.017.
[26] J.D. Zea-Garcia, A.G. de la Torre, M.A.G. Aranda, I. Santacruz, Processing and characterisation of standard and doped alite-belite-ye'elimite ecocement pastes and mortars, Cement and Concrete Research. 127 (2020). https://doi.org/10.1016/j.cemconres.2019.105911.
[27] B. Lothenbach, P.T. Durdziński, K. de Weerdt, Thermogravimetric analysis, in: K. Scrivener, R. Snellings, B. Lothenbach (Eds.), A Practical Guide to Microstructural Analysis of Cementitious Materials, 1st ed., CRC Press, 2016: pp. 177–212.
[28] A.A. Coelho, TOPAS and TOPAS-Academic: An optimization program integrating computer algebra and crystallographic objects written in C++: An, Journal of Applied Crystallography. 51 (2018) 210–218. https://doi.org/10.1107/S1600576718000183.
[29] P.R. de Matos, J.S. Andrade Neto, D. Jansen, Á.G. de la Torre, A.P. Kirchheim, C.E.M. Campos, In-situ laboratory X-ray diffraction applied to cement-based materials, Cement and Concrete Research (Under Review). (2022).
[30] R. Snellings, X-ray powder diffraction applied to cement, in: K. Scrivener, R. Snellings, B. Lothenbach (Eds.), A Practical Guide to Microstructural Analysis of Cementitious Materials, 1st ed., CRC Press, 2016: pp. 107–176.
[31] S.T. Bergold, F. Goetz-Neunhoeffer, J. Neubauer, Quantitative analysis of C-S-H in hydrating alite pastes by in-situ XRD, Cement and Concrete Research. 53 (2013) 119–126. https://doi.org/10.1016/j.cemconres.2013.06.001.
[32] S. Scherb, N. Beuntner, K.C. Thienel, J. Neubauer, Quantitative X-ray diffraction of free, not chemically bound water with the PONKCS method, Journal of Applied Crystallography. 51 (2018) 1535–1543. https://doi.org/10.1107/S1600576718012888.
[33] B.H. O'Connor, M.D. Raven, Application of the Rietveld Refinement Procedure in Assaying Powdered Mixtures, Powder Diffraction. 3 (1988) 2–6. https://doi.org/10.1017/S0885715600013026.
[34] D. Jansen, F. Goetz-Neunhoeffer, C. Stabler, J. Neubauer, A remastered external standard method applied to the quantification of early OPC hydration, Cement and Concrete Research. 41 (2011) 602–608. https://doi.org/10.1016/j.cemconres.2011.03.004.
[35] A. Cuesta, J.D. Zea-Garcia, D. Londono-Zuluaga, A.G. de La Torre, I. Santacruz, O. Vallcorba, M. Dapiaggi, S.G. Sanfélix, M.A.G. Aranda, Multiscale understanding of tricalcium silicate hydration reactions, Scientific Reports. 8 (2018) 1–11. https://doi.org/10.1038/s41598-018-26943-y.
[36] A. Cuesta, Á.G. de La Torre, I. Santacruz, A. Diaz, P. Trtik, M. Holler, B. Lothenbach, M.A.G. Aranda, Quantitative disentanglement of nanocrystalline phases in cement pastes by synchrotron ptychographic X-ray tomography, IUCrJ. 6 (2019) 473–491. https://doi.org/10.1107/S2052252519003774.
[37] L. Valentini, M.C. Dalconi, M. Favero, G. Artioli, G. Ferrari, In-Situ XRD measurement and quantitative analysis of hydrating cement: Implications for sulfate incorporation in C-S-H, Journal of the American Ceramic Society. 98 (2015) 1259–1264. https://doi.org/10.1111/jace.13401.
[38] N.I. Golovastikov, R.G. Matveeva, N. v. Belov, Crystal structure of the tricalcium silicate 3CaO SiO2 = C3S, Soviet Physics - Crystallography. 20 (1975) 441–445.

[39] M.N. de Noirfontaine, M. Courtial, F. Dunstetter, G. Gasecki, M. Signes-Frehel, Tricalcium silicate Ca3SiO5 superstructure analysis: A route towards the structure of the M1 polymorph, Zeitschrift Fur Kristallographie. 227 (2012) 102–112. https://doi.org/10.1524/zkri.2012.1425.
[40] P. Mondal, J.W. Jeffery, The Crystal Structure of Triealeium Aluminate, Ca3Al2O6, Acta Crystallographica. (1975) 689.
[41] F. Nishi, Y. Takeuchi, The A16018 Rings of Tetrahedra in the Structure of Cas.sNaA16O18, Acta Crystallographica Section B Structural Crystallography and Crystal Chemistry. 31 (1975) 1169–1173.
[42] H.E. Petch, The hydrogen positions in portlandite, Ca(OH)2, as indicated by the electron distribution, Acta Crystallographica. 14 (1961) 950–957. https://doi.org/10.1107/s0365110x61002771.
[43] F. Goetz-Neunhoeffer, J. Neubauer, Refined ettringite (Ca 6 Al 2 (SO 4) 3 (OH) 12 ·26H 2 O) structure for quantitative X-ray diffraction analysis , Powder Diffraction. 21 (2006) 4–11. https://doi.org/10.1154/1.2146207.
[44] Á.G. de la Torre, M.-G. López-Olmo, C. Álvarez-Rua, S. García-Granda, Miguel.A.G. Aranda, Structure and microstructure of gypsum and its relevance to Rietveld quantitative phase analyses, Powder Diffraction. 19 (2004) 240–246. https://doi.org/10.1154/1.1725254.
[45] C. Bezou, A. Nonat, J.C. Mutin, A. Nørlund Christensen, M.S. Lehmann, Investigation of the crystal structure of γ-CaSO4, CaSO4 · 0.5 H2O, and CaSO4 · 0.6 H2O by powder diffraction methods, Journal of Solid State Chemistry. 117 (1995) 165–176. https://doi.org/10.1006/jssc.1995.1260.
[46] T. Runčevski, R.E. Dinnebier, O. v. Magdysyuk, H. Pöllmann, Crystal structures of calcium hemicarboaluminate and carbonated calcium hemicarboaluminate from synchrotron powder diffraction data, Acta Crystallographica Section B: Structural Science. 68 (2012) 493–500. https://doi.org/10.1107/S010876811203042X.
[47] P. Juilland, L. Nicoleau, R.S. Arvidson, E. Gallucci, Advances in dissolution understanding and their implications for cement hydration, RILEM Technical Letters. 2 (2017) 90. https://doi.org/10.21809/rilemtechlett.2017.47.
[48] F.P. Glasser, M.B. Marinho, Early stages of the hydration of tricalcium aluminate and its sodium-cotaining solid solutions, Proceedings of the British Ceramic Society. 35 (1984) 221–236.
[49] A.P. Kirchheim, V. Fernàndez-Altable, P.J.M. Monteiro, D.C.C. Dal Molin, I. Casanova, Analysis of cubic and orthorhombic C3A hydration in presence of gypsum and lime, Journal of Materials Science. 44 (2009) 2038–2045. https://doi.org/10.1007/s10853-009-3292-3.
[50] S.T. Bergold, F. Goetz-Neunhoeffer, J. Neubauer, Interaction of silicate and aluminate reaction in a synthetic cement system: Implications for the process of alite hydration, Cement and Concrete Research. 93 (2017) 32–44. https://doi.org/10.1016/j.cemconres.2016.12.006.
[51] C. Jakob, D. Jansen, N. Ukrainczyk, E. Koenders, U. Pott, D. Stephan, J. Neubauer, Relating ettringite formation and rheological changes during the initial cement hydration: A comparative study applying XRD analysis, rheological measurements and modeling, Materials. 12 (2019). https://doi.org/10.3390/ma12182957.
[52] D. Jansen, J. Neubauer, F. Goetz-Neunhoeffer, R. Haerzschel, W.D. Hergeth, Change in reaction kinetics of a Portland cement caused by a superplasticizer - Calculation of heat flow curves from XRD data, Cement and Concrete Research. 42 (2012) 327–332. https://doi.org/10.1016/j.cemconres.2011.10.005.
[53] M. García-Maté, A.G. de La Torre, L. León-Reina, E.R. Losilla, M.A.G. Aranda, I. Santacruz, Effect of calcium sulfate source on the hydration of calcium sulfoaluminate eco-cement, Cement and Concrete Composites. 55 (2015) 53–61. https://doi.org/10.1016/j.cemconcomp.2014.08.003.
[54] X. Kong, J. Pakusch, D. Jansen, S. Emmerling, J. Neubauer, F. Goetz-Neuhoeffer, Effect of polymer latexes with cleaned serum on the phase development of hydrating cement pastes, Cement and Concrete Research. 84 (2016) 30–40. https://doi.org/10.1016/j.cemconres.2016.02.013.
[55] P.R. de Matos, J. Andrade Neto, R. Sakata, A.P. Kirchheim, E.D. Rodríguez, C. Campos, Strategies for XRD quantitative phase analysis of blended Portland cements, Cement and Concrete Research. Under revi (2022) 104571. https://doi.org/10.1016/j.cemconcomp.2022.104571.
[56] J.W. Bullard, H.M. Jennings, R.A. Livingston, A. Nonat, G.W. Scherer, J.S. Schweitzer, K.L. Scrivener, J.J. Thomas, Mechanisms of cement hydration, Cement and Concrete Research. 41 (2011) 1208–1223. https://doi.org/10.1016/B978-0-08-100693-1.00008-4.

[57] L. Huang, L. Tang, H. Gu, Z. Li, Z. Yang, New insights into the reaction of tricalcium silicate (C3S) with solutions to the end of the induction period, Cement and Concrete Research. 152 (2022) 106688. https://doi.org/10.1016/j.cemconres.2021.106688.
[58] J. Plank, M. Schönlein, V. Kanchanason, Study on the early crystallization of calcium silicate hydrate (C-S-H) in the presence of polycarboxylate superplasticizers, Journal of Organometallic Chemistry. 869 (2018) 227–232. https://doi.org/10.1016/j.jorganchem.2018.02.005.
[59] M.J. Sánchez-Herrero, A. Fernández-Jiménez, A. Palomo, C4A3Š hydration in different alkaline media, Cement and Concrete Research. 46 (2013) 41–49. https://doi.org/10.1016/j.cemconres.2013.01.008.
[60] B. Mota, T. Matschei, K. Scrivener, The influence of sodium salts and gypsum on alite hydration, Cement and Concrete Research. 75 (2015) 53–65. https://doi.org/10.1016/j.cemconres.2015.04.015.
[61] M.M. Alonso, F. Puertas, Adsorption of PCE and PNS superplasticisers on cubic and orthorhombic C3A. Effect of sulfate, Construction and Building Materials. 78 (2015) 324–332. https://doi.org/10.1016/j.conbuildmat.2014.12.050.
[62] C.W. Chung, P. Suraneni, J.S. Popovics, L.J. Struble, Using ultrasonic wave reflection to monitor false set of cement paste, Cement and Concrete Composites. 84 (2017) 10–18. https://doi.org/10.1016/j.cemconcomp.2017.08.010.
[63] R.M. Mota, A.S. Silva, V.H.S. Ramos, J.C.T. Rezende, E. de Jesus, Effects of storage temperature and time on false setting behavior of CPI-S Portland cement, Ceramica. 66 (2020) 321–329. https://doi.org/10.1590/0366-69132020663792842.